RADIATION CHARACTERISTICS OF MICROSTRIP FED YAGIS PLACED ON A RECTANGULAR DIELECTRIC PLATE OF FINITE DIMENSIONS

by

Darius Romanek

A Thesis
Submitted to the Faculty of Graduate Studies
in Partial Fulfillment of the Requirements
for the Degree of

MASTER OF SCIENCE

Department of Electrical and Computer Engineering
University of Manitoba
Winnipeg, Manitoba

THE UNIVERSITY OF MANITOBA

FACULTY OF GRADUATE STUDIES

*****

COPYRIGHT PERMISSION

RADIATION CHARACTERSITCS OF MICROSTRIP FED YAGIS PLACED ON A RECTANGULAR DIELECTRIC PLATE OF FINITE DIMENSIONS

BY

Darius Romanek

A Thesis/Practicum submitted to the Faculty of Graduate Studies of The University of Manitoba in partial fulfillment of the requirement of the degree

Of

MASTER OF SCIENCE

Abstract

Printed Yagi or microstrip-fed Yagi Uda antennas placed on dielectric plates of finite dimensions are a natural evolution of wire Yagis. Due to recent developments in the area of wireless communication systems these antennas can be useful as they are compatible with microstrip circuitry used in microwave devices. The basic antenna concept involves printed dipole antenna element fed by a microstrip line to a balun transition. This antenna system is actually a two-element Yagi with a ground plane acting as a reflecting element and the dipole being the feeding element. The concept can be extended to lengthened or thickened dielectric plates with or without the inclusion of the parasitics. Such antennas enjoy good impedance bandwidth and low levels of cross polarization.

Directors prevent the higher order mode(s) from radiating thus narrowing the beam and increasing the directivity. Similar results can be achieved with longer plates although they are not able to prevent the higher order mode(s) from radiating as well as the parasitics do; patterns do however enjoy lower sidelobes. Director addition introduces multiple resonances extending the pattern bandwidth but at the expense of higher sidelobes.

Exact form of the radiation pattern solution is found using Ansoft's High Frequency Structure Simulator, HFSS. Cross-sectional field values can also be calculated. Given the field inside the plate (determined with the aid of HFSS) and its general expression, orthogonality of modes theorem is applied to extract the values of field coefficients for different propagating modes. Once known, these values can provide insight into an entire mechanism of radiation.

Acknowledgements

First of all I would like to thank professor L. Shafai for teaching me the value of self-effort, perseverance and determination without which this work would not have been brought to a successful completion. I am likewise indebted to professor Shafai for his patience, extended financial aid as well as on-going contact and advice while I was away and working which were also significant factors that allowed me to carry this work to successful completion.

I would also like to thank professor John Volakis and Dr. C.J. Reddy for their continued encouragement and inspiration in Virginia that only boosted my self-confidence and technical expertise.

Last but not least I would like to thank my mother and my brother from whom I received most of the emotional support I needed and to whom I dedicate this work.

Table of Contents

List of Figures

List of Tables

Chapter 1: Introduction

Printed Yagi or microstrip-fed Yagi Uda antennas are a natural evolution of wire Yagis. The total field is found by superposition of the fields radiated from the physically existing sources, the dipole currents and the surface current distribution on the surface wave reflector (that is the finite microstrip ground plane supporting the feed structure) [17]. One might also think of them as a combination of wire Yagi and dielectric rod antennas. Much attention has been given to both antenna types in the past.

Historically, dielectric rod antenna research is the older of the two. As early as 1910, dielectric rods were investigated as candidates for transmission lines [12], [16]. Further research indicated that they acted better as efficient radiators [12].

The main bulk of early theoretical work devoted to rod radiation pattern characteristics has produced three different methods of approach to the problem. All three methods attempted to derive a radiation pattern expression for rods of rectangular or circular cross section excited by dominant modes of waveguides of circular or rectangular cross section [12]. The first method, devised by Mallach [7], [12], assumed radiation to occur continuously along a rod's length. Purely practical objection to that theory was that it failed to predict the observed dependence of the beam width of the aerial on the length of the rod. According to the theory, beam width should decrease steadily with increasing rod length, tending to zero as the length tends to infinity. In practice, beam width never tends to zero, regardless of rod length. Spector and Brown [7] explained that increasing

the length of a uniform dielectric rod diminishes the amplitude of the evanescent field which extends from the feed to the radiating aperture, and once the length is sufficient to make this diminishing field small compared with the dipole wave, further increases in rod length will not change the radiation from the aperture. The second method interpreted rod aerials as a type of lens [12]. The third, and the most successful of these methods, proved to be the theory developed in 1948 by Horton and Watson [25], [12] using Schelkunoff's Equivalence Principle and postulating a set of quite fictitious electric and magnetic surface currents in the rod from which the radiation pattern expression was derived. However, in order to carry out this calculation exactly, the electromagnetic field inside a dielectric must be known. Due to the inability of finding an exact expression for this field, Horton and Watson made reasonable approximations and achieved agreement with experimental observations for rods not longer than six wavelengths [25].

Recently, Jasik and Johnson [10] shed more light on the radiation characteristics of dielectric rod antennas. They used the term surface wave antenna when referring to the dielectric rod whose surface wave is a slow wave because it does not radiate along the length of the guide as well as a trapped wave since it carries its energy within a small distance from the interface. They stated that the total pattern of this antenna is formed by the interference between the feed and terminal patterns and gave a simple but approximate expression for the terminal radiation pattern of the dielectric rods.

Originally, treatment of wire Yagi antennas was mostly experimental. By 1957 [7], it was known that the physical action of the directors was to reduce the phase velocity of the wave traveling along the axis of the Yagi, making the wave appear as if it was traversing a region of refractive index greater than unity, whose variation depends on

the dimensions and spacing of the directors. A method of theoretically studying the complex current distributions on all the elements of a Yagi-Uda array, the phase velocity and the corresponding radiation patterns was described by Thiele [23]. Thiele's theory clearly showed the dependence of the far-field patterns on the phase velocity along the array.

The advantages of circular-loop antennas over dipole antennas led to the investigation of yagi arrays of two concentric loops by Shoamanesh and Shafai [21]. The phase velocity of the propagating wave along the array had revealed that the array possessed two distinct pass bands, corresponding respectively to the resonance of the outer and the inner sub arrays and separated by a stop band.

To the best of author's knowledge, the first microstrip-fed Yagi Uda antenna was designed and reported by Qassim and McEwan back in 1991 [19]. The design was based on an equivalent Yagi in which the conductors would be cylindrical and in free space. The dielectric effect was therefore minimized by using thin, low permittivity substrate. Though minimized, the dielectric effect had to be allowed for and this was done by postulating that the dielectric would mainly lower the resonant frequency of an element. The equivalence was therefore found by increasing the element length by a suitable factor. Dielectric proved to have negligible effect on the inter-element spacing.

The work presented in this report is a study of radiation characteristics of microstrip-fed Yagi Uda antennas placed on a dielectric plate of finite dimensions and varying dielectric constant. To this effect, although only high and low dielectric constants were chosen, middle values could be found by interpolation. The feed used in this work has originally been designed and presented by Itoh and Kaneda in their paper from 1998

[20]. Original feed design consisted of a novel Yagi-like printed dipole array antenna, which uses the truncated microstrip ground plane as its reflecting element. The antenna is fed by a uniplanar, broadband microstrip-to-coplanar strip (CPS) transition. The transition can be realized by designing impedance matched T-junction and delaying one side of the microstrip line by half wavelength at the desired frequency. The details of this feed design will be presented in chapter 2. Two improvements of the original feed design followed in the next 4 years [9], [26]. The main purpose of these improvements was to seek better bandwidth and directivity. Recently, Song optimized the design parameters to obtain better bandwidth [27].

Exact form of the radiation pattern solution is found using Ansoft's HFSS (High Frequency Structure Simulator). Cross-sectional field values can also be calculated. Given the field inside the plate (determined with the aid of HFSS) and its general expression (presented in [14]), orthogonality of modes theorem (found in [22]) is applied to extract the values of field coefficients for different propagating modes. Once known, these values can provide insight into an entire mechanism of radiation.

Chapter 2: Problem Description and Analysis

2.1: Introduction

There are several advantages of microstrip-fed Yagi Uda antennas. The antennas are very compact and easy to fabricate due to their uniplanar nature and show great promise for monolithic integration with Si, GaAs, InP-based or other RF front-end circuitry for higher frequency applications such as wireless communications, phased arrays, power combining and millimeter-wave imaging arrays [20].

This chapter discusses the feed used, which includes its original design as well as three others that followed. Then, the routine for extraction of the values of field coefficients for different propagating modes and finding the power in each mode is presented.

2.2: Problem Description

Figure 2.1 (page 6) shows basic problem geometry. This type of Yagi antenna has several advantages over more traditional wire antennas radiating in free space. First, the presence of the substrate provides mechanical support for the antenna and planar transmission-line compatibility. Wire-type antennas in free space are extremely fragile at high frequencies and difficult to feed. Secondly, use of a high-permittivity substrate

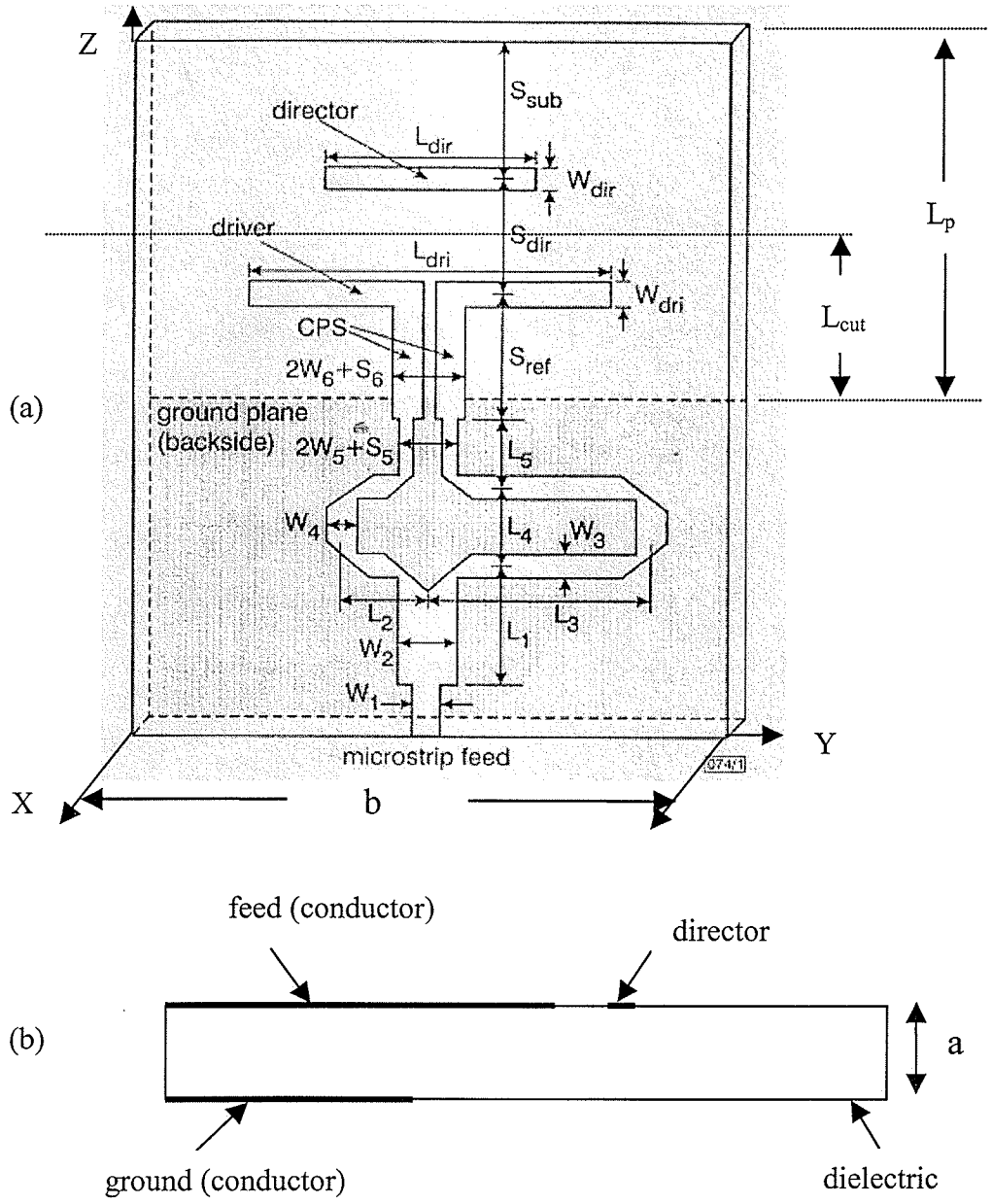

Figure 2.1: Problem Geometry (a) top view (b) side view.

means that the antenna will be extremely compact in terms of free space wavelengths. Thirdly, the length of the antenna's director element is shorter than the conventional Yagi-Uda antenna design and contributes to the broadband characteristics of the antenna

[9]. One of the most unique and effective features of this antenna is the use of the truncated ground plane as the reflector element. The driven printed dipole is used to generate a TE_0 surface wave with very little undesired TM_0 content, which can contribute to cross-polarization. The truncated ground plane acts as an ideal reflector for this TE_0 mode, which is completely cutoff in the grounded dielectric slab region [9], [26]. Bold lines in figure 2.1(b) indicate copper surfaces.

2.2.1: Design Parameters

Chosen design frequency for the circuit in figure 2.1 above was 10 GHz. The chosen dielectric constant equaled 10.2. The plate wavelength (λ_g) at that frequency is 9.4 mm. The circuit dimensions in terms of plate wavelength are [9]:

$W_3 = W_4 = W_6 = W_{dri} = W_{dir} = 0.064\lambda_g$

$W_2 = 0.13\lambda_g$

$W_5 = 0.032\lambda_g$

$L_1 = 0.335\lambda_g$

$L_2 = 0.19\lambda_g$

$L_3 = 0.495\lambda_g$

$L_4 = 0.22\lambda_g$

$L_5 = 0.19\lambda_g$

$S_5 = 0.064\lambda_g$

$S_6 = 0.032\lambda_g$

$S_{ref} = 0.35\lambda_g$

$L_{dri} = 0.8\lambda_g$

$L_{dir} = 0.45\lambda_g$

Parameters S_{dir} and S_{sub} have not been mentioned as parameter S_{sub} was not used in this work and parameter S_{dir} was altered for director studies; it was chosen to be equal to $0.4\lambda_g$ (where subscript g refers to the wavelength in the plate). Parameter L_p measures

length of the plate and parameter L_{cut} represents the cut plane for mode extraction. The design achieved an impedance bandwidth of 17% and gain of 6.5dB.

2.2.2: Design Improvements

In the years following the initial feed design, Itoh and Kaneda re-designed the feed twice [20], [26] to first achieve a tremendous increase in bandwidth (between 43% and 48%) at a price of a lower gain (3-5dB) and second to obtain good gain (5-7dB) at the expense of a slightly smaller bandwidth (11%). In both cases, parameters had been adjusted. Then, Song investigated the effects of five main design parameters of the microstrip-fed quasi-Yagi antenna on its operational frequency and impedance bandwidth [27]. The parameters included length of the director, distance between the director and the driver, distance between the coupled microstrip lines, length of the driver and the distance from the driver to the reflector. It was found that the most sensitive parameters of the quasi-Yagi antenna were the length of the driver and the distance from the driver to the reflector.

Although this work is primarily based on the initial design, these improvements could be used as an enhancement or as alternatives to the current work.

2.3: Field Analysis of a Rectangular Dielectric Plate

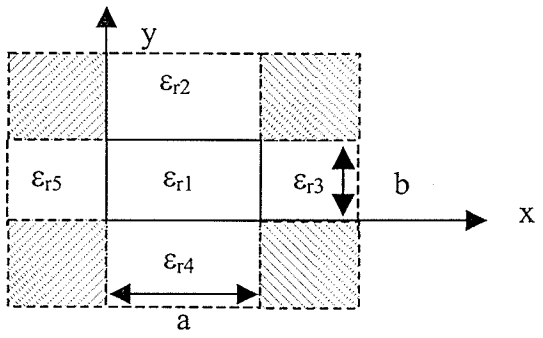

Figure 2.2: Cross-section of a dielectric plate.

Figure 2.2 above shows the primary regions of field existence. The field also exists in shaded regions but it is so small that it can be ignored. The value of a need also not be greater than the value of b. Dimension a is much smaller than b in our case as illustrated in figure 2.1. According to Marcatili [14], the field components in each of the five areas of Figure 2.1 can be written as

$$
\begin{aligned}
H_{x1}^{mn} &= A_{mn_1}\cos(k_{xm}x+\alpha)\cos(k_{yn}y+\beta)\exp(-jk_z z),\ 0\le x\le a,\ 0\le y\le b \\
H_{x2}^{mn} &= A_{mn_2}\cos(k_{xm}x+\alpha)\exp(-jk_{yn_2}y)\exp(-jk_z z),\ 0\le x\le a,\ b<y<\infty \\
H_{x3}^{mn} &= A_{mn_3}\cos(k_{yn}y+\beta)\exp(-jk_{xm_3}x)\exp(-jk_z z),\ a<x<\infty,\ 0\le y\le b \\
H_{x4}^{mn} &= A_{mn_4}\cos(k_{xm}x+\alpha)\exp(jk_{yn_4}y)\exp(-jk_z z),\ 0\le x\le a,\ -\infty<y<0 \\
H_{x5}^{mn} &= A_{mn_5}\cos(k_{yn}y+\beta)\exp(jk_{xm_5}x)\exp(-jk_z z),\ -\infty<x<0,\ 0\le y\le b
\end{aligned}
\tag{1a}
$$

$$
H_{yv}^{mn} = 0,\ v = 1,2\ldots5 \tag{1b}
$$

$$
\begin{aligned}
H_{z1}^{mn} &= \frac{-jk_{xm}k_{yn}}{k_z}A_{mn_1}\sin(k_{xm}x+\alpha)\sin(k_{yn}y+\beta)\exp(-jk_z z),0\le x\le a,\ 0\le y\le b \\
H_{z2}^{mn} &= \frac{k_{xm}k_{yn_2}}{k_z}A_{mn_2}\sin(k_{xm}x+\alpha)\exp(-jk_{yn_2}y)\exp(-jk_z z),0\le x\le a,\ b<y<\infty \\
H_{z3}^{mn} &= \frac{k_{xm_3}k_{yn}}{k_z}A_{mn_3}\sin(k_{yn}y+\beta)\exp(-jk_{xm_3}x)\exp(-jk_z z),a<x<\infty,\ 0\le y\le b \\
H_{z4}^{mn} &= \frac{-k_{xm}k_{yn_4}}{k_z}A_{mn_4}\sin(k_{xm}x+\alpha)\exp(jk_{yn_4}y)\exp(-jk_z z),0\le x\le a,\ -\infty<y<0 \\
H_{z5}^{mn} &= \frac{-k_{xm_5}k_{yn}}{k_z}A_{mn_5}\sin(k_{yn}y+\beta)\exp(jk_{xm_5}x)\exp(-jk_z z),-\infty<x<0,\ 0\le y\le b
\end{aligned}
\tag{1c}
$$

where superscripts m and n indicate the number of extrema each component has within the guide, α and β locate the field maxima and minima in region 1, k_z is the axial propagation constant and k_{xm} and k_{yn} are the transverse propagation constants along the x and y directions, respectively.

In order to find the electric field components, the following equations can be used:

$$E_{xv}^{mn} = \frac{-1}{\omega\varepsilon_o\varepsilon_{rv}k_z}\frac{\partial^2 H_{xv}}{\partial x\partial y},\ v = 1,2...5 \tag{2a}$$

$$E_{yv}^{mn} = \frac{k_o^2\varepsilon_{rv} - k_{yn}^2}{\omega\varepsilon_o\varepsilon_{rv}k_z}H_{xv},\ v = 1,2...5 \tag{2b}$$

$$E_{zv}^{mn} = \frac{j}{\omega\varepsilon_o\varepsilon_{rv}}\frac{\partial H_{xv}}{\partial y},\ v = 1,2...5 \tag{2c}$$

where k_o is the free space propagation constant and $k_o = \omega\sqrt{\varepsilon_o\mu_o}$.

Hence, equations (2a) to (2c) can be written as

$$\begin{aligned}
E_{x1}^{mn} &= -B_{mn_1}\sin(k_{xm}x+\alpha)\sin(k_{yn}y+\beta)\exp(-jk_z z),\ 0\le x\le a,\ 0\le y\le b\\
E_{x2}^{mn} &= -jB_{mn_2}\sin(k_{xm}x+\alpha)\exp(-jk_{yn_2}y)\exp(-jk_z z),\ 0\le x\le a,\ b<y<\infty\\
E_{x3}^{mn} &= -jB_{mn_3}\sin(k_{yn}y+\beta)\exp(-jk_{xm_3}x)\exp(-jk_z z),\ a<x<\infty,\ 0\le y\le b\\
E_{x4}^{mn} &= jB_{mn_4}\sin(k_{xm}x+\alpha)\exp(jk_{yn_4}y)\exp(-jk_z z),\ 0\le x\le a,\ -\infty<y<0\\
E_{x5}^{mn} &= jB_{mn_5}\sin(k_{yn}y+\beta)\exp(jk_{xm_5}x)\exp(-jk_z z),\ -\infty<x<0,\ 0\le y\le b
\end{aligned} \tag{3a}$$

$$\begin{aligned}
E_{y1}^{mn} &= C_{mn_1}\cos(k_{xm}x+\alpha)\cos(k_{yn}y+\beta)\exp(-jk_z z),\ 0\le x\le a,\ 0\le y\le b\\
E_{y2}^{mn} &= C_{mn_2}\cos(k_{xm}x+\alpha)\exp(-jk_{yn_2}y)\exp(-jk_z z),\ 0\le x\le a,\ b<y<\infty\\
E_{y3}^{mn} &= C_{mn_3}\cos(k_{yn}y+\beta)\exp(-jk_{xm_3}x)\exp(-jk_z z),\ a<x<\infty,\ 0\le y\le b\\
E_{y4}^{mn} &= C_{mn_4}\cos(k_{xm}x+\alpha)\exp(jk_{yn_4}y)\exp(-jk_z z),\ 0\le x\le a,\ -\infty<y<0\\
E_{y5}^{mn} &= C_{mn_5}\cos(k_{yn}y+\beta)\exp(jk_{xm_5}x)\exp(-jk_z z),\ -\infty<x<0,\ 0\le y\le b
\end{aligned} \tag{3b}$$

$$\begin{aligned}
E_{z1}^{mn} &= -jD_{mn_1}\cos(k_{xm}x+\alpha)\sin(k_{yn}y+\beta)\exp(-jk_z z),\ 0\le x\le a,\ 0\le y\le b\\
E_{z2}^{mn} &= D_{mn_2}\cos(k_{xm}x+\alpha)\exp(-jk_{yn_2}y)\exp(-jk_z z),\ 0\le x\le a,\ b<y<\infty\\
E_{z3}^{mn} &= -jD_{mn_3}\sin(k_{yn}y+\beta)\exp(-jk_{xm_3}x)\exp(-jk_z z),\ a<x<\infty,\ 0\le y\le b\\
E_{z4}^{mn} &= -D_{mn_4}\cos(k_{xm}x+\alpha)\exp(jk_{yn_4}y)\exp(-jk_z z),\ 0\le x\le a,\ -\infty<y<0
\end{aligned} \tag{3c}$$

$$E_{z5}^{mn} = -jD_{mn_5}\sin(k_{yn}y+\beta)\exp(jk_{xm_5}x)\exp(-jk_z z),\ -\infty < x < 0,\ 0 \le y \le b$$

where: $B_{mn} = \dfrac{k_{xm}k_{yn}A_{mn_v}}{\omega\varepsilon_o\varepsilon_{rv}k_z}$, $v = 1,2...5$

$$C_{mn} = \frac{k_v^2\varepsilon_{rv} - k_{yn}^2}{\omega\varepsilon_o\varepsilon_{rv}k_z}A_{mn_v},\ v = 1,2...5$$

$$D_{mn} = \frac{k_{yn}A_{mn_v}}{\omega\varepsilon_o\varepsilon_{rv}},\ v = 1,2...5$$

and where k_v is the propagation constant of a plane wave in the v^{th} medium (v = 1,2…5).

Equations (1) to (3) assume polarization along y as the dipole in figure 1 is y-polarized. Constants k_{xm}, k_{yn} and k_z can be found by matching tangential components along the edges of region 1. In order to do that we choose two of three possible combinations of matched fields. For regions 1, 2 and 4 we make use of the fact that H_{xv}, H_{zv} and E_{zv} are all equal at the interfaces between regions 1 and 2 as well as regions 1 and 4. Likewise, for regions 1,3 and 5 we note that H_{zv}, E_{yv} and E_{zv} are equal at the region interfaces. Let us first match the fields at the interfaces between regions 1, 2 and 4. We will choose the relationships between H_{xv} and E_{zv}. We obtain the following set of relations,

$$A_{mn_1}\cos(k_{yn}b+\beta) = A_{mn_2}\exp(-ik_{yn_2}b) \tag{4a}$$

$$A_{mn_1}\cos(\beta) = A_{mn_4} \tag{4b}$$

$$A_{mn_1}\left(\frac{-ik_{yn}}{\omega\varepsilon_o\varepsilon_{r1}}\right)\sin(k_{yn}b+\beta) = A_{mn_2}\left(\frac{k_{yn_2}}{\omega\varepsilon_o\varepsilon_{r2}}\right)\exp(-ik_{yn_2}b) \tag{4c}$$

$$A_{mn_1}\left(\frac{ik_{yn}}{\omega\varepsilon_o\varepsilon_{r1}}\right)\sin(\beta) = A_{mn_4}\left(\frac{k_{yn_4}}{\omega\varepsilon_o\varepsilon_{r4}}\right) \tag{4d}$$

If we now divide equations (4c) and (4d) by (4a) and (4b) respectively, we obtain,

$$\frac{k_{yn}}{i\varepsilon_{r1}}\tan(k_{yn}b+\beta)=\frac{k_{yn_2}}{\varepsilon_{r2}} \tag{5a}$$

and

$$\frac{ik_{yn}}{\varepsilon_{r1}}\tan(\beta)=\frac{k_{yn_4}}{\varepsilon_{r4}} \tag{5b}$$

Equations (5a) and (5b) can be rewritten as,

$$\tan(k_{yn}b+\beta)=i\frac{k_{yn_2}}{k_{yn}}\frac{\varepsilon_{r1}}{\varepsilon_{r2}} \tag{6a}$$

and

$$\tan(\beta)=-i\frac{k_{yn_4}}{k_{yn}}\frac{\varepsilon_{r1}}{\varepsilon_{r4}} \tag{6b}$$

Similarly, we match the fields at the interfaces between regions 1, 3 and 5 by choosing the relationships between H_{zv} and E_{zv} to obtain,

$$\tan(\alpha)=i\frac{k_{xn_3}}{k_{xn}} \tag{7a}$$

and

$$\tan(k_{xn}a+\alpha)=-i\frac{k_{xn_5}}{k_{xn}} \tag{7b}$$

Equations (6) and (7) can be rewritten as,

$$k_{yn}b = q\pi - \tan^{-1}\frac{\varepsilon_{r2}k_{yn}}{\varepsilon_{r1}\left|k_{yn_2}\right|} - \tan^{-1}\frac{\varepsilon_{r4}k_{yn}}{\varepsilon_{r1}\left|k_{yn_4}\right|} \tag{8}$$

and

$$k_{xm}a = p\pi - \tan^{-1}\frac{k_{xm}}{\left|k_{xm_3}\right|} - \tan^{-1}\frac{k_{xm}}{\left|k_{xm_5}\right|} \tag{9}$$

where,

$$\left|k_{yn_{2,4}}\right| = \left[\left(\frac{\pi}{A_{2,4}}\right)^2 - k_{yn}^2\right]^{\frac{1}{2}} \tag{10}$$

$$\left|k_{xm_{3,5}}\right| = \left[\left(\frac{\pi}{A_{3,5}}\right)^2 - k_{xm}^2\right]^{\frac{1}{2}} \tag{11}$$

and

$$A_{2,3,4,5} = \frac{\pi}{(k_1^2 - k_{2,3,4,5}^2)^{\frac{1}{2}}} \tag{12}$$

Equations (8) and (9) cannot be solved exactly in closed form. Nevertheless, for well-guided modes, most of the power travels within medium 1, which implies that the terms k_{yn}^2 and k_{xm}^2 in equations (10) and (11) can be neglected [14]. By solving for k_{xm} and k_{yn}, the following expression for the guide wavelength is obtained,

$$\lambda_z = \frac{2\pi}{k_z} \tag{13}$$

where [14]:

$$k_z = \sqrt{k_1^2 - k_{xm}^2 - k_{yn}^2}$$

$$k_{xm} = \frac{m\pi}{a}\left(1 + \frac{A_3 + A_5}{\pi a}\right)^{-1} \qquad \text{for } E_{mn}^{y} \text{ modes}$$

$$k_{xm} = \frac{m\pi}{a}\left(1 + \frac{\varepsilon_{r_3} A_3 + \varepsilon_{r_5} A_5}{\pi \varepsilon_r a}\right)^{-1} \qquad \text{for } E_{mn}^{x} \text{ modes}$$

$$k_{yn} = \frac{n\pi}{b}\left(1 + \frac{\varepsilon_{r_2} A_2 + \varepsilon_{r_4} A_4}{\pi \varepsilon_r b}\right)^{-1} \qquad \text{for } E_{mn}^{y} \text{ modes}$$

$$k_{yn} = \frac{n\pi}{b}\left(1 + \frac{A_2 + A_4}{\pi b}\right)^{-1} \qquad \text{for } E_{mn}^{x} \text{ modes}$$

$$A_i = \frac{\pi}{\sqrt{k_1^2 - k_i^2}} = \frac{\lambda}{2\sqrt{\varepsilon_r - \varepsilon_{r_i}}} \qquad , \text{i} = 2,3,4,5$$

$$k_i = \frac{2\pi\sqrt{\varepsilon_{r_i}}}{\lambda_o} \qquad , \text{i} = 1,2,3,4,5$$

The total fields can be written as follows,

$$\vec{E}(x,y,z) = \sum_m \sum_n \hat{x} E_{xv}^{mn} + \hat{y} E_{yv}^{mn} + \hat{z} E_{zv}^{mn} \tag{14a}$$

$$\vec{H}(x,y,z) = \sum_m \sum_n \hat{x} H_{xv}^{mn} + \hat{z} H_{zv}^{mn} \tag{14b}$$

Equations (14a) and (14b) give the volume fields. If we now dissect the guide at some $z = z_o$, multiply each of the components of any given mode by the complex conjugate of a specific mode on the right hand side of equations (14a) and (14b) [22] and the total field components by the complex conjugate of a specific mode on the left hand side of equations (14a) and (14b) and then integrate both sides over the dissecting surface to obtain

$$\iint_S \vec{E}(x,y,z=z_o)\cdot(\vec{E}_v^{mn})^* dxdy = \iint_S \left|\vec{E}_v^{mn}\right|^2 dxdy \tag{15a}$$

and

$$\iint_S \vec{H}(x,y,z=z_o)\cdot(\vec{H}_v^{mn})^* dxdy = \iint_S \left|\vec{H}_v^{mn}\right|^2 dxdy \tag{15b}$$

where superscript *mn* represents a specific mode.

Due to the orthogonal nature of the fields, equations (15a) and (15b) allow us to determine the coefficients for each and every mode (refer to Appendix B). Functions $\vec{E}(x,y,z=z_o)$ and $\vec{H}(x,y,z=z_o)$ can be determined using Ansoft's HFSS. Moreover, by analyzing $\vec{E}(x,y,z=z_l)$ and $\vec{H}(x,y,z=z_l)$ (l = *1,2...n*) we can study and determine the path of radiation along the guide.

2.4: Power Analysis of a Rectangular Dielectric Plate

The fields that are created and propagating inside and outside the plate have power associated with them [3]. To find the power flowing in each of the regions shown in figure 2.2, it is first necessary to find the average power density in each of the regions directed along the axis of the plate. The power flowing along the plate can then be found by integrating the axial directed power density over the cross section of each of the regions shown in figure 2.1. Since regions 2, 3, 4 and 5 must be finite, appropriate boundaries have been chosen to capture a great majority of the field in those regions.

The regions are defined as follows:

Region 1: $0 \le x \le a$, $0 \le y \le b$

Region 2: $0 \le x \le a$, $b < y < d$

Region 3: $a < x < d$, $0 \le y \le b$

Region 4: $0 \le x \le a,\ -d < y < 0$

Region 5: $-d < x < 0,\ 0 \le y \le b$

For the plate geometry of figure 2.1, the z-directed power density can be written as,

$$\left(\vec{S}_z\right)^v_{mn} = \hat{a}_z S_{zv} = \hat{a}_z \frac{1}{2}\mathrm{Re}[E_{xv}H^*_{yv} - E_{yv}H^*_{xv}] \tag{16}$$

Since $H_{yv} = 0$ and E_{xv} is negligible [14], equation (16) can be rewritten as

$$\left(\vec{S}_z\right)^v_{mn} = -\hat{a}_z \frac{1}{2}\mathrm{Re}[E_{yv}H^*_{xv}] \tag{17}$$

Therefore,

$$\left(\vec{S}_z\right)^1_{mn} = \hat{a}_z S_{z1} = \hat{a}_z \frac{|A_{mn}|^2}{2} \cdot \frac{k_{yn}^2 - k_o^2\varepsilon_{r1}}{\omega\varepsilon_o\varepsilon_{r1}k_z}[\cos^2(k_{xm}x)\cos^2(k_{yn}y)]$$

$$\left(\vec{S}_z\right)^2_{mn} = \hat{a}_z S_{z2} = \hat{a}_z \frac{|A_{mn}|^2}{2} \cdot \frac{k_{yn}^2 - k_o^2\varepsilon_{r2}}{\omega\varepsilon_o\varepsilon_{r2}k_z}[\cos^2(k_{xm}x)]$$

$$\left(\vec{S}_z\right)^3_{mn} = \hat{a}_z S_{z3} = \hat{a}_z \frac{|A_{mn}|^2}{2} \cdot \frac{k_{yn}^2 - k_o^2\varepsilon_{r3}}{\omega\varepsilon_o\varepsilon_{r3}k_z}[\cos^2(k_{yn}y)] \tag{18}$$

$$\left(\vec{S}_z\right)^4_{mn} = \hat{a}_z S_{z4} = \hat{a}_z \frac{|A_{mn}|^2}{2} \cdot \frac{k_{yn}^2 - k_o^2\varepsilon_{r4}}{\omega\varepsilon_o\varepsilon_{r4}k_z}[\cos^2(k_{xm}x)]$$

$$\left(\vec{S}_z\right)^5_{mn} = \hat{a}_z S_{z5} = \hat{a}_z \frac{|A_{mn}|^2}{2} \cdot \frac{k_{yn}^2 - k_o^2\varepsilon_{r5}}{\omega\varepsilon_o\varepsilon_{r5}k_z}[\cos^2(k_{yn}y)]$$

The associated power is obtained by integrating equation (17) over each region's cross-section as shown in figure 2.3 below.

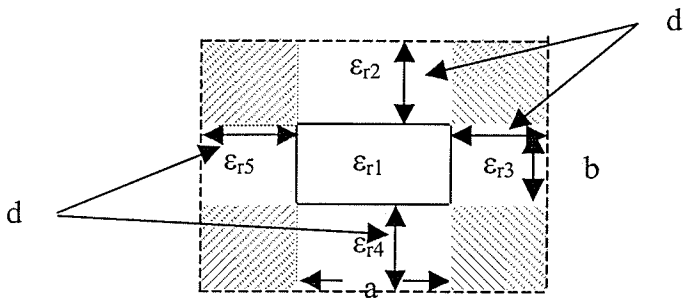

Figure 2.3: Area of Integration.

The distance d is made sufficiently large to capture most of the field in the surrounding regions.

$$P_{mn}^{1} = \iint_{A_1} \left(\vec{S}_z\right)_{mn}^{1} \cdot d\vec{s} = \int_0^b \int_0^a S_{z_1} dxdy$$

$$P_{mn}^{2} = \iint_{A_2} \left(\vec{S}_z\right)_{mn}^{2} \cdot d\vec{s} = \int_b^{b+d} \int_0^a S_{z_2} dxdy = d\int_0^a S_{z_2} dx$$

$$P_{mn}^{3} = \iint_{A_3} \left(\vec{S}_z\right)_{mn}^{3} \cdot d\vec{s} = \int_0^b \int_a^{a+d} S_{z_3} dxdy = d\int_0^b S_{z_3} dy \qquad (19)$$

$$P_{mn}^{4} = \iint_{A_4} \left(\vec{S}_z\right)_{mn}^{4} \cdot d\vec{s} = \int_{-d}^0 \int_0^a S_{z_4} dxdy = d\int_0^a S_{z_4} dx$$

$$P_{mn}^{5} = \iint_{A_5} \left(\vec{S}_z\right)_{mn}^{5} \cdot d\vec{s} = \int_0^b \int_{-d}^0 S_{z_5} dxdy = d\int_0^b S_{z_5} dy$$

Since

$$\int_0^c \cos^2(kx)dx = \frac{c}{2} + \frac{\sin(2kc)}{4k} \qquad (20),$$

equation (19) becomes

$$P_{mn}^{1} = \frac{\left|A_{mn}\right|^2}{2} \cdot \frac{k_{yn}^2 - k_o^2 \varepsilon_{r1}}{\omega \varepsilon_o \varepsilon_{r1} k_z} \left[\left(\frac{a}{2} + \frac{\sin(2k_{xm}a)}{4k_{xm}}\right)\left(\frac{b}{2} + \frac{\sin(2k_{yn}b)}{4k_{yn}}\right)\right]$$

$$P_{mn}^{2} = d \cdot \frac{\left|A_{mn}\right|^2}{2} \cdot \frac{k_{yn}^2 - k_o^2 \varepsilon_{r2}}{\omega \varepsilon_o \varepsilon_{r2} k_z} \left[\left(\frac{a}{2} + \frac{\sin(2k_{xm}a)}{4k_{xm}}\right)\right]$$

$$P_{mn}^{3} = d \cdot \frac{|A_{mn}|^2}{2} \cdot \frac{k_{yn}^2 - k_o^2 \varepsilon_{r3}}{\omega \varepsilon_o \varepsilon_{r3} k_z} [(\frac{b}{2} + \frac{\sin(2k_{yn} b)}{4k_{yn}})] \tag{21}$$

$$P_{mn}^{4} = d \cdot \frac{|A_{mn}|^2}{2} \cdot \frac{k_{yn}^2 - k_o^2 \varepsilon_{r4}}{\omega \varepsilon_o \varepsilon_{r4} k_z} [(\frac{a}{2} + \frac{\sin(2k_{xm} a)}{4k_{xm}})]$$

$$P_{mn}^{5} = d \cdot \frac{|A_{mn}|^2}{2} \cdot \frac{k_{yn}^2 - k_o^2 \varepsilon_{r5}}{\omega \varepsilon_o \varepsilon_{r5} k_z} [(\frac{b}{2} + \frac{\sin(2k_{yn} b)}{4k_{yn}})]$$

By the use of superposition [3], the total power associated with a wave is equal to the sum of all the power components associated with each mode that exists inside the area of figure 2.3. Thus

$$P_{total} = \sum_{m,n} P_{mn}^{v} \text{ , } v = 1,2...5 \tag{22}$$

2.5: Discussion

As an electromagnetic wave is launched into the dielectric plate, fields exist both inside as well as outside the plate. Obviously, most of the field will be concentrated in region 1 of figure 2.3 whereas some of it will be found in regions 2, 3, 4 and 5. Shaded regions can be assumed to contain no field at all since the value of it is negligible compared with the fields in other regions.

Equations 1 through 3 represent the basic form of these fields in the cross-section of the plate. The fields inside the plate are cosinusoidal in nature and decaying in regions outside the plate. Each of these fields is a summation of modes that exist inside the plate of specific dimensions. The basic shape and size of this field pattern depends on the number of modes existing inside the plate and their individual strength. To this effect, if the plate were to support only one mode that is the dominant mode, the form of the cross-

sectional field pattern would be a pure cosinusoid. Introduction of higher order modes distorts the field pattern inside the plate. The higher the distortion, the stronger the influence of higher order modes.

The key now is to extract the values of the coefficients of all these modes (both dominant and higher order) using the mechanism of equation 15. This can be done as we move along the plate probing the field and extracting the coefficients at various cross-sections. Equations 21 and 22 allow us to find the percentage of power in each given mode based on which predictions of pattern behavior can be made.

2.6: Concluding Remarks

Since wire Yagis in free space are extremely fragile at high frequencies, printed Yagis have been used. To this effect, several works dealing with the design of printed Yagi antennas have been published in recent years all striving to achieve good gain and impedance characteristics. The method proposed here has been devised to predict and study pattern behavior and characteristics based on the extraction of values of mode coefficients. Given these values, the percentage of power carried by each given mode could be obtained.

Chapter 3: Length Studies of Microstrip-Fed Yagi Uda Antennas Placed On a Plate of Final Dimensions With and Without Directors

3.1: Introduction

Pattern Analysis with and without directors naturally follows work done by previous authors. This chapter shows how the modal coefficient theory presented in chapter 2 can be applied to both predict and understand pattern performance as we increase the dielectric plate length with and/or without directors. This can be done by analyzing radiation pattern bandwidth, which here refers to pattern shape and size in reference to center frequency with directivity values falling within at least 3 dB below the values at center frequency.

Phase velocity and pattern and its directivity are no longer just controlled by element spacing but also by the adjustment of plate dimensions. Of course, adjustment of plate dimensions influences higher order modes, which has the potential of further affecting the phase velocity, pattern and directivity as will be shown in this and the following chapter. In fact, as plate itself has a tendency of slowing down the wave (as it typically travels through a medium with a permittivity higher than unity), directors act to slow it down even further making the effective permittivity even higher than the permittivity of the plate itself from the point of view of a traveling wave.

3.2: Microstrip-Fed Yagis Placed On High Permittivity Plates

Figures 3.1 to 3.11 (pages 23 to 33) demonstrate an increase in radiation pattern bandwidth, as the plate is gradually made longer. The effects are particularly noticeable at the upper end of the frequency spectrum. Let us now analyze the patterns as we traverse different plate lengths. Figures 3.1 and 3.2 (pages 23 and 24) show the patterns of the two-element microstrip fed Yagi placed on a plate with an electrical length of $1.04\lambda_g$ (λ_g=9.4mm at 10GHz). Figure 3.2c shows the pattern at 12GHz in phi=0° plane which, according to Figure 3.1c, is located at the upper end of the frequency spectrum. The pattern suffers from much lower gain (4dB below peak level) and relatively high levels of cross-polarization; in phi=90° plane (shown in Fig. 3.2d) it is quite asymmetrical with peak gain shifted by about 40° to the left of $\theta = 0°$ axis. Figures 3.1a and 3.1b show nearly identical patterns at the center frequency. Figures 3.2a and 3.2b demonstrate that patterns change quite rapidly at the lower end of the frequency spectrum. Slight increase in plate length makes the pattern lose its uniformity, as illustrated in Figure 3.3 (page 25). Figures 3.4 and 3.5 (pages 26 and 27) show the patterns of the two-element microstrip fed Yagi placed on a plate with an electrical length of $1.91\lambda_g$. A comparison of figures 3.2 and 3.5 shows a definite improvement in pattern bandwidth both at the lower as well as the upper end of the frequency spectrum. The pattern at the upper part of the spectrum still suffers from relatively low gain (which is now 3.5dB below peak level) and high cross-polarization (figures 3.5c and 3.5d). We also observe that the pattern in phi=90° plane (Fig. 3.5d) remains symmetrical with peak gain now shifted by about 35° to the left of $\theta = 0°$ axis. Patterns of the two-element microstrip fed Yagi placed on a plate with an electrical length of $3.2\lambda_g$ are presented in

figures 3.6 and 3.7 (pages 28 and 29). A comparison of figures 3.6 and 3.7 shows a further improvement in pattern bandwidth. The pattern at the upper part of the frequency spectrum now peaks within 2.5dB of the peak level at the center frequency (Fig. 3.7c); cross-polarization remains high. We observe that the pattern in phi=90° plane (Fig. 3.7d) gains symmetry with peak gain now shifted by about 25° to the left of $\theta = 0°$ axis. As we now increase the plate length to $4.15\lambda_g$ we observe that the pattern at the upper part of the frequency spectrum now peaks at peak level (figures 3.8 and 3.9 on pages 30 and 31); cross-polarization decreases (Fig. 3.9c). The pattern in phi=90° plane (Fig. 3.9d) becomes more symmetrical and its peak is no longer shifted. Further increases in length (figures 3.10 and 3.11 on pages 32 and 33) have minimal effect on pattern bandwidth.

Careful analysis of figures 3.13 and 3.14 (page 37) reveals beam's oscillatory nature. Beam tilt oscillates until it eventually settles for plates longer than $4\lambda_g$. Table 3.1 (page 34) illustrates that the values of return loss change quite dramatically for plates shorter than $4\lambda_g$ showing a direct relationship between the oscillation of the beam and return loss. They settle at around –16.5dB for longer plates. Furthermore, table 3.1 shows the value of operating frequency to be very sensitive to the changes in plate length in case of electrically short plates. It settles at around 10GHz for plates longer than $1.28\lambda_g$ and is no longer affected by increasing the plate length. Additionally, slight increase in plate length at shorter lengths has an effect of increasing the impedance bandwidth. Further length extensions have very little effect on impedance bandwidth.

Tables 3.2 through 3.6 (pages 34 and 35) as well as Fig. 3.15 (page 38) show a gradual decrease in the rate of decay of a higher order mode defined by the derivative of each of the curves in Fig. 3.15.

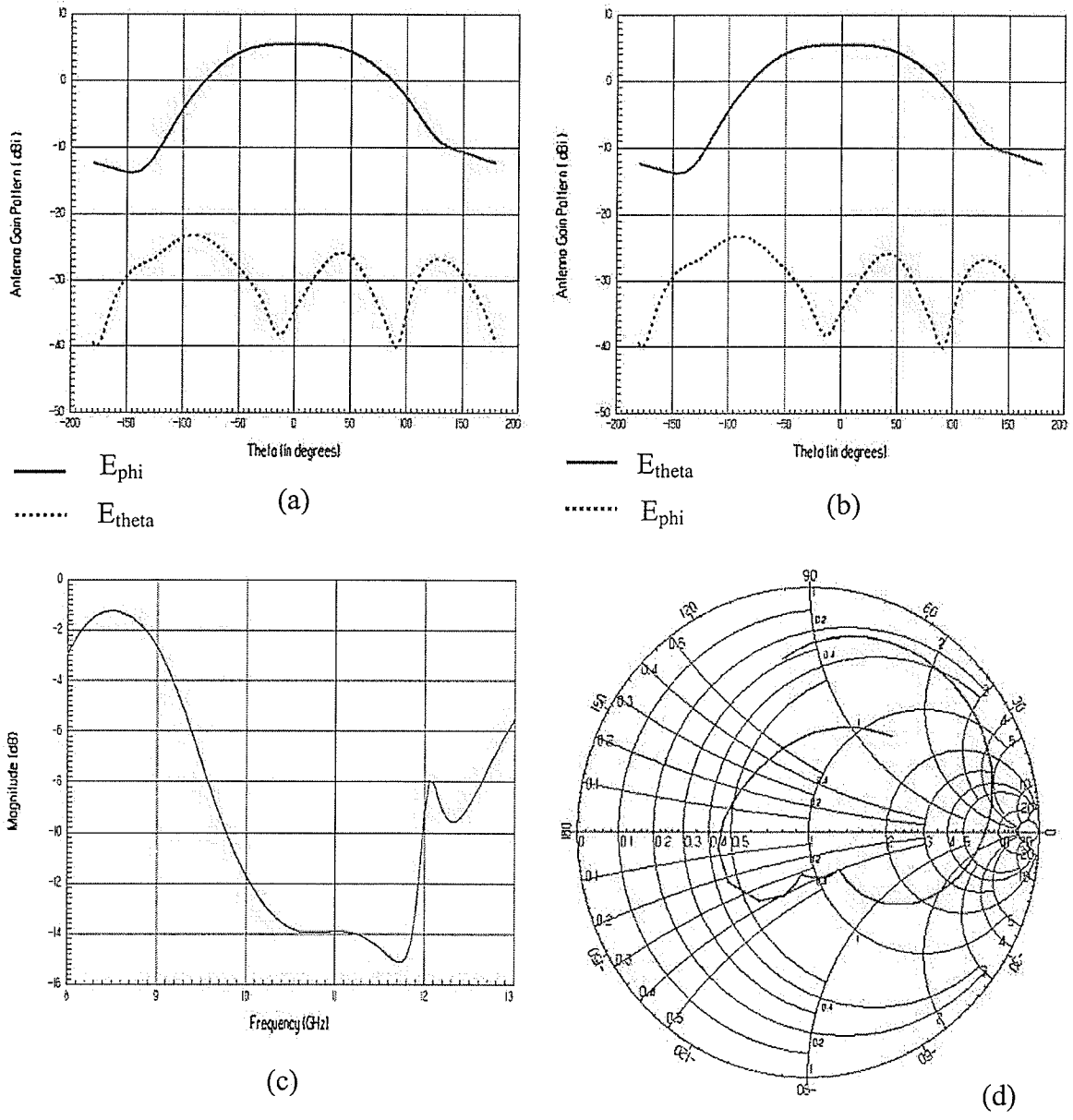

Figure 3.1. Antenna Gain Patterns and Return Loss at the center frequency of a Yagi on a plate with a dielectric constant of 10.2 and an electrical length of $1.04\lambda_g$, (a) radiation pattern at 10 GHz at phi=0, (b) radiation pattern at 10 GHz at phi=90, (c) linear plot of a return loss, (d) return loss on a smith chart.

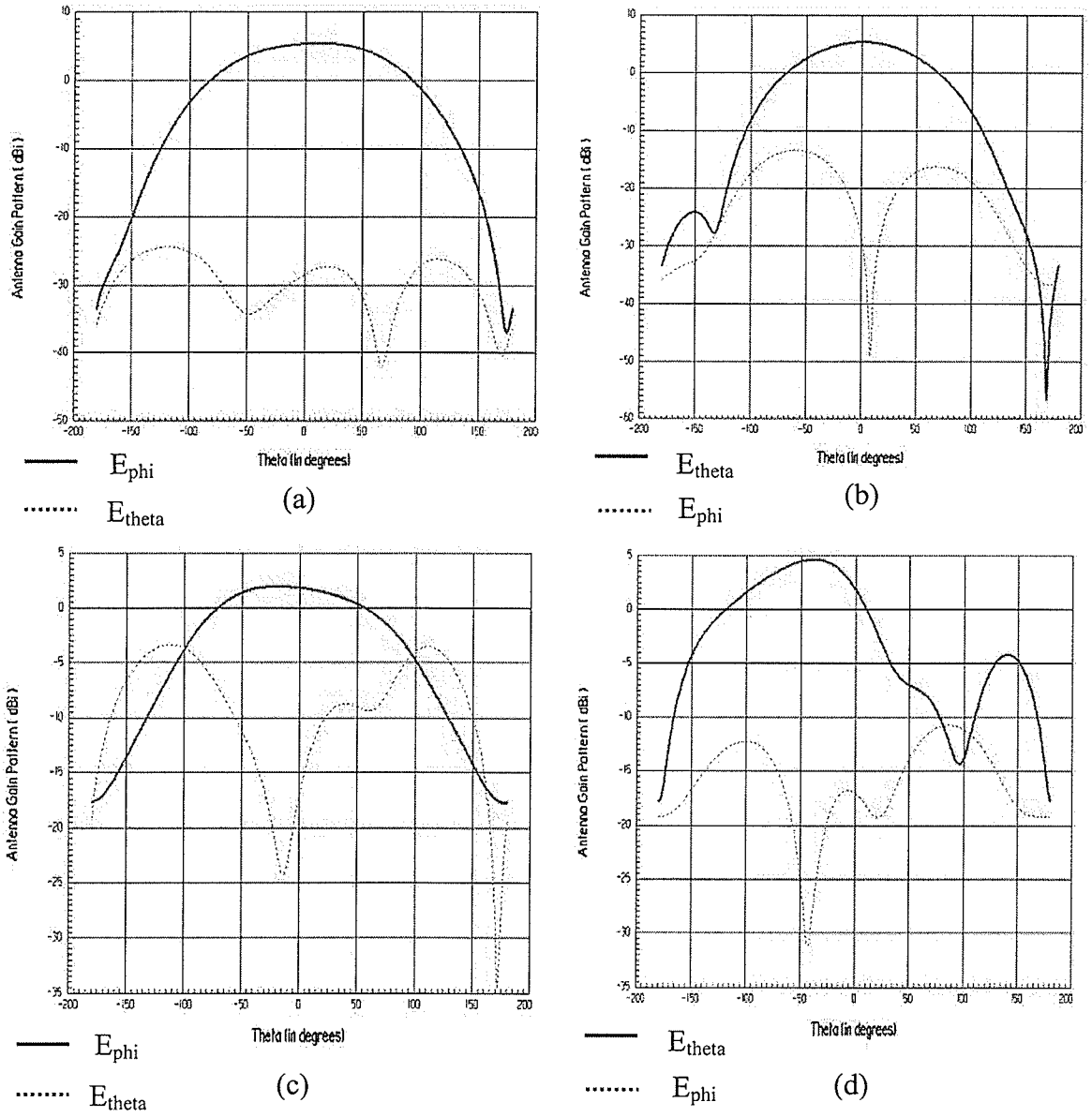

Figure 3.2. Antenna Gain Patterns within the impedance bandwidth of a Yagi on a plate with a dielectric constant of 10.2 and an electrical length of $1.04\lambda_g$, (a) radiation pattern at 9.8 GHz at phi=0, (b) radiation pattern at 9.8 GHz at phi=90, (c) radiation pattern at 12 GHz at phi=0, (d) radiation pattern at 12 GHz at phi=90.

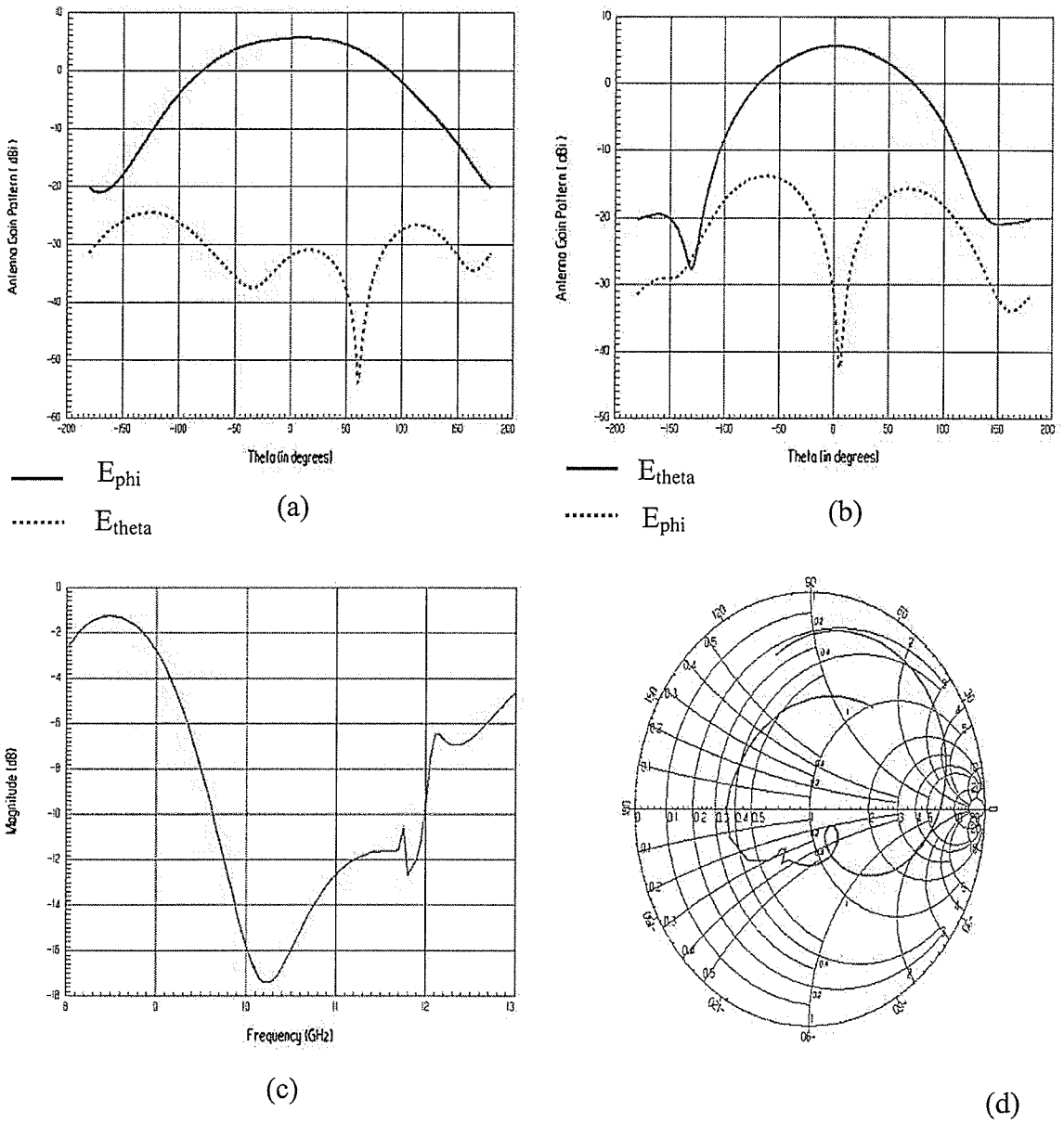

Figure 3.3. Antenna Gain Patterns and Return Loss at the center frequency of a Yagi on a plate with a dielectric constant of 10.2 and an electrical length of $1.28\lambda_g$, (a) radiation pattern at 10 GHz at phi=0, (b) radiation pattern at 10 GHz at phi=90, (c) linear plot of a return loss, (d) return loss on a smith chart.

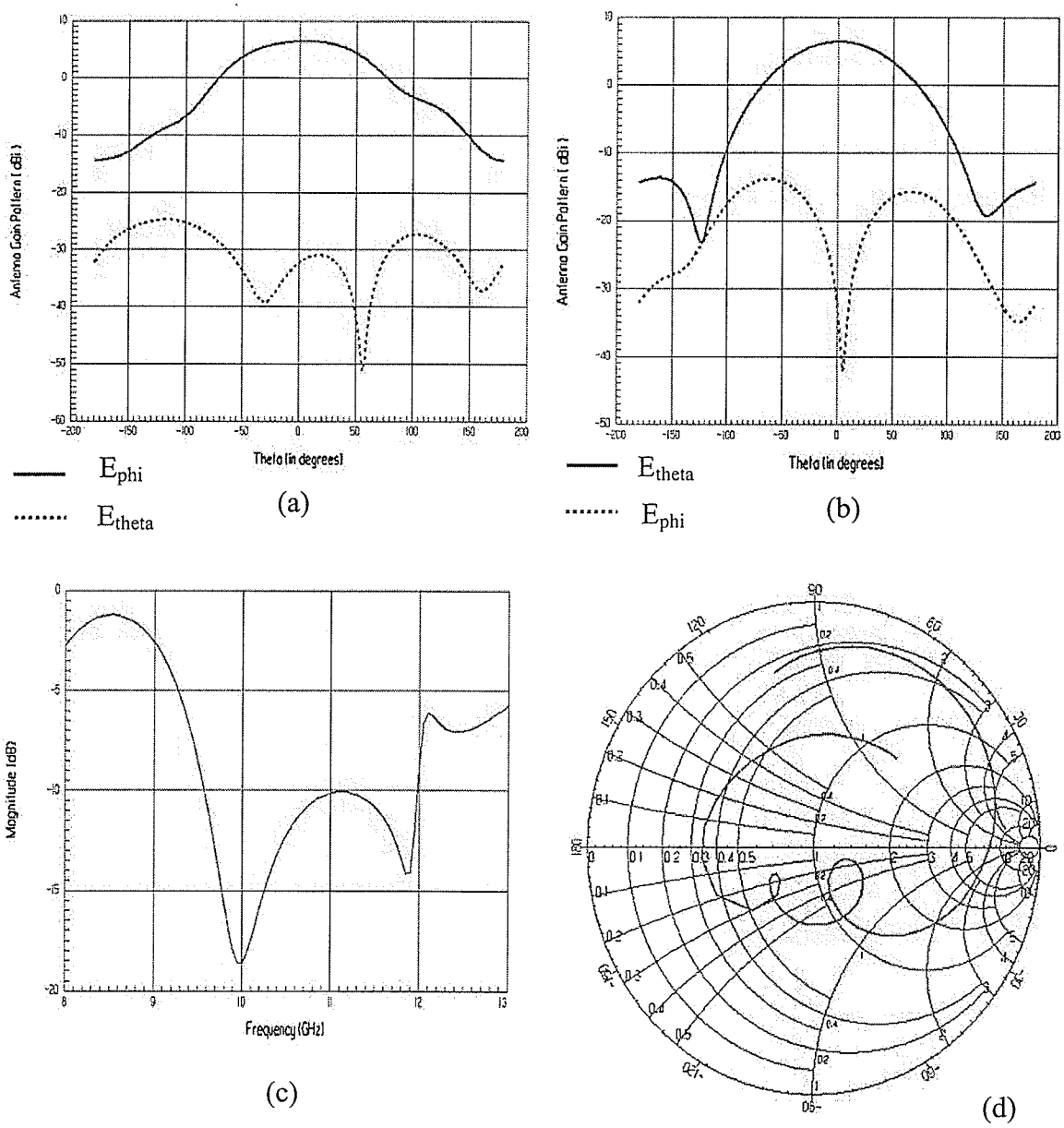

Figure 3.4. Antenna Gain Patterns and Return Loss at the center frequency of a Yagi on a plate with a dielectric constant of 10.2 and an electrical length of $1.91\lambda_g$, (a) radiation pattern at 10 GHz at phi=0, (b) radiation pattern at 10 GHz at phi=90, (c) linear plot of a return loss, (d) return loss on a smith chart.

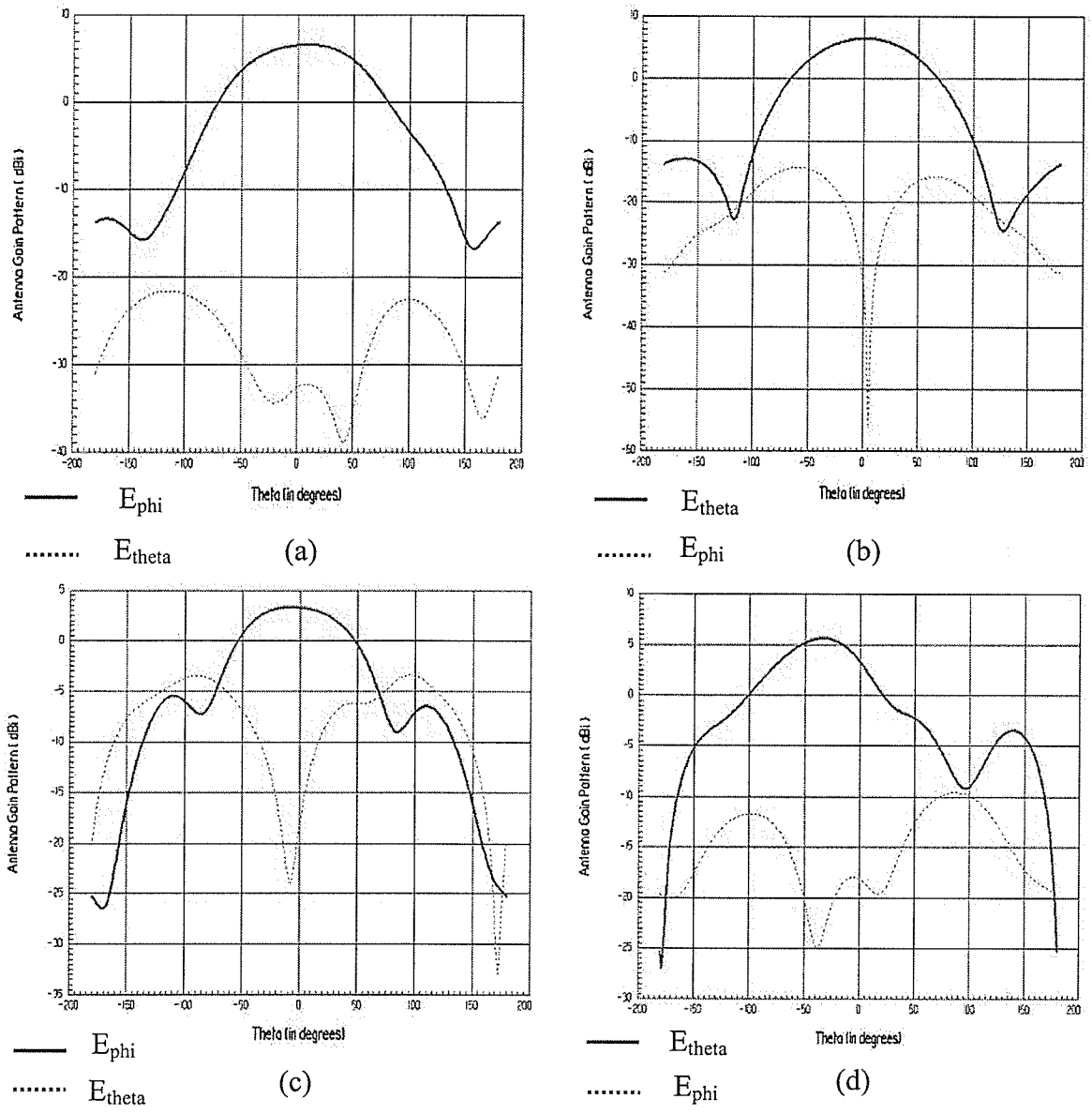

Figure 3.5. Antenna Gain Patterns within the impedance bandwidth of a Yagi on a plate with a dielectric constant of 10.2 and an electrical length of $1.91\lambda_g$, (a) radiation pattern at 9.5 GHz at phi=0, (b) radiation pattern at 9.5 GHz at phi=90, (c) radiation pattern at 12 GHz at phi=0, (d) radiation pattern at 12 GHz at phi=90.

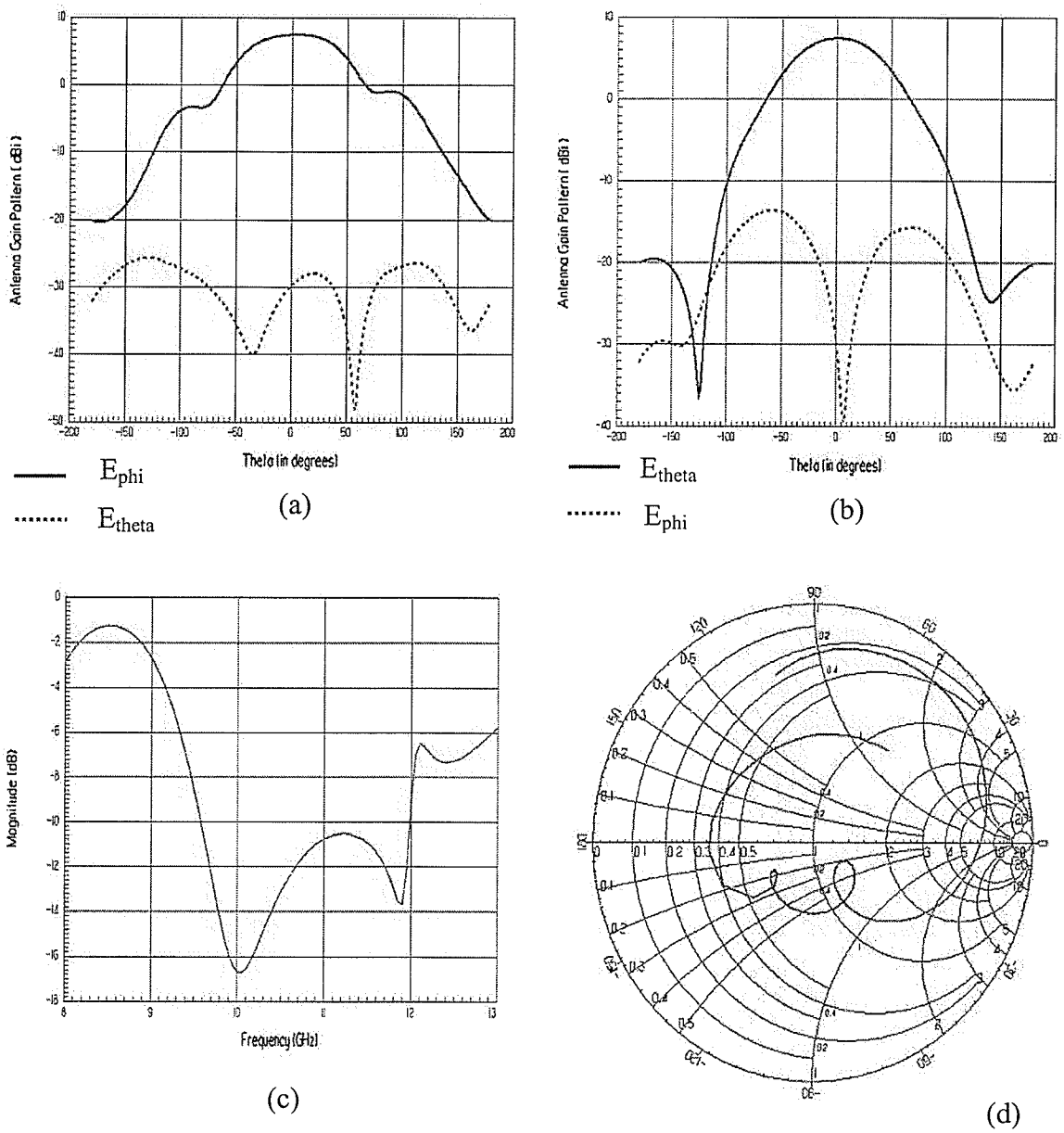

Figure 3.6. Antenna Gain Patterns and Return Loss at the center frequency of a Yagi on a plate with a dielectric constant of 10.2 and an electrical length of $3.2\lambda_g$, (a) radiation pattern at 10 GHz at phi=0, (b) radiation pattern at 10 GHz at phi=90, (c) linear plot of a return loss, (d) return loss on a smith chart.

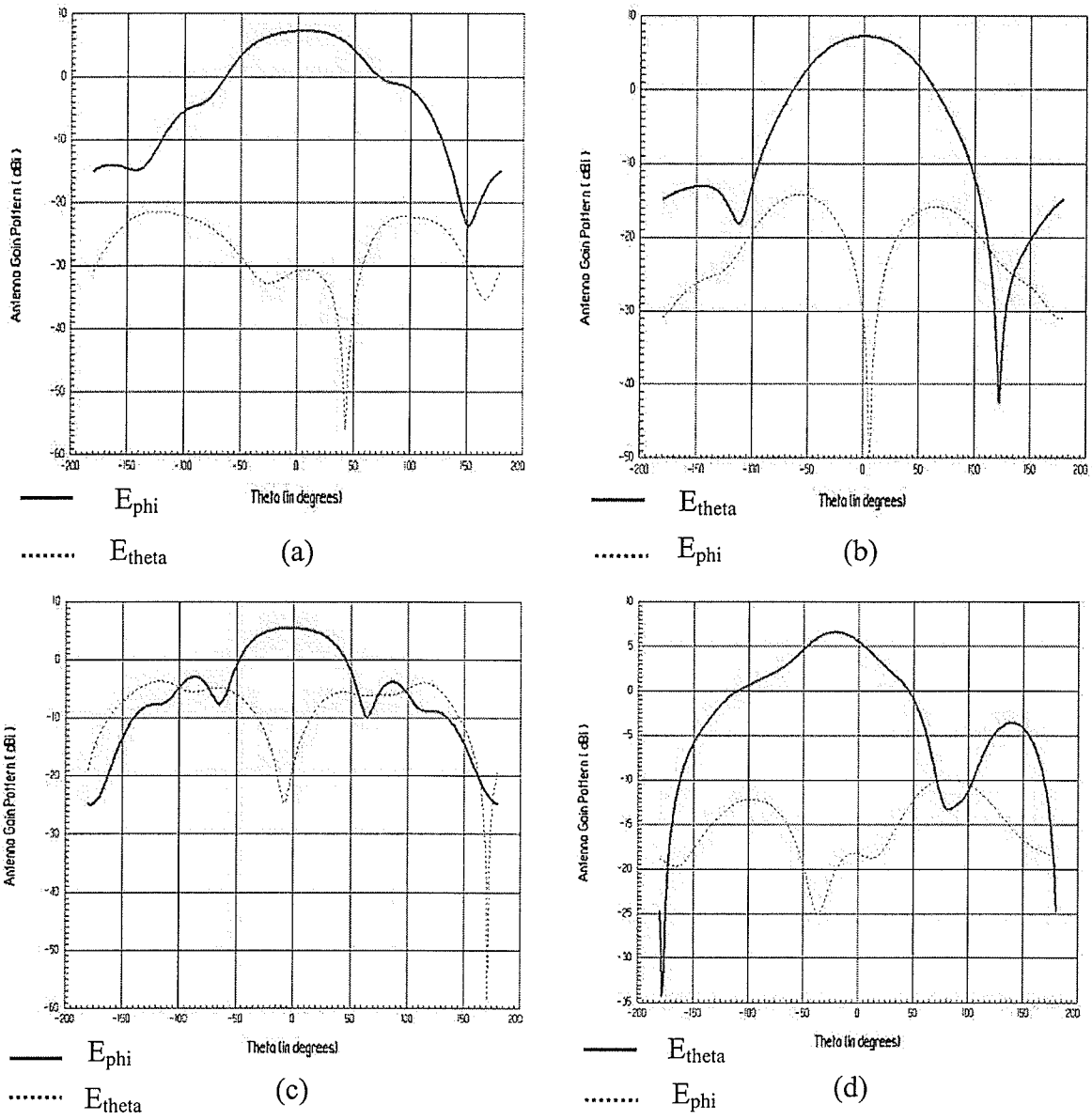

Figure 3.7. Antenna Gain Patterns within the impedance bandwidth of a Yagi on a plate with a dielectric constant of 10.2 and an electrical length of $3.2\lambda_g$, (a) radiation pattern at 9.5 GHz at phi=0, (b) radiation pattern at 9.5 GHz at phi=90, (c) radiation pattern at 12 GHz at phi=0, (d) radiation pattern at 12 GHz at phi=90.

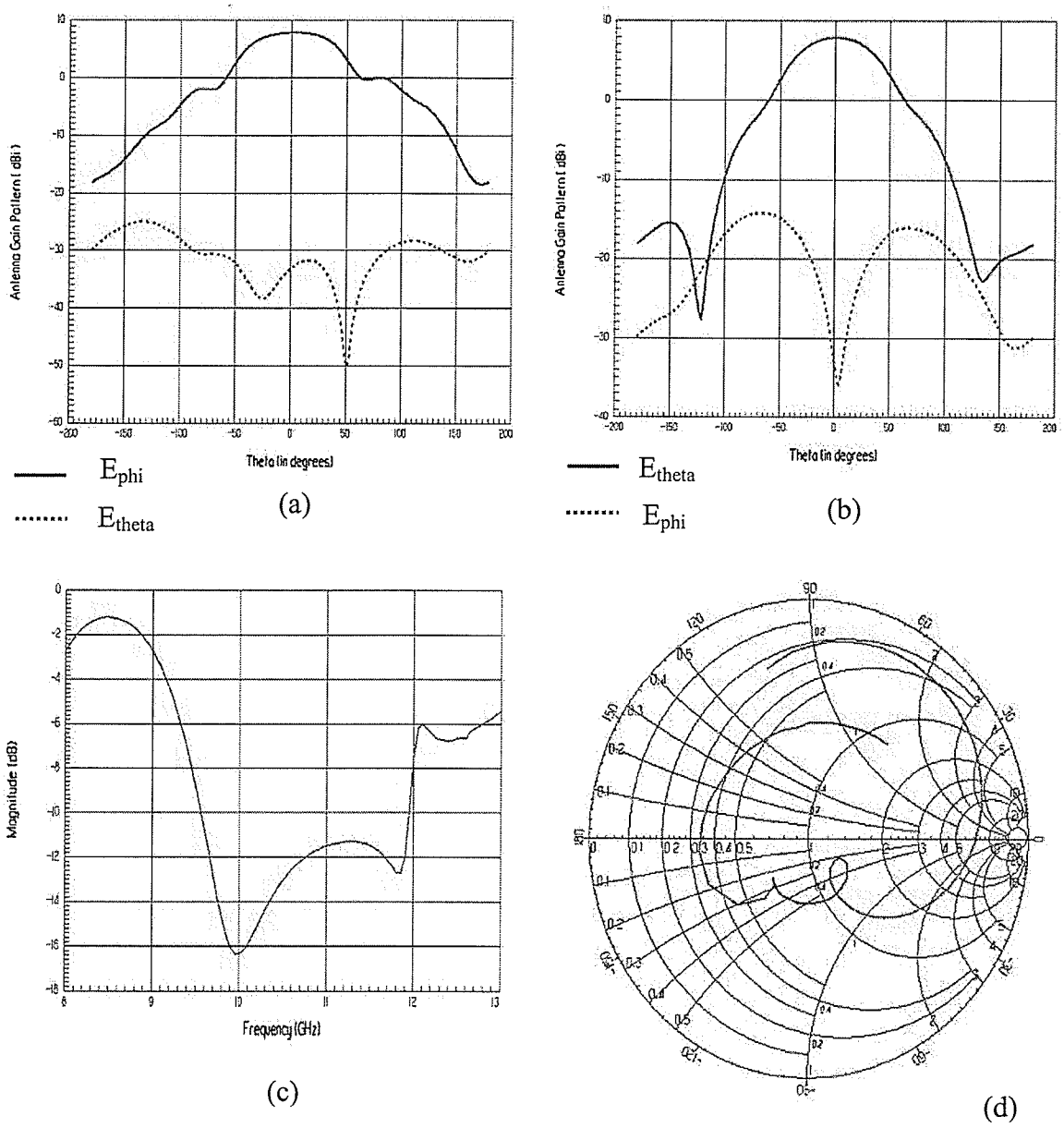

Figure 3.8. Antenna Gain Patterns and Return Loss at the center frequency of a Yagi on a plate with a dielectric constant of 10.2 and an electrical length of $4.15\lambda_g$, (a) radiation pattern at 10 GHz at phi=0, (b) radiation pattern at 10 GHz at phi=90, (c) linear plot of a return loss, (d) return loss on a smith chart.

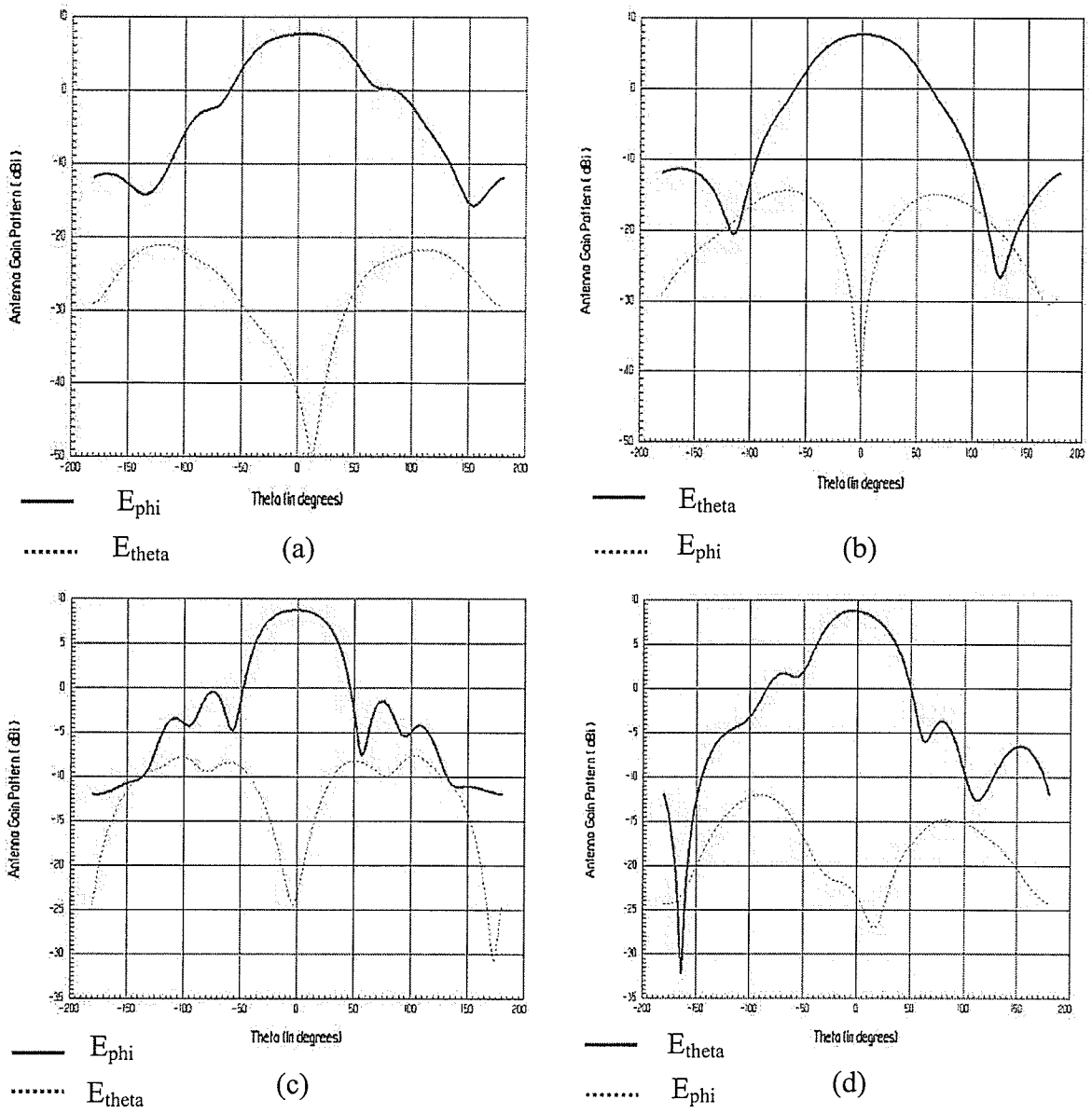

Figure 3.9. Antenna Gain Patterns within the impedance bandwidth of a Yagi on a plate with a dielectric constant of 10.2 and an electrical length of $4.15\lambda_g$, (a) radiation pattern at 9.5 GHz at phi=0, (b) radiation pattern at 9.5 GHz at phi=90, (c) radiation pattern at 11.9 GHz at phi=0, (d) radiation pattern at 11.9 GHz at phi=90.

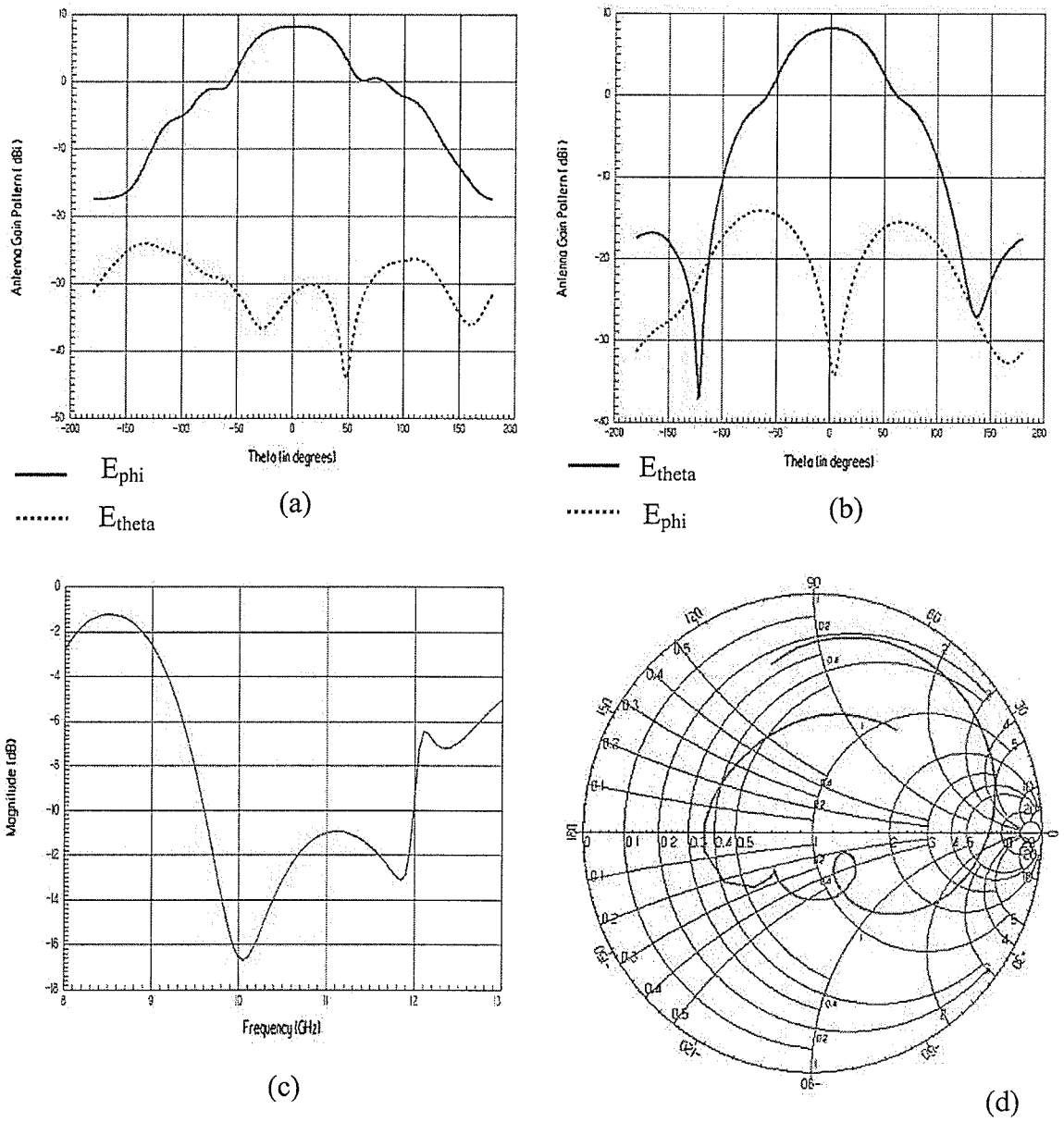

Figure 3.10. Antenna Gain Patterns and Return Loss at the center frequency of a Yagi on a plate with a dielectric constant of 10.2 and an electrical length of $5\lambda_g$, (a) radiation pattern at 10 GHz at phi=0, (b) radiation pattern at 10 GHz at phi=90, (c) linear plot of a return loss, (d) return loss on a smith chart.

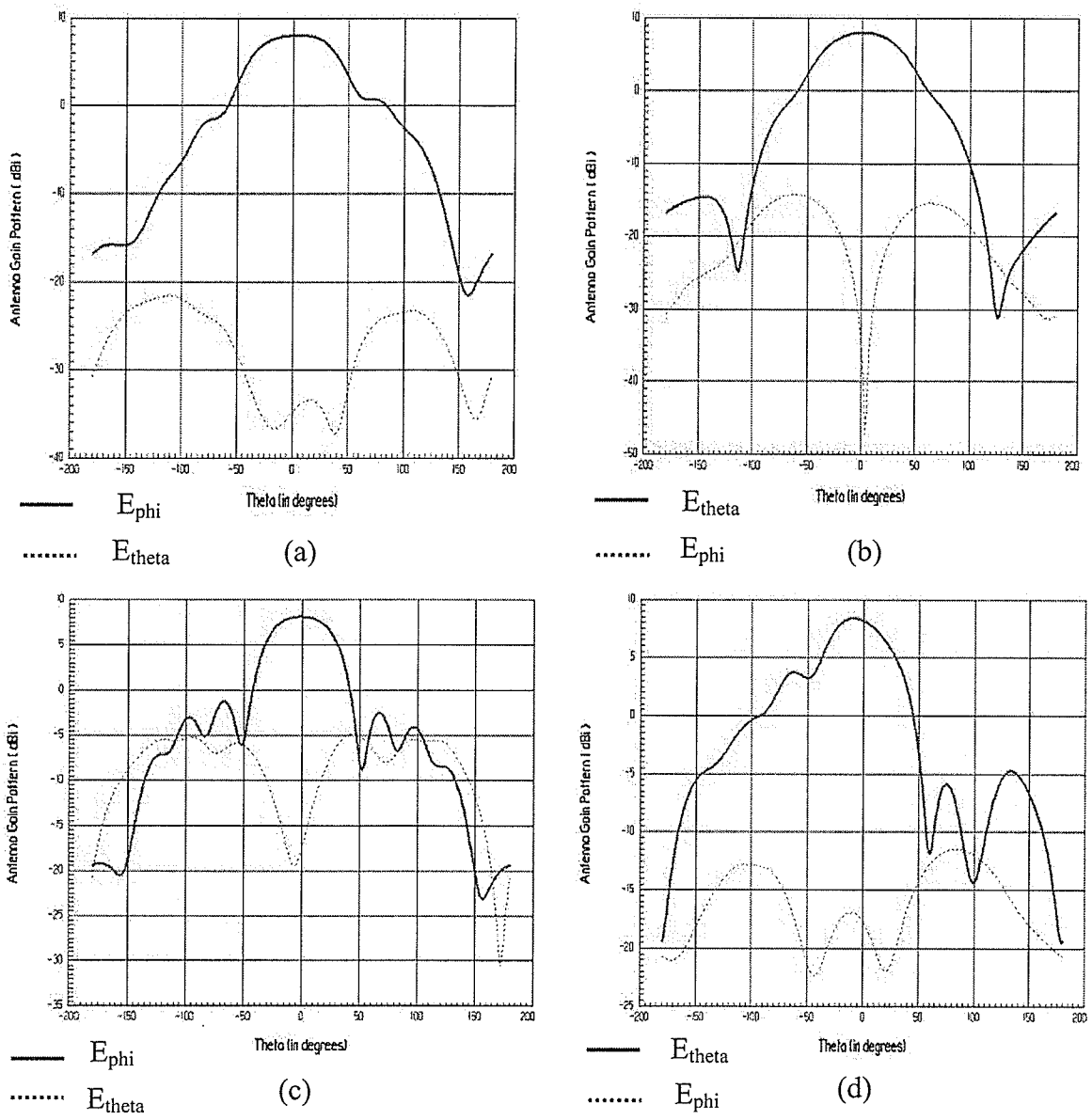

Figure 3.11. Antenna Gain Patterns within the pattern bandwidth of a Yagi on a plate with a dielectric constant of 10.2 and an electrical length of $5\lambda_g$, (a) radiation pattern at 9.6 GHz at phi=0, (b) radiation pattern at 9.6 GHz at phi=90, (c) radiation pattern at 12 GHz at phi=0, (d) radiation pattern at 12 GHz at phi=90.

Table 3.1: Return Loss and Pattern data for the two element microstrip-fed Yagi (ε_r=10.2, a=0.06755λ_g, b=1.3163λ_g, freq = 10GHz), λ_g=9.4mm, Figures 3.13 and 3.14.

L_p (λ_g)	Return Loss (dB)	Frequency (GHz)	Impedance Bandwidth (%)	Beam Tilt (θ) E-plane (phi=90)	Beam Tilt (θ) H-plane (phi=0)
1.04	-15.2	11.7	18.8	1	2
1.28	-17.4	10.2	23.53	1	10
1.6	-19.5	10	24	1	7
1.91	-18.5	10	24	1	6
2.23	-16.2	9.9	23.23	1	9
2.55	-15	10	25	1	5
2.87	-15	10.1	23.76	-1	7
3.2	-16.7	10	24	1	4
3.51	-16.1	10	23	0	6
3.83	-16.2	10	24	0	3
4.15	-16.3	10	23	1	4
4.5	-16.4	10.1	23.76	1	4
5	-16.6	10.1	23.76	0	3

Table 3.2: Percentage of modal power for the two element microstrip-fed Yagi (ε_r=10.2, a=0.06755λ_g, b=1.3163λ_g, freq = 10GHz) with plate length equal to 1.04λ_g, λ_g=9.4mm, Figure 3.15.

L_{cut} (λ_g)	P(TM_{01}) (%)	P(TM_{02}) (%)
0.53	88.33246	11.66754
1.04	99.20126	0.7987432

Table 3.3: Percentage of modal power for the two element microstrip-fed Yagi (ε_r=10.2, a=0.06755λ_g, b=1.3163λ_g, freq = 10GHz) with plate length equal to 1.91λ_g, λ_g=9.4mm, Figure 3.15.

L_{cut} (λ_g)	P(TM_{01}) (%)	P(TM_{02}) (%)
0.53	87.16214	12.83786
1.06	94.02689	5.973105
1.6	96.619	3.380991
1.91	99.99184	8.1649264E-03

Table 3.4: Percentage of modal power for the two element microstrip-fed Yagi (ε_r=10.2, a=0.06755λ_g, b=1.3163λ_g, freq = 10GHz) with plate length equal to 3.2λ_g, λ_g=9.4mm, Figure 3.15.

L_{cut} (λ_g)	P(TM_{01}) (%)	P(TM_{02}) (%)
0.53	87.05219	12.94782
1.06	93.40872	6.591282
1.6	96.71976	3.280232
2.13	96.74722	3.252778
2.66	98.68217	1.317827
3.2	99.87254	0.1274621

Table 3.5: Percentage of modal power for the two element microstrip-fed Yagi (ε_r=10.2, a=0.06755λ_g, b=1.3163λ_g, freq = 10GHz) with plate length equal to 4.15λ_g, λ_g=9.4mm, Figure 3.15.

L_{cut} (λ_g)	P(TM_{01}) (%)	P(TM_{02}) (%)
0.53	86.99046	13.00954
1.06	93.93998	6.060029
1.6	96.70313	3.296859
2.13	96.3993	3.600699
2.66	98.86436	1.135632
3.19	98.86585	1.13415
3.72	98.98135	1.01865
4.15	99.85483	0.1451688

Table 3.6: Percentage of modal power for the two element microstrip-fed Yagi (ε_r=10.2, a=0.06755λ_g, b=1.3163λ_g, freq = 10GHz) with plate length equal to 5λ_g, λ_g=9.4mm, Figure 3.15.

L_{cut} (λ_g)	P(TM_{01}) (%)	P(TM_{02}) (%)
0.53	87.09356	12.90644
1.06	93.86046	6.139538
1.6	96.61644	3.383556
2.13	96.80763	3.192369
2.66	98.91123	1.088768
3.19	98.95171	1.048285
3.72	98.69261	1.30739
4.25	98.54781	1.45218
4.78	99.4794	0.5205986
5	99.95287	4.7129985E-02

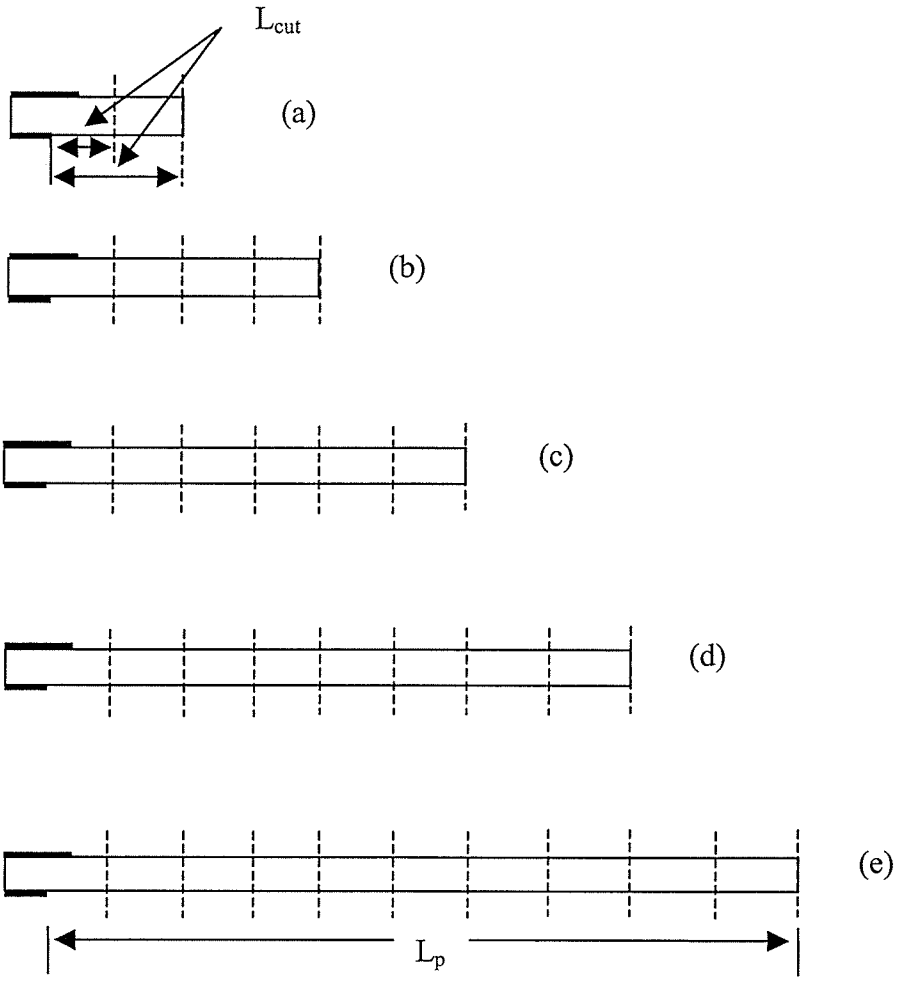

Figure 3.12. Side View of a two-element microstrip-fed Yagi antenna without parasitics and a dielectric constant of 10.2, (a) $L_p = 1.04\lambda_g$, (b) $L_p = 1.91\lambda_g$, (c) $L_p = 3.2\lambda_g$, (d) $L_p = 4.15\lambda_g$, (e) $L_p = 5\lambda_g$.

Figure 3.12 above shows the side view of 5 two-element microstrip-fed Yagi antennas of varying lengths as outlined in Tables 3.2 through 3.6. The two-element Yagi refers here to the microstrip fed dipole/ground plane configuration as shown in each of the figures (bold lines indicating copper lines). The dotted lines indicate the cut planes as indicated by each of the rows in Tables 3.2 through 3.6.

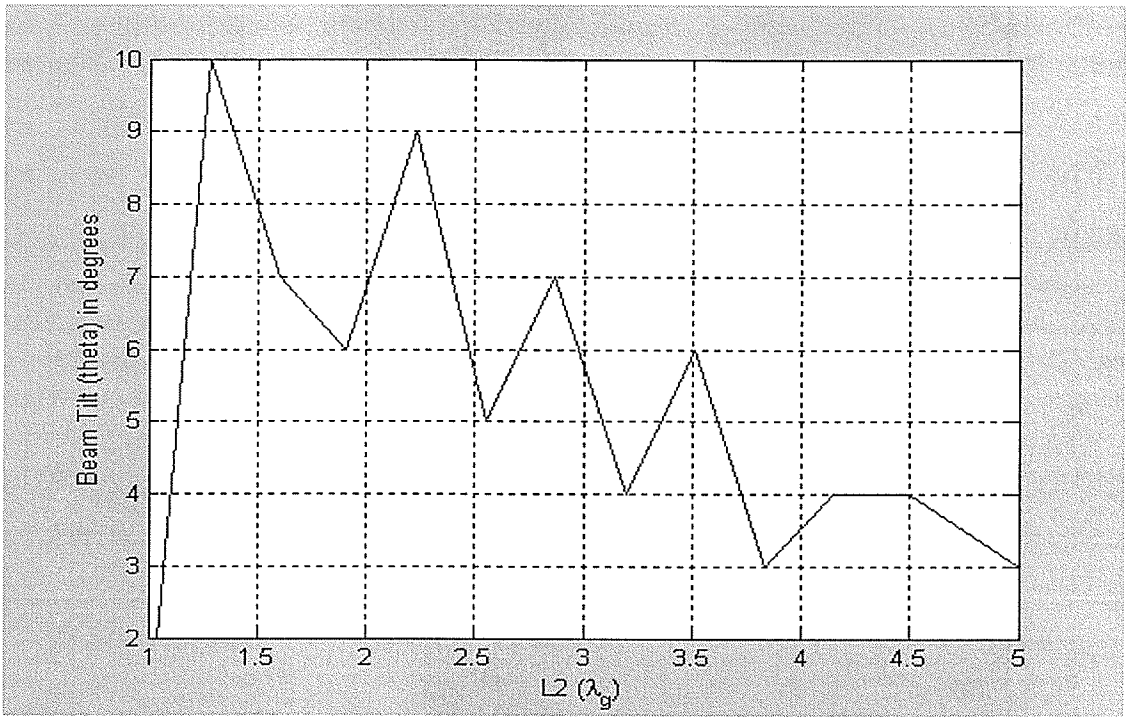

Figure 3.13. Beam tilt vs. plate length for the two element microstrip-fed Yagi (ε_r=10.2, a=0.06755λ_g, b=1.3163λ_g, freq = 10GHz) for plates of varying lengths.

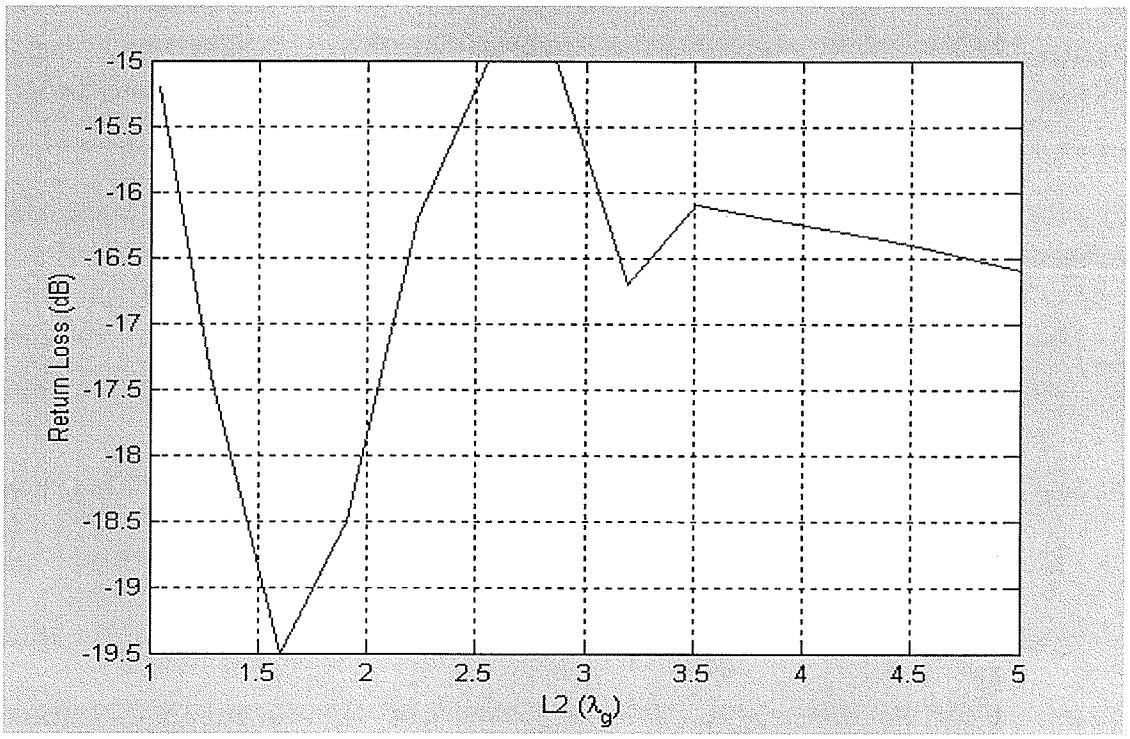

Figure 3.14. Return Loss vs. plate length for the two element microstrip-fed Yagi (ε_r=10.2, a=0.06755λ_g, b=1.3163λ_g, freq = 10GHz) for plates of varying lengths.

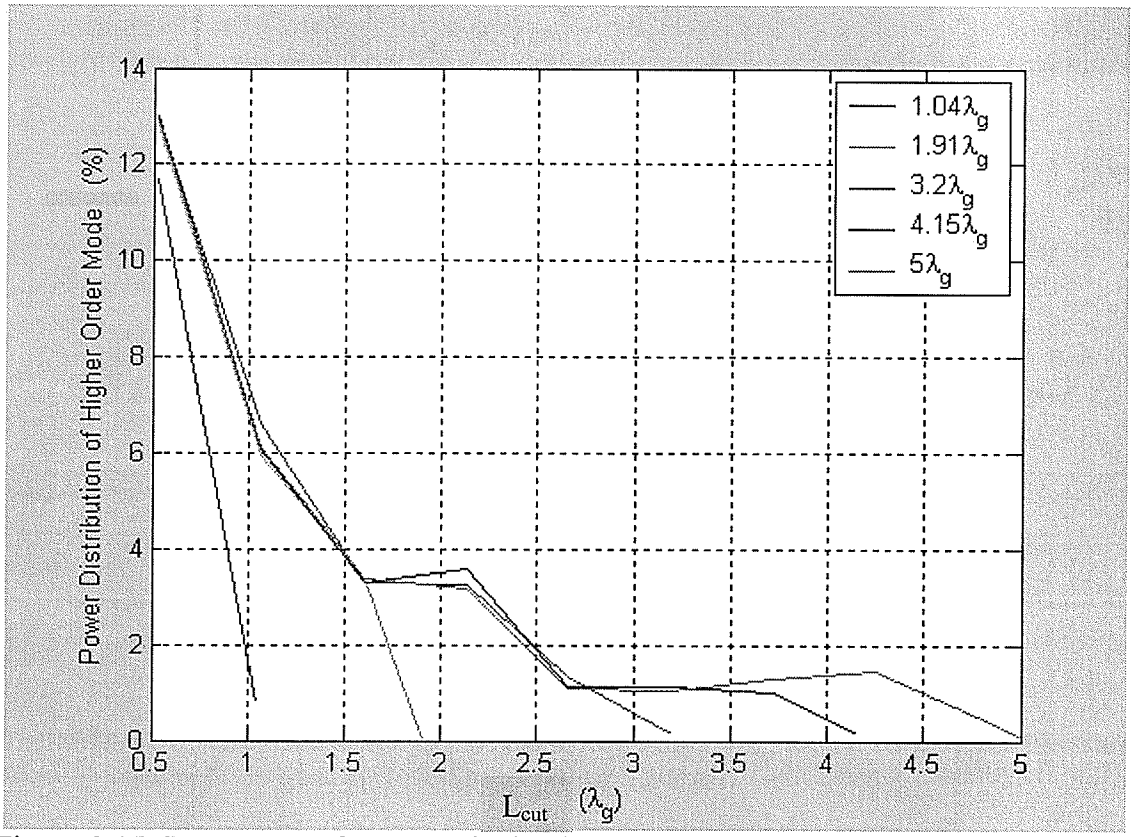

Figure 3.15. Percentage of Power Distribution of Higher Order (TM_{02}) Mode vs. Plate Length along the two element microstrip-fed Yagi with five different plate lengths (ε_r=10.2, a=0.06755λ_g, b=1.3163λ_g, freq = 10GHz).

Let us now correlate the pattern performance with Fig. 3.15. Looking at the curves in Fig. 3.15 we observe that the decay of a higher order mode is much more rapid for shorter plates, as we observe the curves for plate lengths of $1.04\lambda_g$ and $1.91\lambda_g$. The rate of decay for those lengths is greater than for longer plates. In that range we observe a more rapid improvement in pattern bandwidth. Curves for plate lengths of $3.2\lambda_g$, $4.15\lambda_g$ and $5\lambda_g$ are nearly the same, proving that further improvements in pattern bandwidth and directivity are minimal due to the similar pattern of power distribution of higher order modes.

3.3: Microstrip-Fed Yagis Placed On Low Permittivity Plates

Let us analyze the radiation patterns as we did before for the high permittivity plates. Figures 3.16 and 3.17 (pages 40 and 41) show the patterns of the two element microstrip-fed Yagi placed on a plate with an electrical length of λ_g. Figures 3.17c and 3.17d show patterns at 11.3GHz in phi=0° and phi=90° planes, respectively. It is clear that the patterns suffer from distortion and asymmetry at that frequency. Their directivity values are also reduced and peak 2dB below the directivity values at center frequency. Figures 3.18 and 3.19 (pages 42 and 43) show the patterns of the two element microstrip-fed Yagi placed on a plate with an electrical length of $2\lambda_g$. Figures 3.19c and 3.19d show that the patterns continue to suffer from distortion and asymmetry at the upper side of the impedance bandwidth. Their directivity values are now 3dB below the directivity values at center frequency. Figures 3.20 and 3.21 (pages 44 and 45) demonstrate continued distortion and asymmetry of the patterns at the upper side of the impedance bandwidth. Their directivity values are now 1.5dB below the directivity values at center frequency. Figures 3.18a and 3.20a show ripples in the patterns that can be attributed to the rate of decay of a higher order mode which is high for low permittivity plates. The ripples subside as we continue to increase the length of the plate due to reduced rate of decay of a higher order mode.

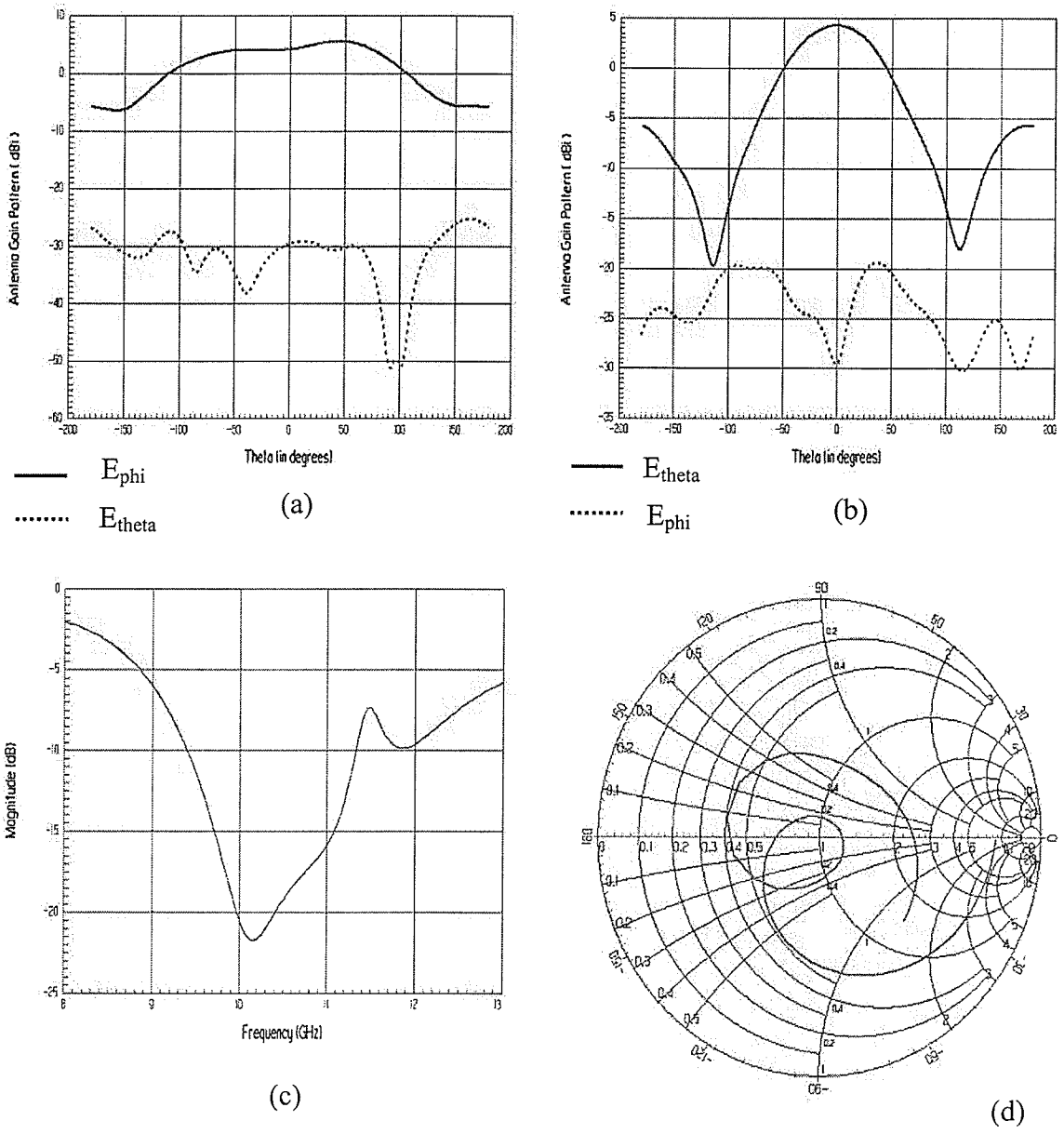

Figure 3.16. Antenna Gain Patterns and Return Loss at a center frequency of a Yagi on a plate with a dielectric constant of 2.5 and an electrical length of λ_g, (a) radiation pattern at 10 GHz at phi=0, (b) radiation pattern at 10 GHz at phi=90, (c) linear plot of a return loss, (d) return loss on a smith chart.

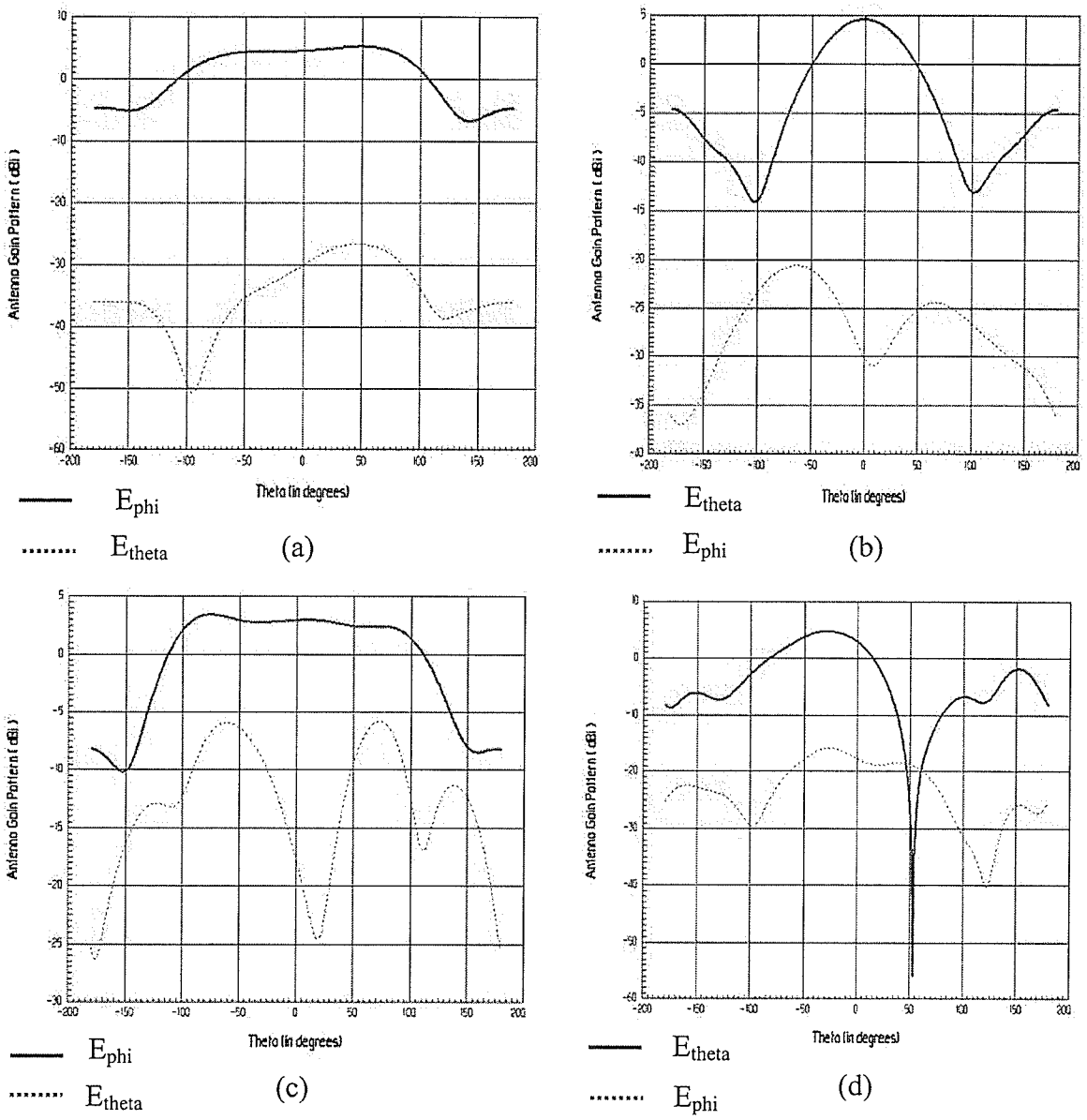

Figure 3.17. Antenna Gain Patterns within the impedance bandwidth of a Yagi on a plate with a dielectric constant of 2.5 and an electrical length of λ_g, (a) radiation pattern at 9.3 GHz at phi=0, (b) radiation pattern at 9.3 GHz at phi=90, (c) radiation pattern at 11.3 GHz at phi=0, (d) radiation pattern at 11.3 GHz at phi=90.

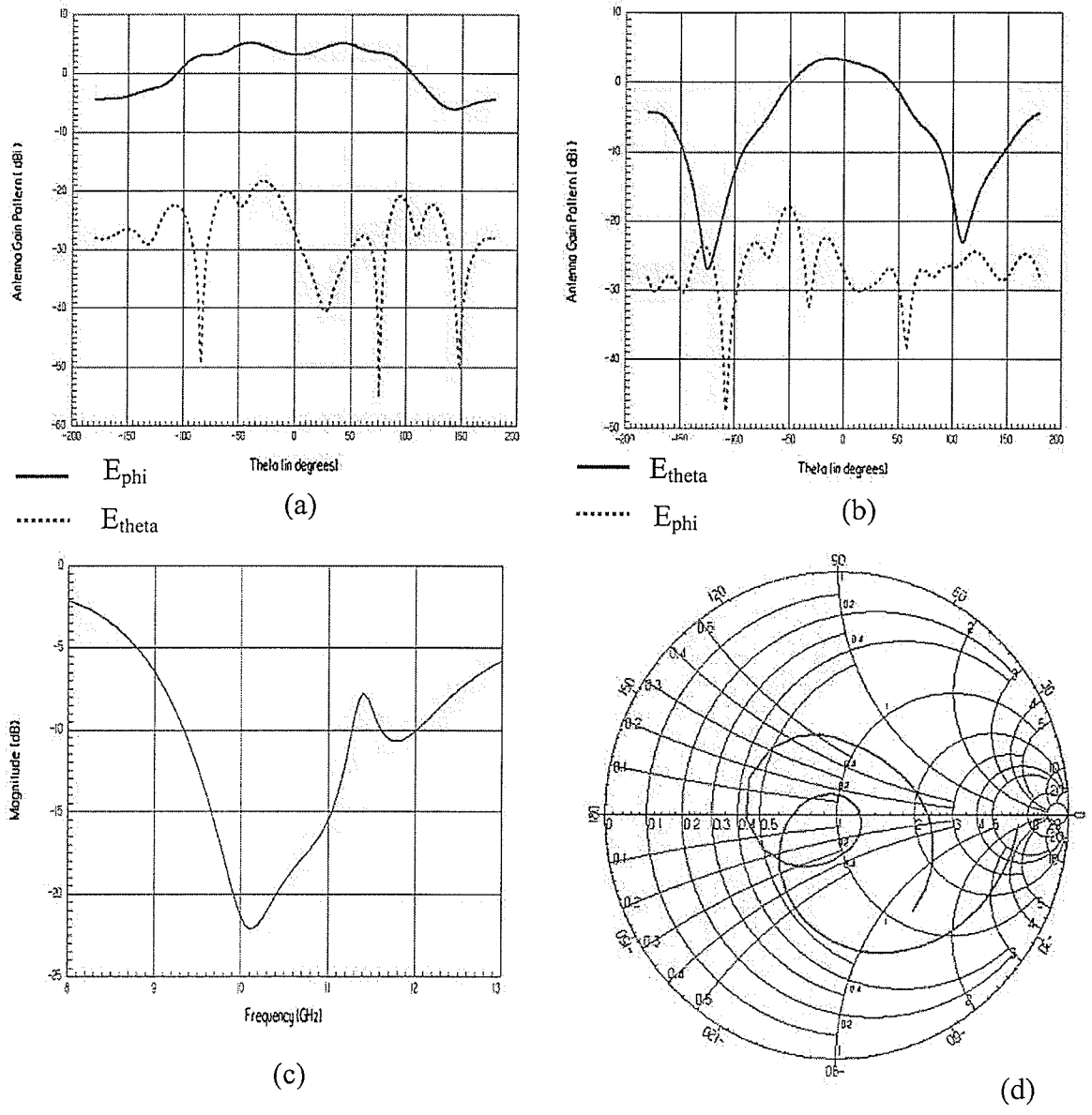

Figure 3.18. Antenna Gain Patterns and Return Loss at the center frequency of a Yagi on a plate with a dielectric constant of 2.5 and an electrical length of $2\lambda_g$, (a) radiation pattern at 10 GHz at phi=0, (b) radiation pattern at 10 GHz at phi=90, (c) linear plot of a return loss, (d) return loss on a smith chart.

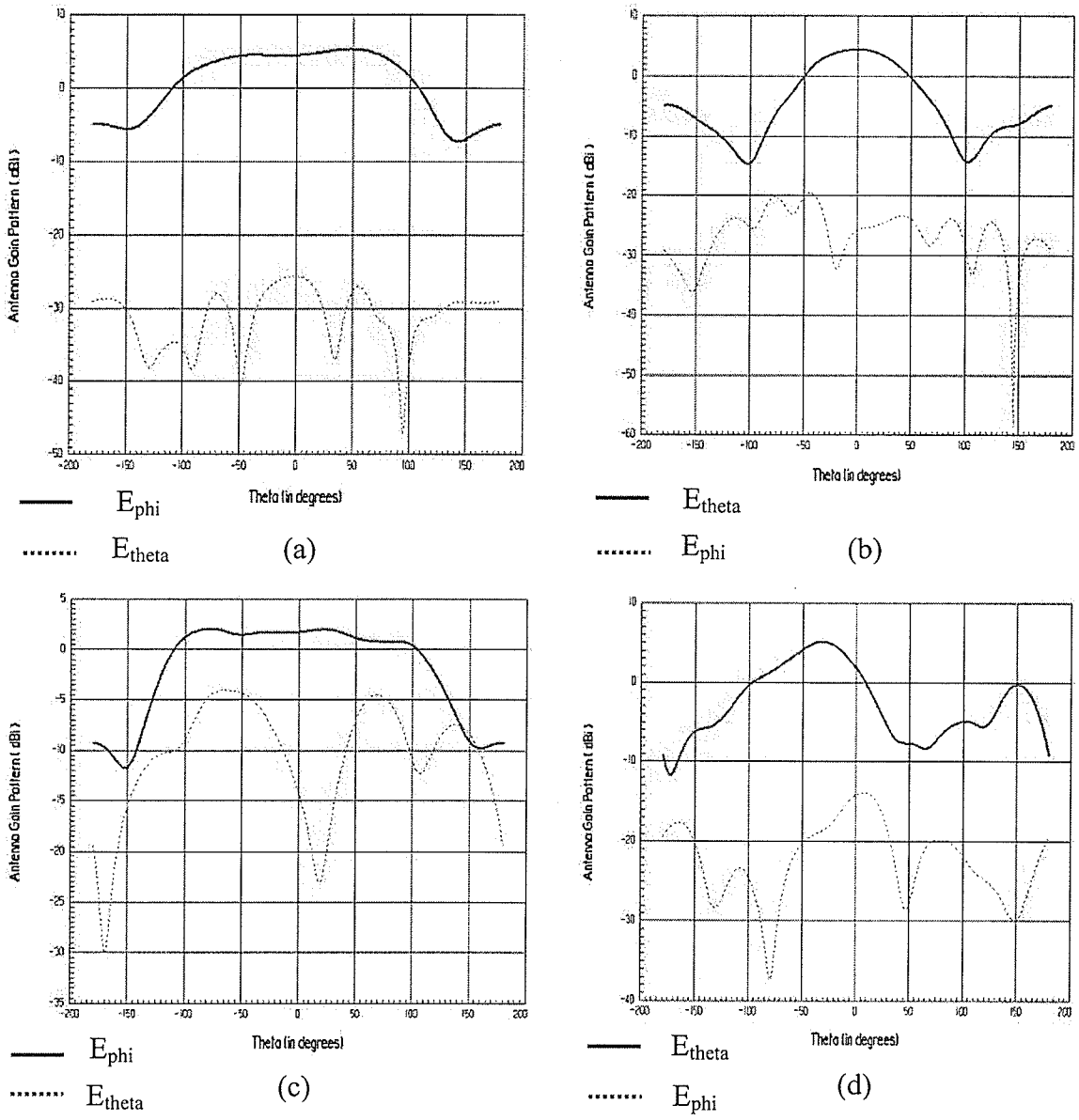

Figure 3.19. Antenna Gain Patterns within the impedance bandwidth of a Yagi on a plate with a dielectric constant of 2.5 and an electrical length of $2\lambda_g$, (a) radiation pattern at 9.3 GHz at phi=0, (b) radiation pattern at 9.3 GHz at phi=90, (c) radiation pattern at 11.3 GHz at phi=0, (d) radiation pattern at 11.3 GHz at phi=90.

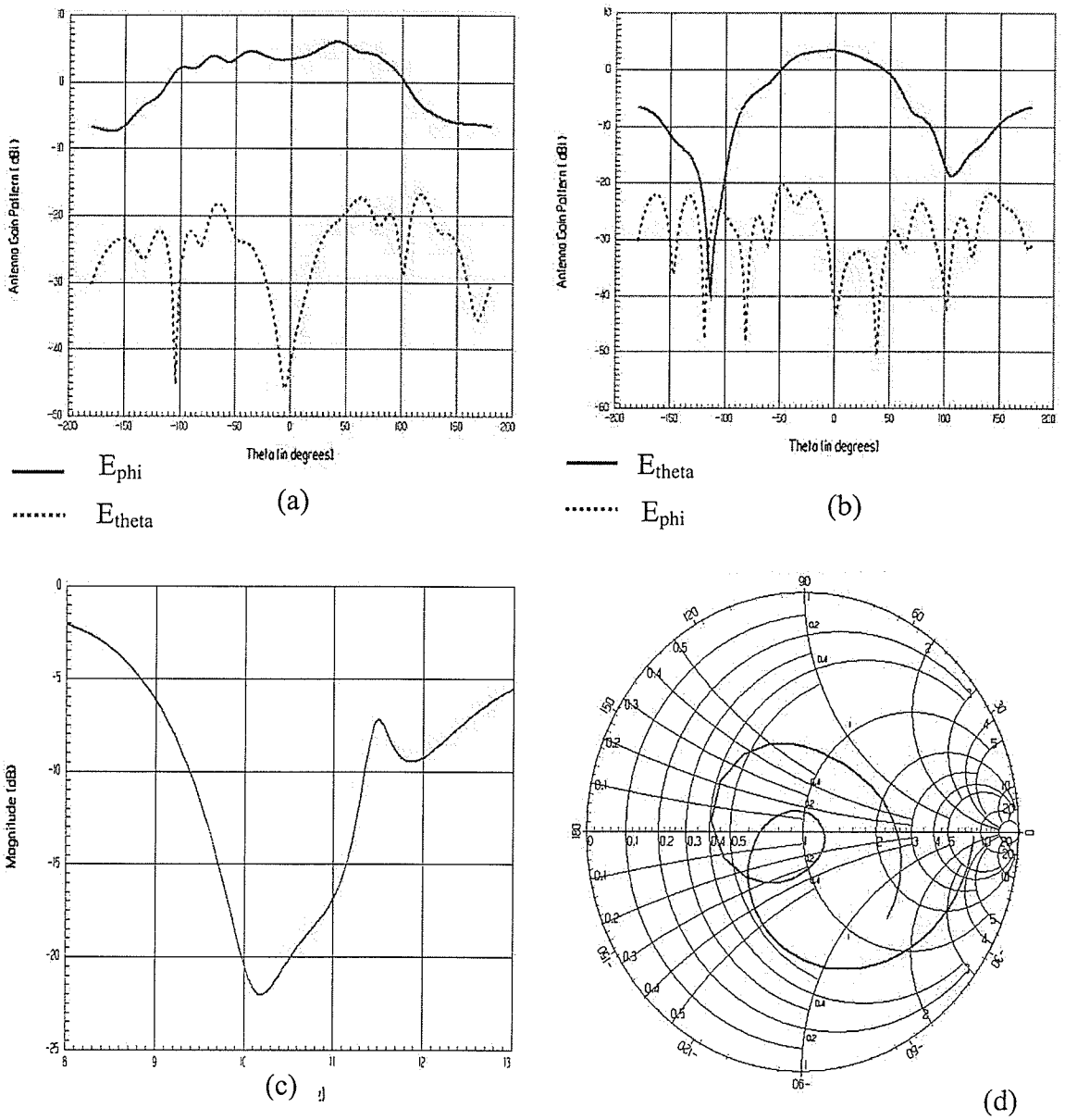

Figure 3.20. Antenna Gain Patterns and Return Loss at the center frequency of a Yagi on a plate with a dielectric constant of 2.5 and an electrical length of $3\lambda_g$, (a) radiation pattern at 10 GHz at phi=0, (b) radiation pattern at 10 GHz at phi=90, (c) linear plot of a return loss, (d) return loss on a smith chart.

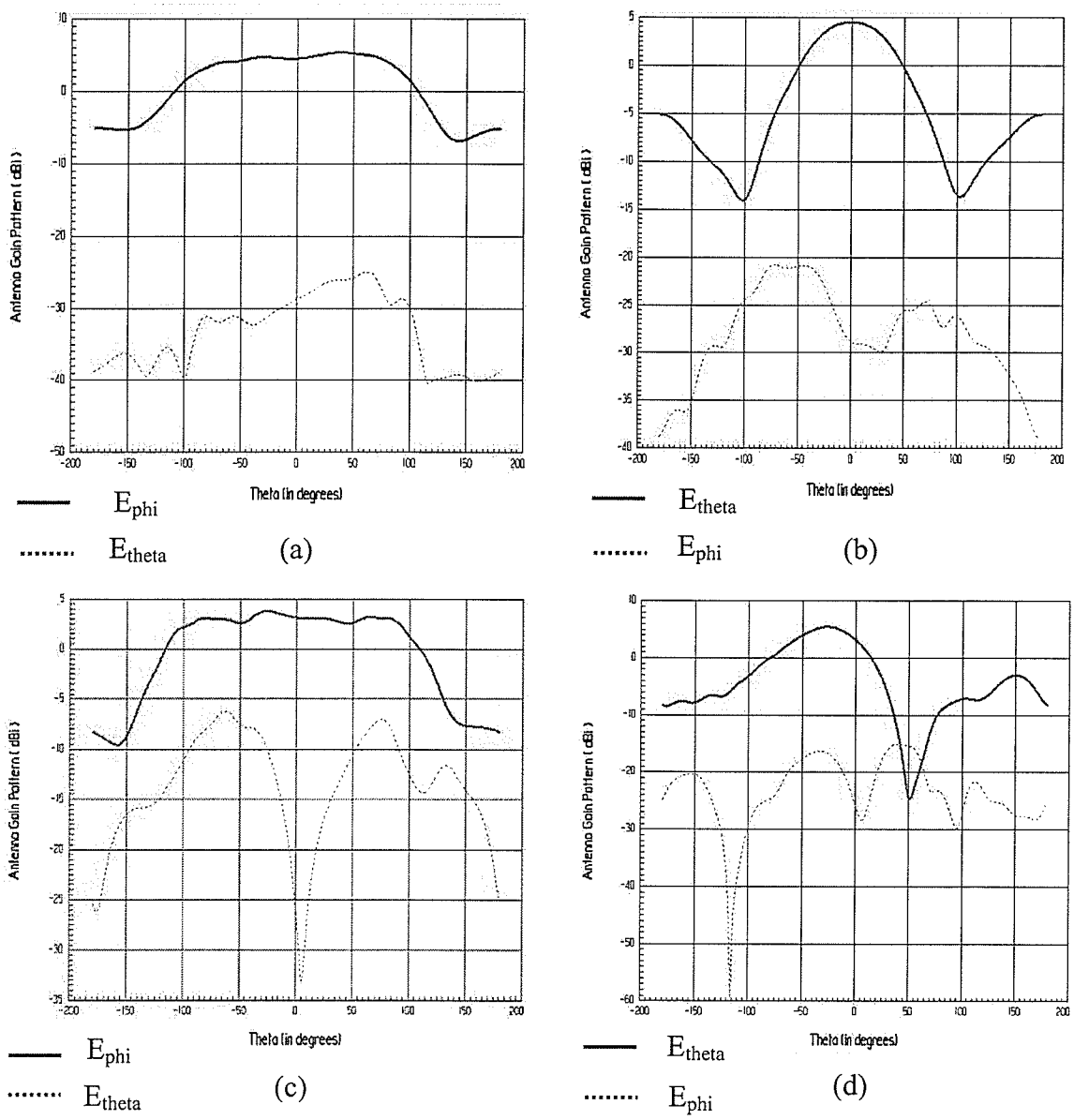

Figure 3.21. Antenna Gain Patterns within the impedance bandwidth of a Yagi on a plate with a dielectric constant of 2.5 and an electrical length of $3\lambda_g$, (a) radiation pattern at 9.4 GHz at phi=0, (b) radiation pattern at 9.4 GHz at phi=90, (c) radiation pattern at 11.3 GHz at phi=0, (d) radiation pattern at 11.3 GHz at phi=90.

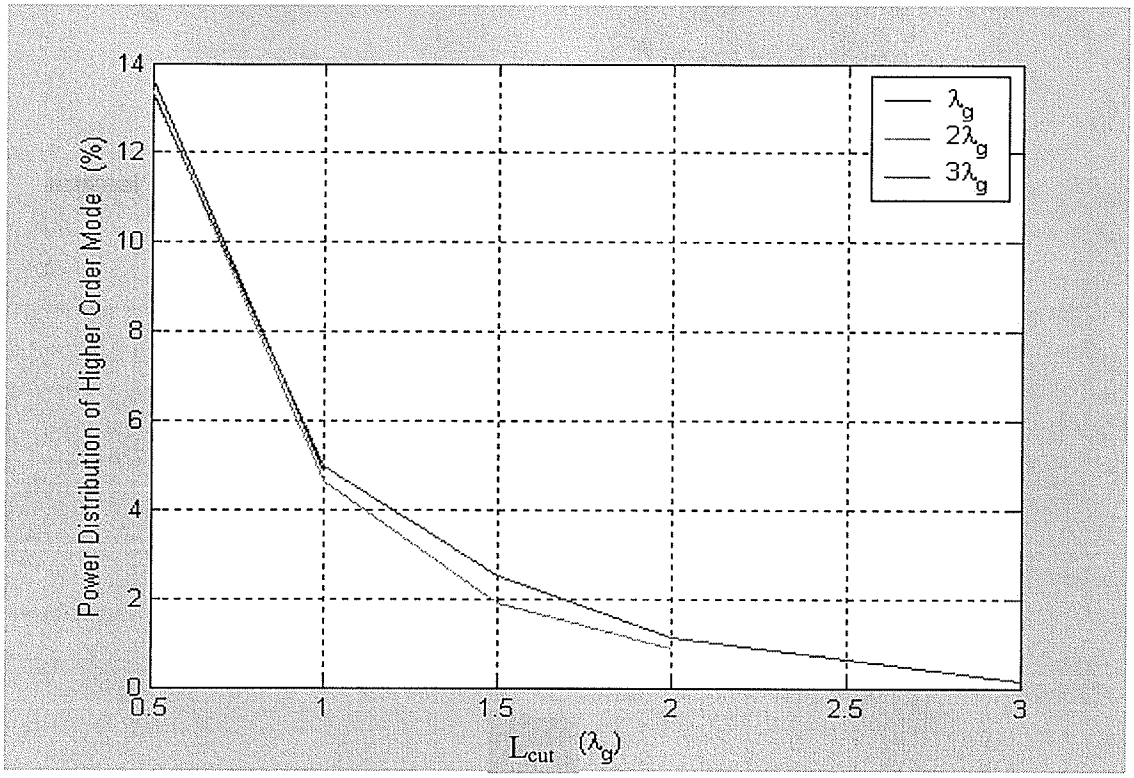

Figure 3.22. Percentage of Power Distribution of Higher Order (TM_{02}) Mode vs. Plate Length for the two element microstrip-fed Yagi with three different plate lengths (ε_r=2.5, a=0.013λ_g, b=1.316λ_g, freq = 10GHz).

We will now correlate the pattern performance with Fig. 3.22. We observe that the rate of decay of a higher order mode is high for shorter plates causing a beam split for plate lengths of $2\lambda_g$ (as shown in Fig. 3.18a). Beyond that point, the rate of decay decreases (as demonstrated in Fig. 3.22) showing that further improvements in pattern bandwidth and directivity are minimal due to the similar pattern of power distribution of higher order modes.

Table 3.7 below illustrates that increasing plate length has little or no effect on return loss. The value of operating frequency is likewise insensitive to the changes in

plate length. Impedance bandwidth also remains relatively unaffected. The pattern also undergoes a slight beam split at guide length equal to $2\lambda_g$.

Table 3.7: Return Loss and Pattern data for the two element microstrip-fed Yagi (ε_r=2.5, a=0.013λ_g, b=1.316λ_g, freq = 10GHz), λ_g=19mm.

L_p (λ_g)	Return Loss (dB)	Frequency (GHz)	Impedance Bandwidth (%)	Beam Tilt (θ) E-plane (phi=90)	Beam Tilt (θ) H-plane (phi=0)
1	-24	10.1	18.27	-2	45
2	-22	10.1	19.8	-13	-41/42
3	-22	10.2	18.63	-4	41

Tables 3.8 through 3.10 on page 48 as well as Fig. 3.22 show a gradual increase in the rate of decay of a higher order mode defined by the derivative of each of the curves in Fig. 3.22. We observe a rapid decay of a higher order mode and a divergence of the gap between the curves.

Comparing patterns of plates with high and low dielectric constant one can see (comparing figure 3.15 with 3.22) that the rate of decay of a higher order mode is much higher for the plates with lower dielectric constant than for plates with higher dielectric constant. Moreover, the rate of decay of a higher order mode in plates with higher dielectric constant appears to settle much faster than the rate of decay of a higher order mode in plates with lower dielectric constant. The settling effect for higher dielectric constants appears to have a more positive effect on pattern bandwidth and directivity. The unsettling effect that takes place with lower dielectric constants appears to have a

Table 3.8: Percentage of modal power for the two element microstrip-fed Yagi (ε_r=2.5, a=0.013λ_g, b=1.316λ_g, freq = 10GHz) with plate length equal to λ_g, λ_g=19mm, Figure 3.22.

L_{cut} (λ_g)	P(TM_{01}) (%)	P(TM_{02}) (%)
0.5	86.39599	13.60401
1.0	95.16393	4.83606

Table 3.9: Percentage of modal power for the two element microstrip-fed Yagi (ε_r=2.5, a=0.013λ_g, b=1.316λ_g, freq = 10GHz) with plate length equal to 2λ_g, λ_g=19mm, Figure 3.22.

L_{cut} (λ_g)	P(TM_{01}) (%)	P(TM_{02}) (%)
0.5	86.64708	13.35292
1.0	95.3476	4.652401
1.5	98.11578	1.884226
2.0	99.11272	0.8872728

Table 3.10: Percentage of modal power for the two element microstrip-fed Yagi (ε_r=2.5, a=0.013λ_g, b=1.316λ_g, freq = 10GHz) with plate length equal to 3λ_g, λ_g=19mm, Figure 3.22.

L_{cut} (λ_g)	P(TM_{01}) (%)	P(TM_{02}) (%)
0.5	86.72874	13.27126
1.0	95.0302	4.969796
1.5	97.47977	2.520233
2.0	98.89195	1.108049
2.5	99.34639	0.6536108
3.0	99.83862	0.1613863

detrimental effect on pattern bandwidth and directivity. In fact, increasing plate length does not make the antenna any more directive.

3.4: Effects of Parasitics On High Permittivity Yagis

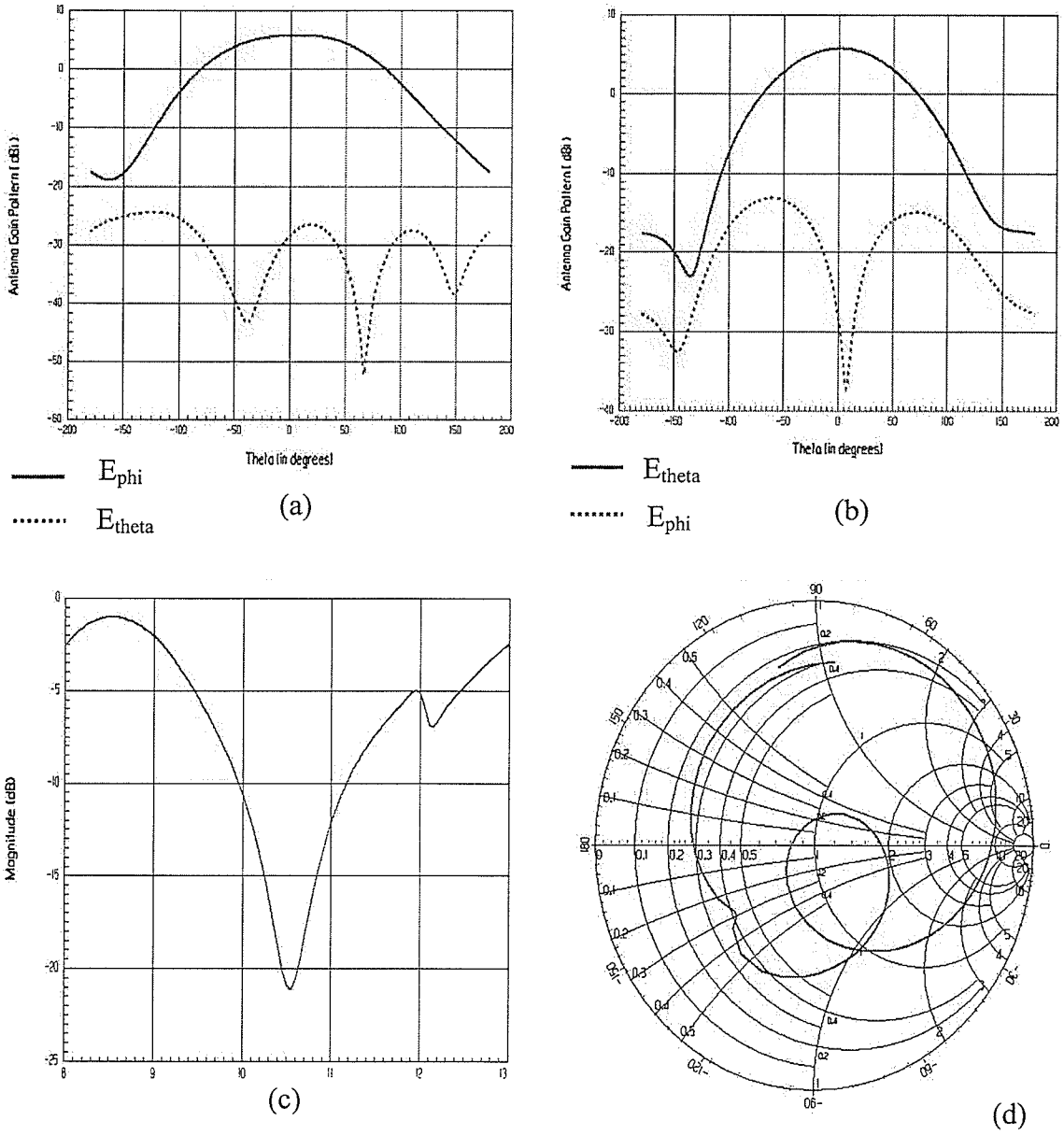

Figure 3.23. Antenna Gain Patterns and Return Loss at the center frequency of a Yagi on a plate with a dielectric constant of 10.2 and an electrical length of $1.04\lambda_g$ with one director, (a) radiation pattern at 10 GHz at phi=0, (b) radiation pattern at 10 GHz at phi=90, (c) linear plot of a return loss, (d) return loss on a smith chart.

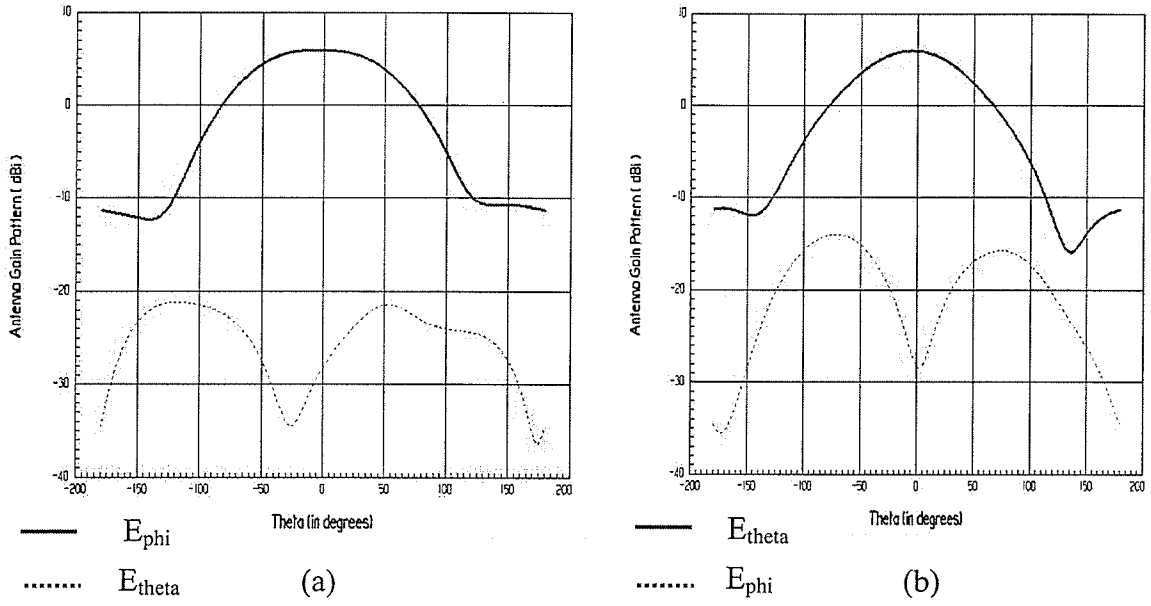

Figure 3.24. Antenna Gain Patterns at the upper side of the frequency range of a Yagi on a plate with a dielectric constant of 10.2 and an electrical length of $1.04\lambda_g$ with one director, (a) radiation pattern at 11.2 GHz at phi=0, (b) radiation pattern at 11.2 GHz at phi=90.

Examination of the patterns in figures 3.23 and 3.24 shows a good pattern bandwidth performance with one director and the plate length of $1.04\lambda_g$. As we extend the plate length to $1.91\lambda_g$ and place three more directors (with a total of four) we notice side lobe formation at center frequency; the side lobes become more pronounced at the upper side of the frequency spectrum. The antenna continues to exhibit good pattern bandwidth performance in the basic frequency range. In addition, directivity values are 1dB higher at the upper side of the frequency range than at the lower but at the expense of higher side lobes (1dB higher at the upper side of the frequency range than at the lower). Figure 3.25c (page 51) also shows a second resonance condition occurring at the frequency of 12.5 GHz. The patterns continue to show good directivity with relatively low cross-polarization although the basic shape of the pattern is now changed (figure 3.26 on page 52). We therefore come to the conclusion that the second resonance

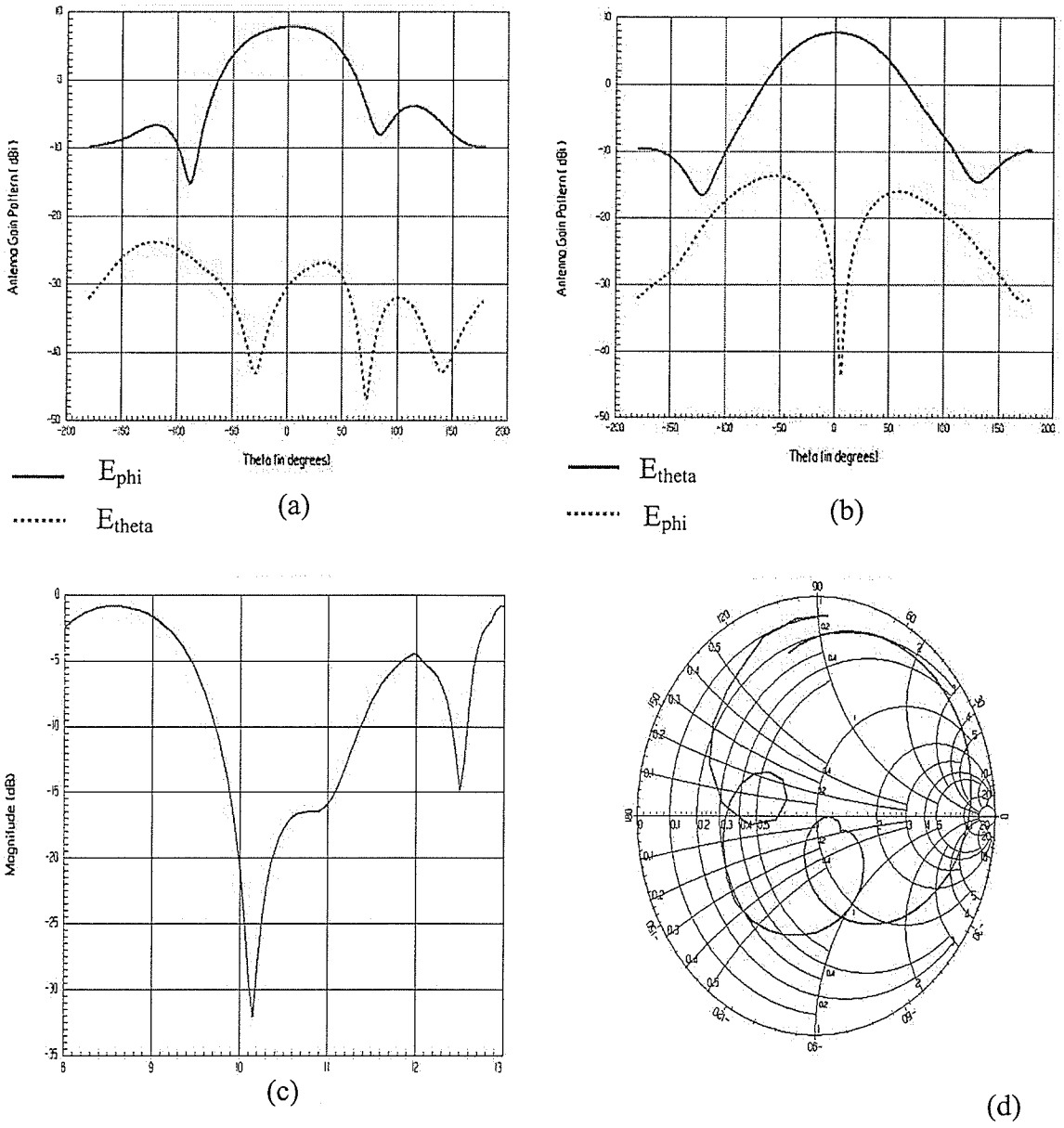

Figure 3.25. Antenna Gain Patterns and Return Loss at the center frequency of a Yagi on a plate with a dielectric constant of 10.2 and an electrical length of $1.91\lambda_g$ with four directors, (a) radiation pattern at 10 GHz at phi=0, (b) radiation pattern at 10 GHz at phi=90, (c) linear plot of a return loss, (d) return loss on a smith chart.

condition thus extends the pattern bandwidth of the antenna but at the expense of higher side lobes. Inclusion of three more parasitics (for a total of seven) on an extended plate length of $3.2\lambda_g$ continues to show a good pattern bandwidth performance at the expense

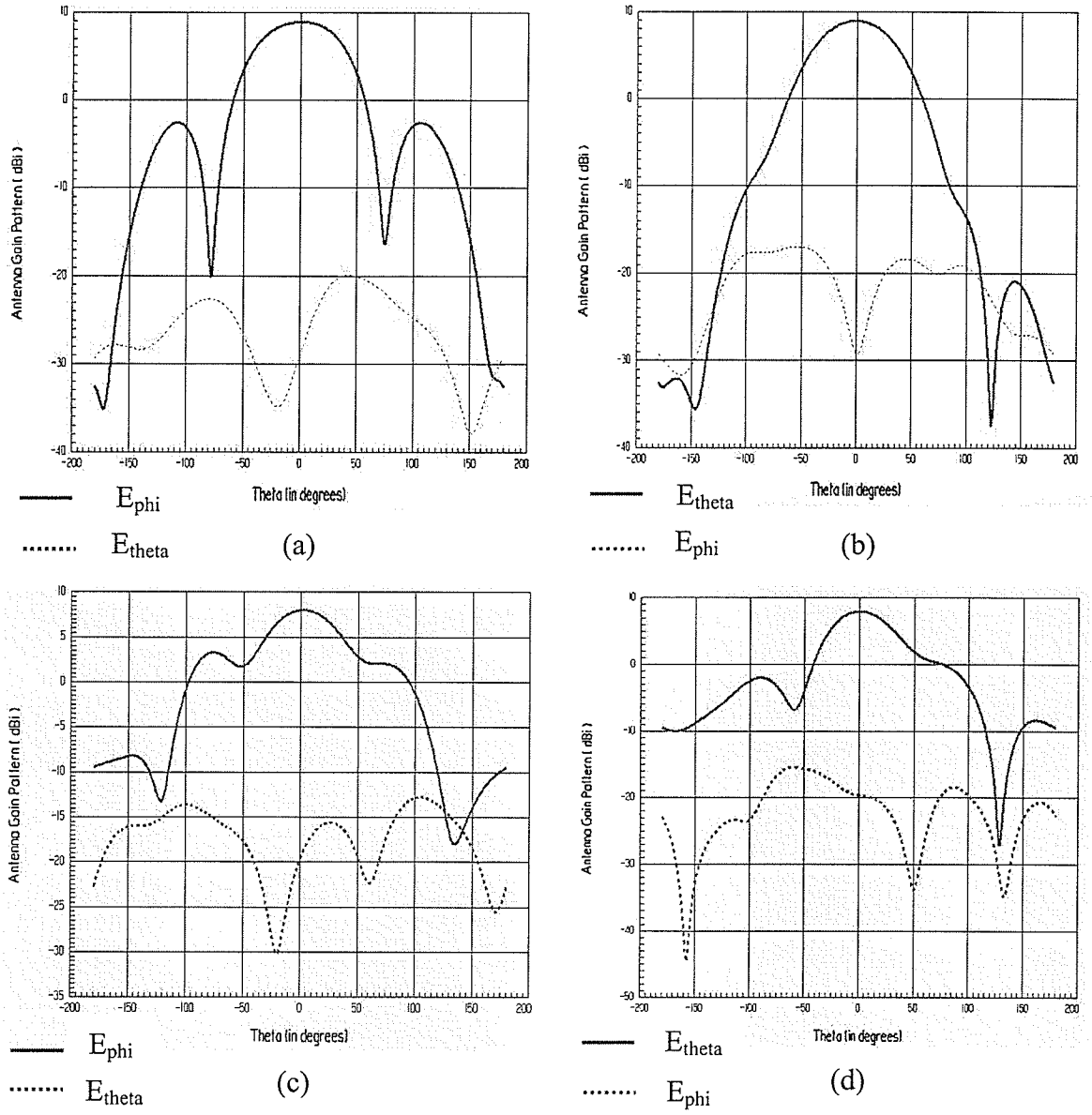

Figure 3.26. Antenna Gain Patterns within the impedance bandwidth and at 2nd resonance of a Yagi on a plate with a dielectric constant of 10.2 and an electrical length of $1.91\lambda_g$ with four directors, (a) radiation pattern at 11.3 GHz at phi=0, (b) radiation pattern at 11.3 GHz at phi=90, (c) radiation pattern at 12.5 GHz at phi=0, (d) radiation pattern at 12.5 GHz at phi=90.

of even higher side lobes (2dB higher at the upper side of the frequency range than at the lower) (figures 3.27 and 3.28 on pages 53 and 54).

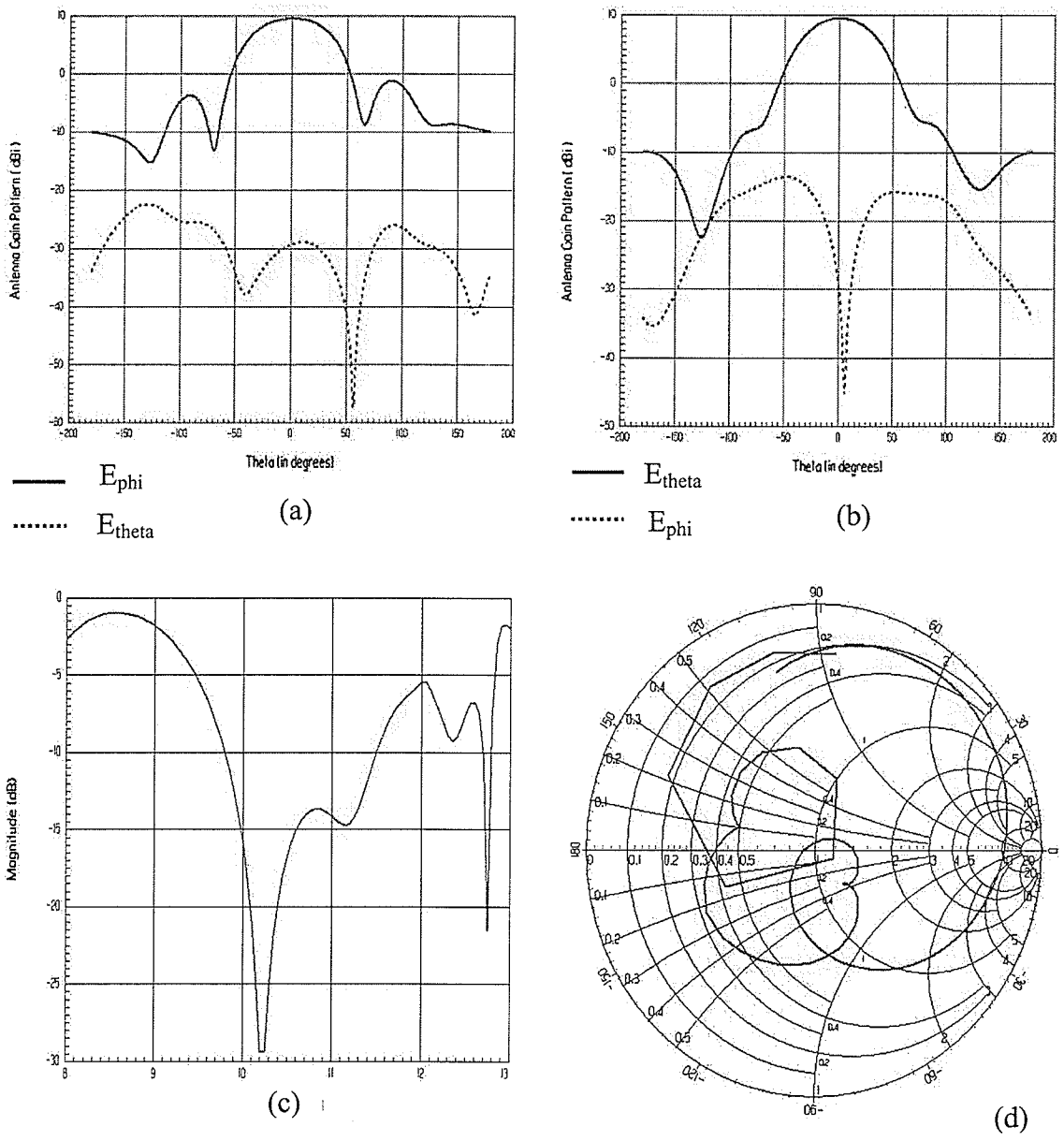

Figure 3.27. Antenna Gain Patterns and Return Loss at the center frequency of a Yagi on a plate with a dielectric constant of 10.2 and an electrical length of $3.2\lambda_g$ with seven directors, (a) radiation pattern at 10 GHz at phi=0, (b) radiation pattern at 10 GHz at phi=90, (c) linear plot of a return loss, (d) return loss on a smith chart.

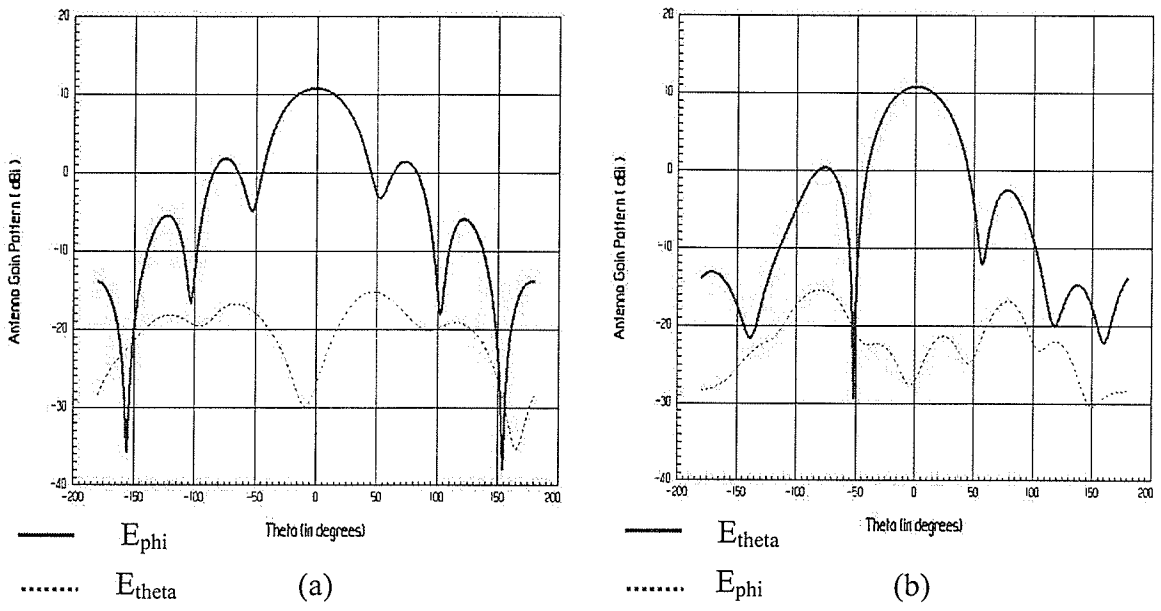

Figure 3.28. Antenna Gain Patterns at the upper side of the frequency range of a Yagi on a plate with a dielectric constant of 10.2 and an electrical length of $3.2\lambda_g$ with seven directors, (a) radiation pattern at 11.5 GHz at phi=0, (b) radiation pattern at 11.5 GHz at phi=90.

The above data is summarized in Table 3.11. It reveals that director addition has an effect of reducing the return loss and causes a shift in operating frequency. The impedance bandwidth also increases and beam tilt reduces. The region of most rapid changes appears to take place for plate lengths of one to two wavelengths with up to 4 parasitics. Adding more parasitics appears to have little or no effect on the return loss, frequency shift or impedance bandwidth but it further reduces the beam tilt and increases directivity.

Table 3.11: Return Loss and Pattern data for the microstrip-fed Yagi (ε_r=10.2, a=0.06755λ_g, b=1.3163λ_g, freq = 10GHz) with directors, λ_g=9.4mm.

L_p (λ_g)	No. of directors	Return Loss (dB)	Frequency (GHz)	Impedance Bandwidth (%)	Beam Tilt (θ) E-plane (phi=90)	Beam Tilt (θ) H-plane (phi=0)
1.04	1	-21	10.5	12.381	1	7
1.91	4	-32	10.1	16.832	1	4
3.2	7	-29.5	10.2	16.667	0	1

Table 3.12: Percentage of modal power for the three element microstrip-fed Yagi (ε_r=10.2, a=0.06755λ_g, b=1.3163λ_g, freq = 10GHz) with plate length equal to 1.04λ_g, λ_g=9.4mm, Figure 3.30.

L_{cut} (λ_g)	P(TM_{01}) (%)	P(TM_{02}) (%)
0.487	84.35262	15.64737
1.04	98.76952	1.23048

Table 3.13: Percentage of modal power for the six element microstrip-fed Yagi (ε_r=10.2, a=0.06755λ_g, b=1.3163λ_g, freq = 10GHz) with plate length equal to 1.91λ_g, λ_g=9.4mm, Figure 3.30.

L_{cut} (λ_g)	P(TM_{01}) (%)	P(TM_{02}) (%)
0.487	84.5403	15.4597
0.823	90.72297	9.277035
1.158	93.02345	6.976545
1.494	95.008	4.992
1.91	99.57635	0.423655

Table 3.14: Percentage of modal power for the nine element microstrip-fed Yagi (ε_r=10.2, a=0.06755λ_g, b=1.3163λ_g, freq = 10GHz) with plate length equal to 3.2λ_g, λ_g=9.4mm, Figure 3.30.

L_{cut} (λ_g)	P(TM_{01}) (%)	P(TM_{02}) (%)
0.487	84.42318	15.57683
0.823	91.34252	8.657481
1.158	93.00414	6.995872
1.494	93.55956	6.44045
1.829	92.9718	7.0282
2.1645	92.92823	7.071763
2.5	93.94847	6.051529
3.2	99.54191	0.4580938

Examination of tables 3.12 through 3.14 as well as figure 3.30 on page 57 reveals a profound reduction in the rate of decay of a higher order mode following resistor placement.

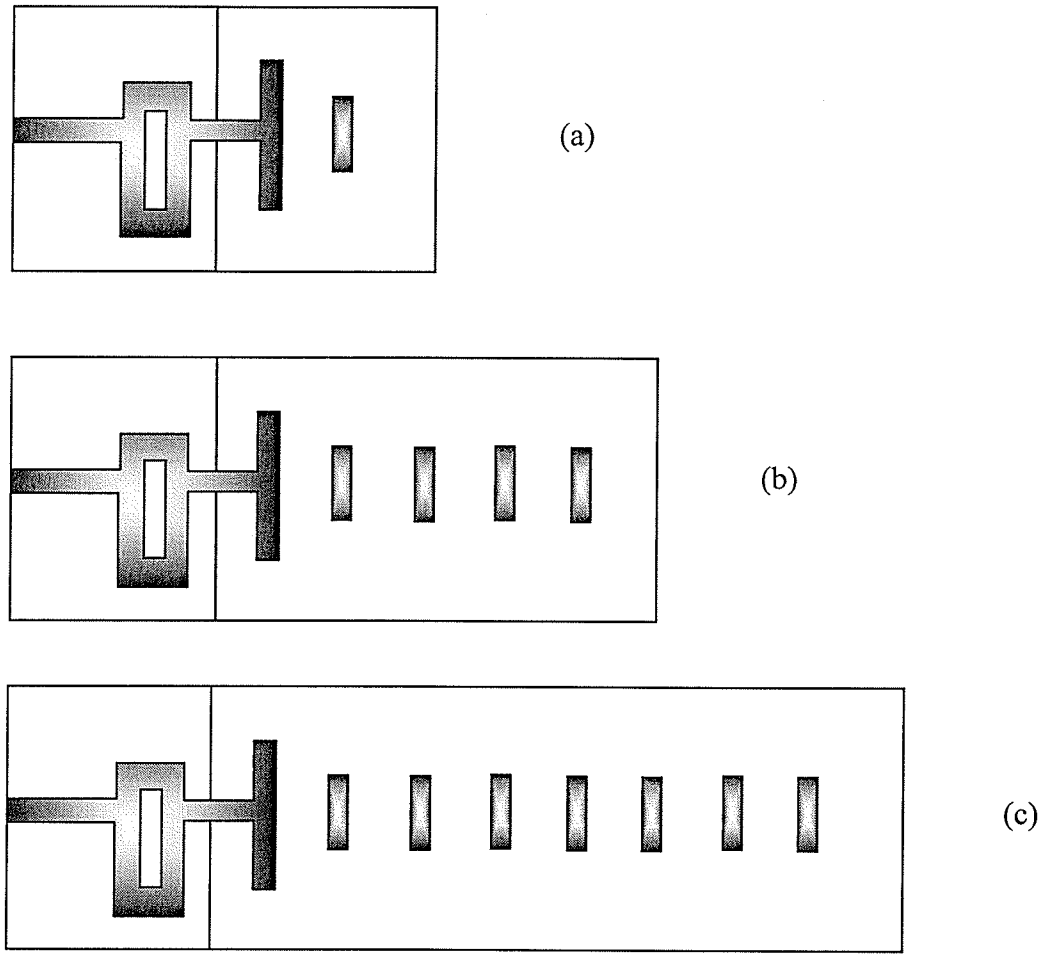

Figure 3.29. Top View of a multi-element microstrip-fed Yagi antenna, (a) 3-element, (b) 6-element, (c) 9-element.

Figure 3.29 above shows three antenna configurations used. 3-element configuration refers to the reflector plane with a feeding element and one director. 6-element configuration contains 4 directors and a 9-element configuration consists of 7 directors. These should be considered as we analyze figure 3.30 below.

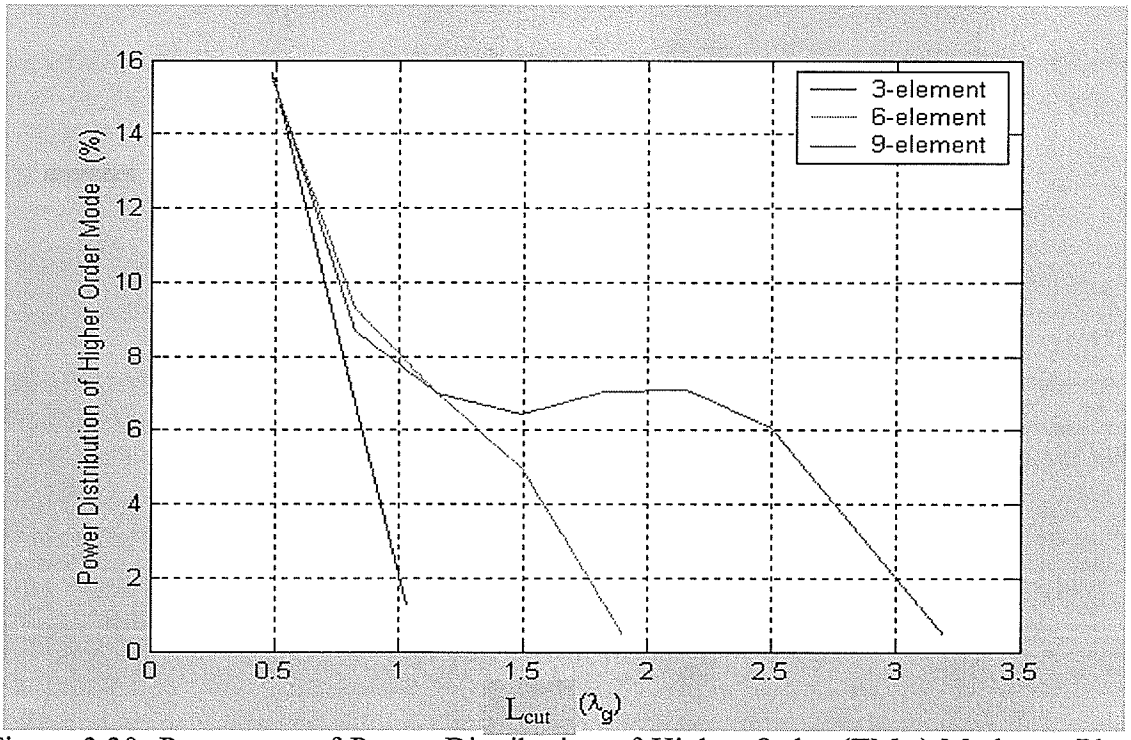

Figure 3.30. Percentage of Power Distribution of Higher Order (TM_{02}) Mode vs. Plate Length for the microstrip-fed Yagi with three different plate lengths and directors (ε_r=10.2, a=0.06755λ_g, b=1.3163λ_g, freq = 10GHz).

Let us then correlate the pattern performance with figure 3.30. At first glance we notice that the rate of decay of a higher order mode is much more controlled when one uses directors as opposed to using an antenna without them. Use of directors improves antenna pattern bandwidth performance as well as directivity although the effects are mostly felt for shorter plate lengths. Beyond that the level of side lobes rises and we do not see much improvement in antenna pattern bandwidth. In fact, examination of the pattern at second resonance does not give promising results.

Comparing figures 3.15 with 3.30 we see how quickly do directors act to reduce the effects of higher order mode radiation by keeping it inside and allowing the dominant mode to participate in radiation. However, higher order modes still do radiate quite rapidly near plate termination giving rise to side lobes and actually reducing the pattern bandwidth by eliminating second resonance condition.

3.5: Effects of Parasitics On Low Permittivity Yagis

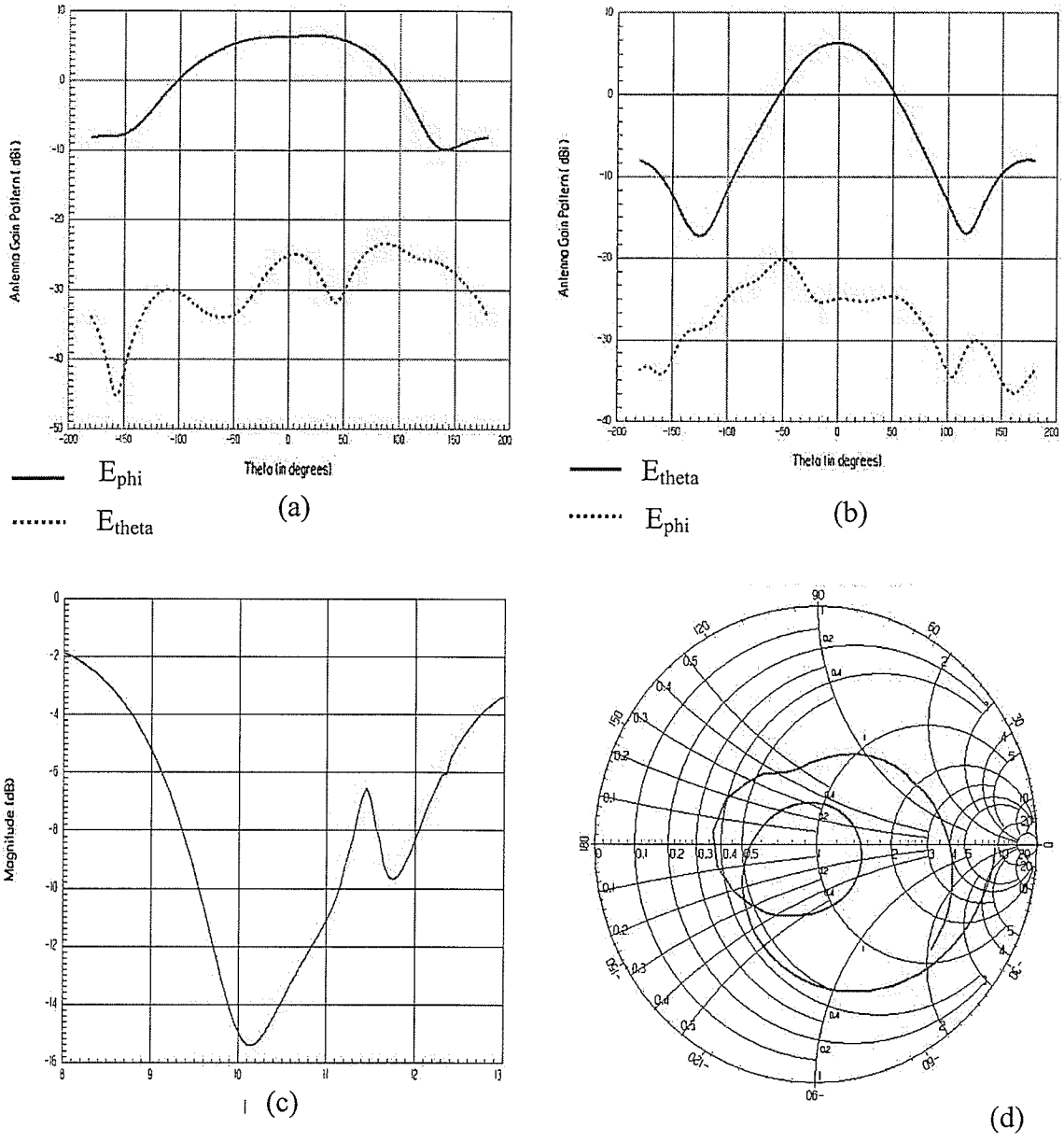

Figure 3.31. Antenna Gain Patterns and Return Loss at the center frequency of a Yagi on a plate with a dielectric constant of 2.5 and an electrical length of λ_g with one director, (a) radiation pattern at 10 GHz at phi=0, (b) radiation pattern at 10 GHz at phi=90, (c) linear plot of a return loss, (d) return loss on a smith chart.

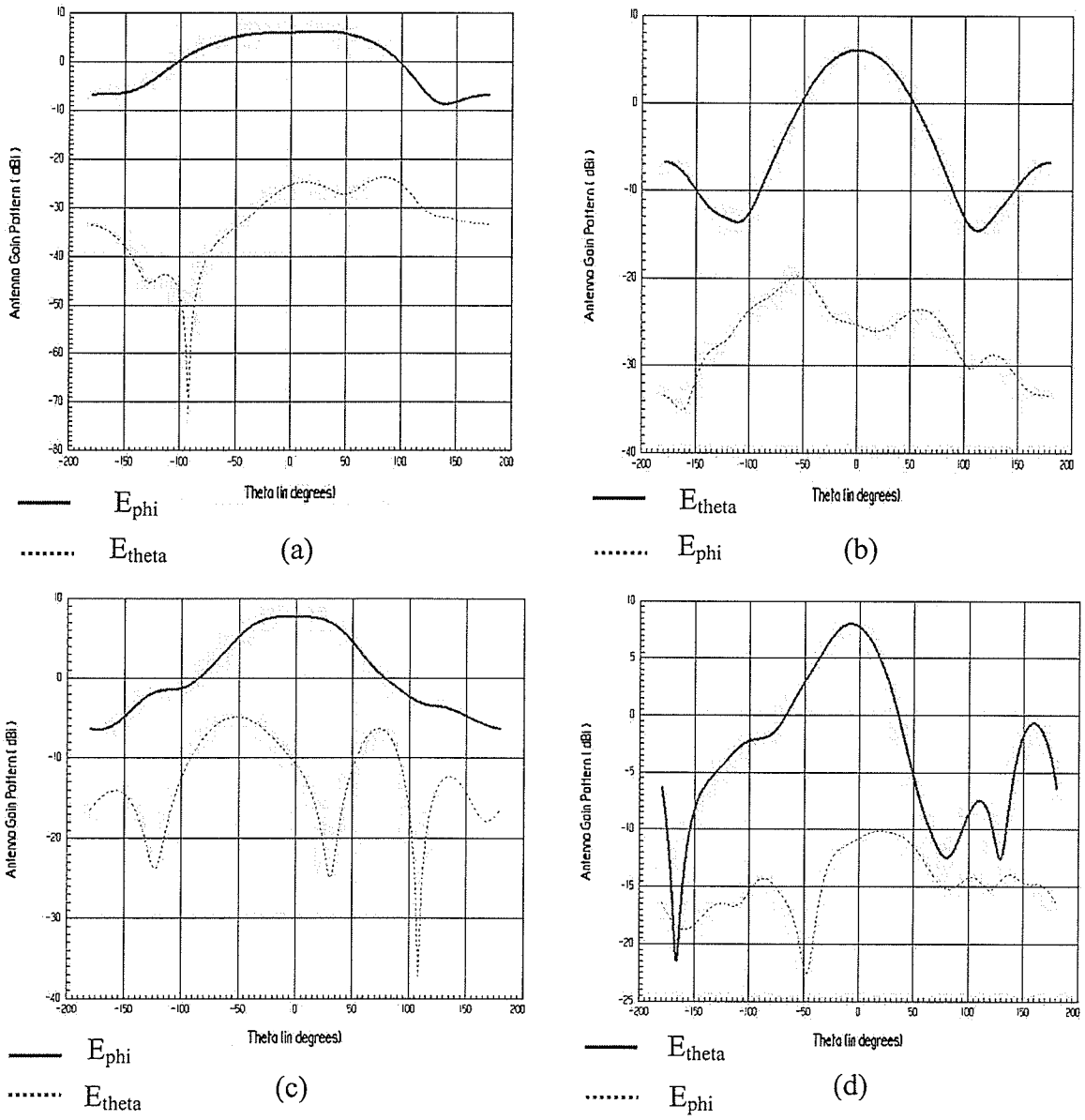

Figure 3.32. Antenna Gain Patterns within the impedance bandwidth of a Yagi on a plate with a dielectric constant of 2.5 and an electrical length of λ_g with one director, (a) radiation pattern at 9.5 GHz at phi=0, (b) radiation pattern at 9.5 GHz at phi=90, (c) radiation pattern at 11.2 GHz at phi=0, (d) radiation pattern at 11.2 GHz at phi=90.

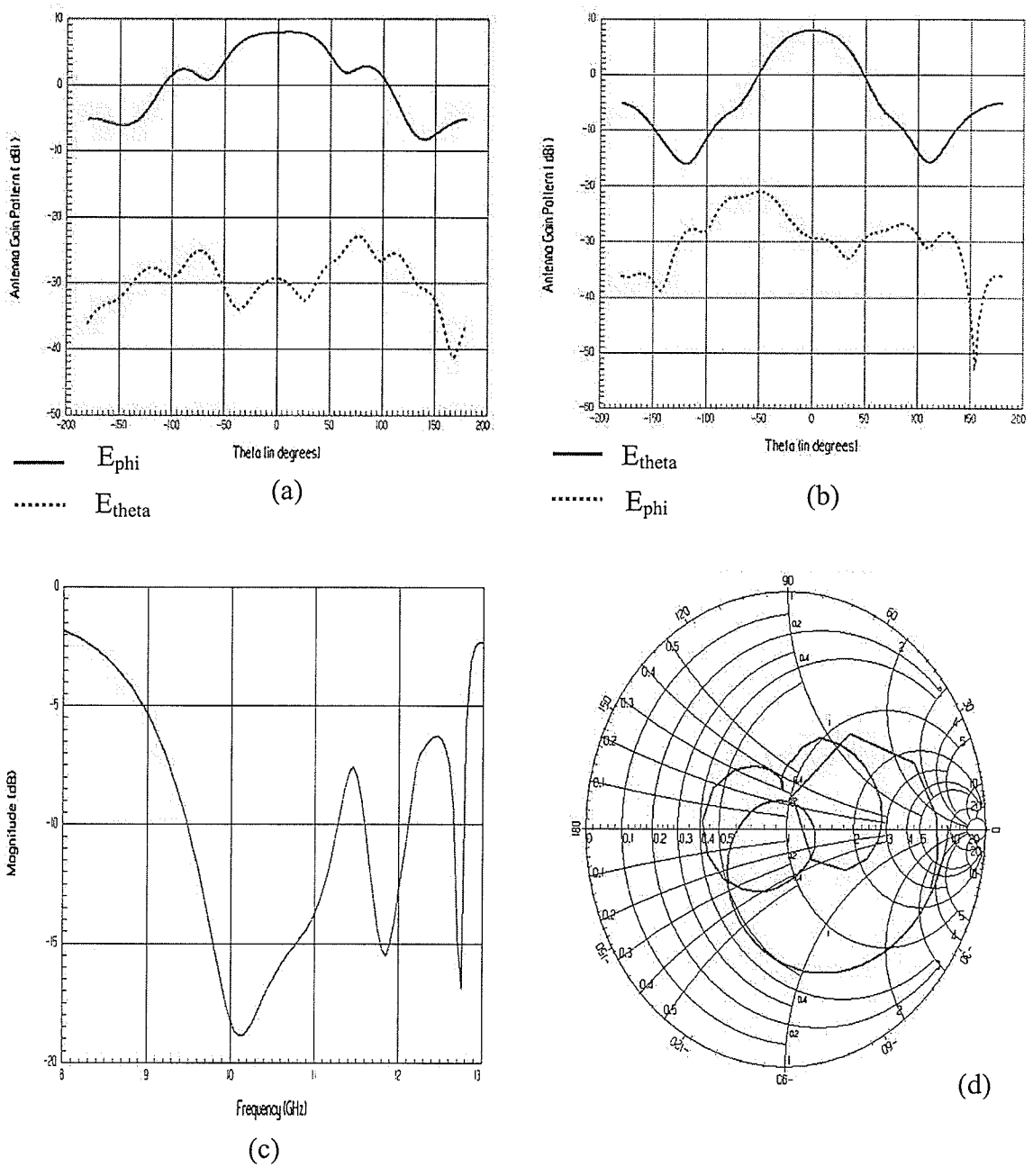

Figure 3.33. Antenna Gain Patterns and Return Loss at the center frequency of a Yagi on a plate with a dielectric constant of 2.5 and an electrical length of $2\lambda_g$ with four directors, (a) radiation pattern at 10 GHz at phi=0, (b) radiation pattern at 10 GHz at phi=90, (c) linear plot of a return loss, (d) return loss on a smith chart.

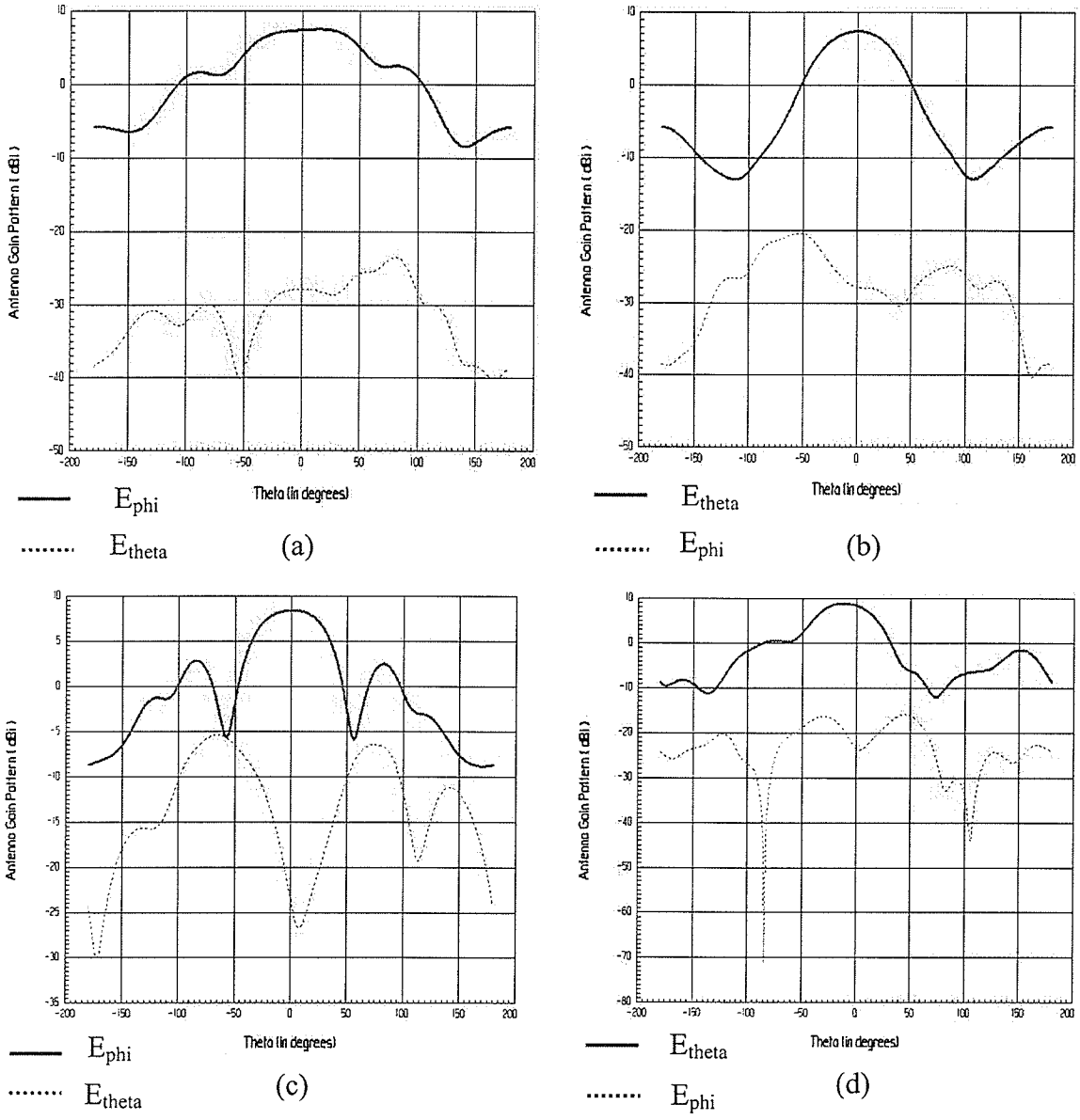

Figure 3.34. Antenna Gain Patterns within the impedance bandwidth of a Yagi on a plate with a dielectric constant of 2.5 and an electrical length of $2\lambda_g$ with four directors, (a) radiation pattern at 9.5 GHz at phi=0, (b) radiation pattern at 9.5 GHz at phi=90, (c) radiation pattern at 11.3 GHz at phi=0, (d) radiation pattern at 11.3 GHz at phi=90.

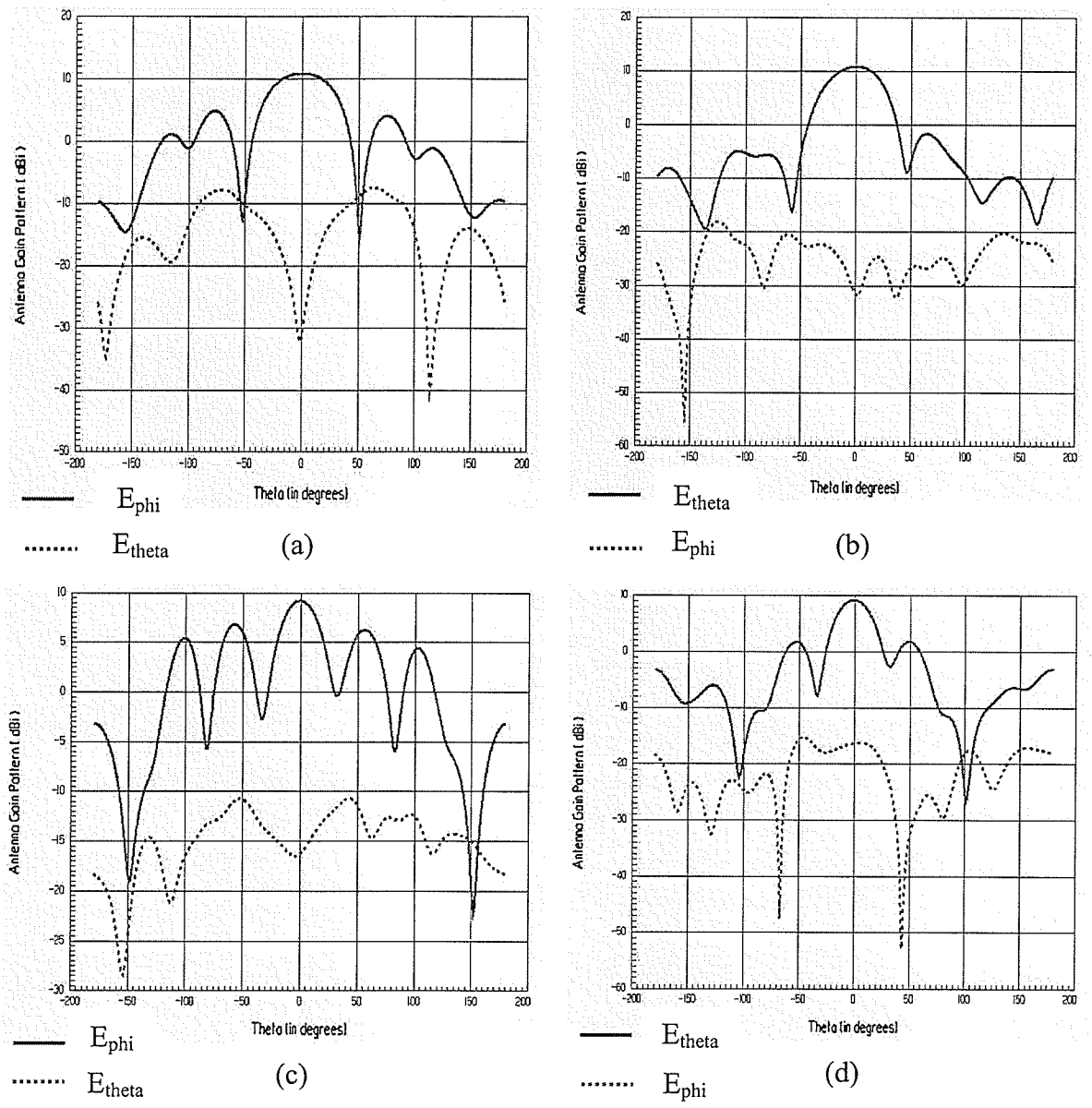

Figure 3.35. Antenna Gain Patterns at 2nd and 3rd resonances of a Yagi on a plate with a dielectric constant of 2.5 and an electrical length of $2\lambda_g$ with four directors, (a) radiation pattern at 11.85 GHz at phi=0, (b) radiation pattern at 11.85 GHz at phi=90, (c) radiation pattern at 12.75 GHz at phi=0, (d) radiation pattern at 12.75 GHz at phi=90.

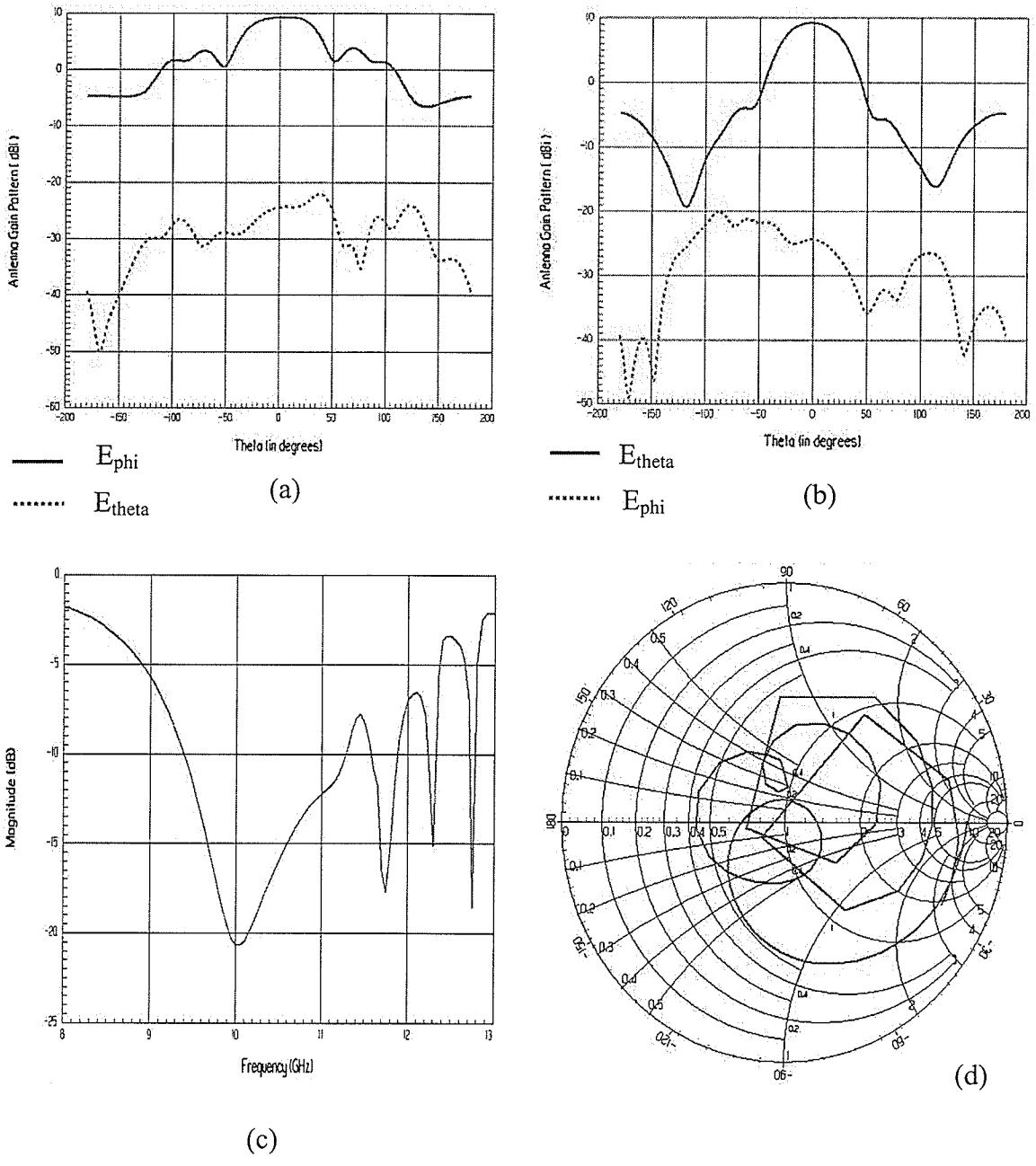

Figure 3.36. Antenna Gain Patterns and Return Loss at the center frequency of a Yagi on a plate with a dielectric constant of 2.5 and an electrical length of $3\lambda_g$ with seven directors, (a) radiation pattern at 10 GHz at phi=0, (b) radiation pattern at 10 GHz at phi=90, (c) linear plot of a return loss, (d) return loss on a smith chart.

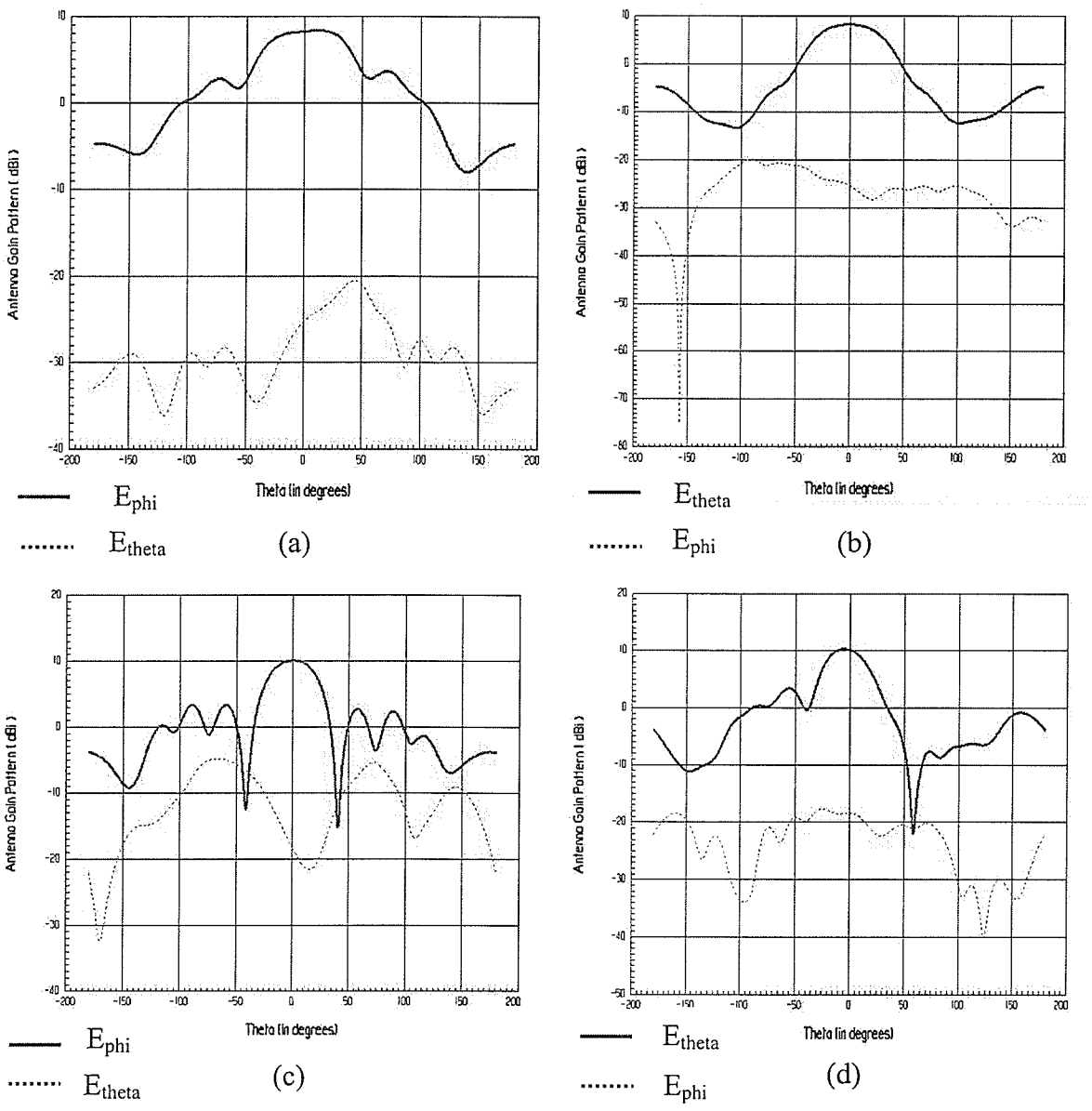

Figure 3.37. Antenna Gain Patterns within the impedance bandwidth of a Yagi on a plate with a dielectric constant of 2.5 and an electrical length of $3\lambda_g$ with seven directors, (a) radiation pattern at 9.4 GHz at phi=0, (b) radiation pattern at 9.4 GHz at phi=90, (c) radiation pattern at 11.3 GHz at phi=0, (d) radiation pattern at 11.3 GHz at phi=90.

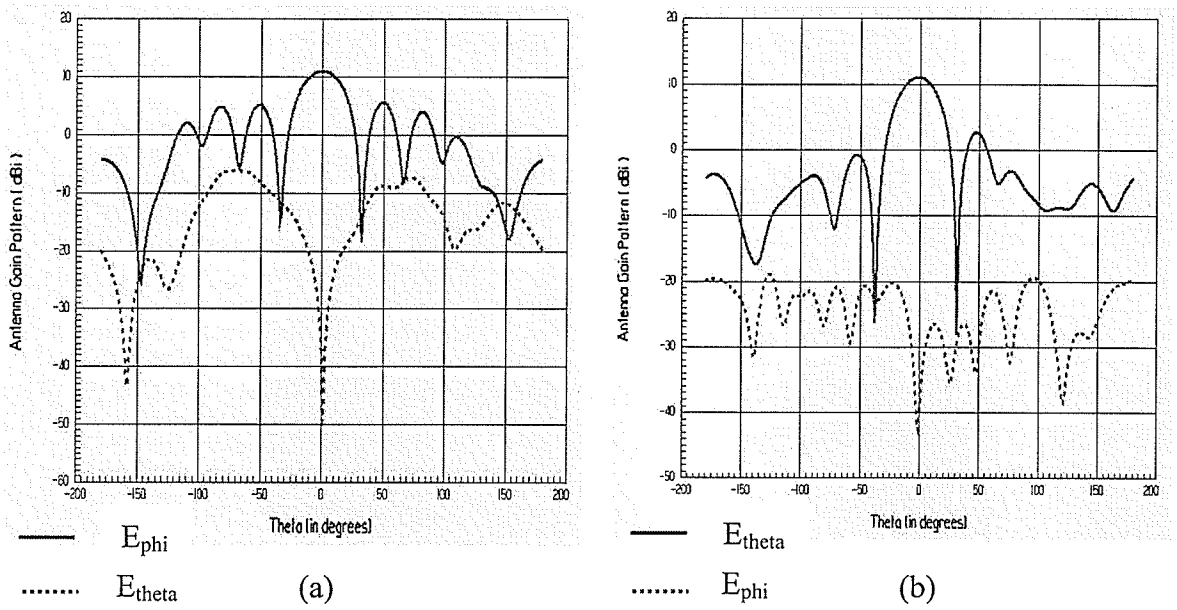

Figure 3.38. Antenna Gain Patterns at 2nd resonance of a Yagi on a plate with a dielectric constant of 2.5 and an electrical length of $3\lambda_g$ with seven directors, (a) radiation pattern at 11.75 GHz at phi=0, (b) radiation pattern at 11.75 GHz at phi=90.

Figures 3.31 and 3.32 (pages 58 and 59) show a relatively good radiation pattern performance over specified band of frequencies. Figure 3.33c (page 60) shows three resonances as we extend the plate length to two guide wavelengths and include 4 parasitics. As shown in figures 3.34 and 3.35 (pages 61 and 62), inclusion of those parasitics has an effect of extending the pattern bandwidth beyond its normal range of frequencies (as defined by impedance bandwidth) at the expense of higher side lobes. The directivity is actually 3dB higher at 2^{nd} resonance (at 11.85GHz) than at 1^{st} and the side lobe level is 1dB lower. On the other hand, the directivity is actually 2dB lower at 3^{rd} resonance (occurring at 12.75GHz) than at 2^{nd} and the side lobe level is 1.5dB higher. Therefore 2^{nd} resonance appears to dominate. Additional extension of the plate to $3\lambda_g$ and an inclusion of seven directors have an effect of eliminating the dominance of the 2^{nd}

resonance and shortening the pattern bandwidth as 3rd and 4th resonances no longer play any significant role. We also do not observe much improvement in pattern directivity (figures 3.36 to 3.38 on pages 63 to 65).

As indicated in table 3.15 below, director addition has an effect of reducing the value of return loss but does not much affect the operating frequency. The impedance bandwidth also increases and beam tilt reduces. The greatest changes take place for plate lengths of one to two guide wavelengths with up to 4 parasitics.

Table 3.15: Return Loss and Pattern data for the microstrip-fed Yagi (ε_r=2.5, a=0.013λ_g, b=1.316λ_g, freq = 10GHz) with directors, λ_g=19mm.

L_p (λ_g)	No. of directors	Return Loss (dB)	Frequency (GHz)	Impedance Bandwidth (%)	Beam Tilt (θ) E-plane (phi=90)	Beam Tilt (θ) H-plane (phi=0)
1.04	1	-15.4	10.1	15.84	-1	23
1.91	4	-19	10.1	17.82	-1	10
3.2	7	-20.5	10	19	-2	7

Examination of tables 3.16 through 3.18 (pages 66 and 67) as well as figure 3.39 (page 68) reveals a profound reduction in the dissipation of a higher order mode following resistor placement.

Table 3.16: Percentage of modal power for the three element microstrip-fed Yagi (ε_r=2.5, a=0.013λ_g, b=1.316λ_g, freq = 10GHz) with plate length equal to λ_g, λ_g=19mm, Figure 3.39.

L_{cut} (λ_g)	P(TM_{01}) (%)	P(TM_{02}) (%)
0.487	84.43602	15.56397
1	98.2019	1.798093

Table 3.17: Percentage of modal power for the six element microstrip-fed Yagi (ε_r=2.5, a=0.013λ_g, b=1.316λ_g, freq = 10GHz) with plate length equal to 2λ_g, λ_g=19mm, Figure 3.39.

L_{cut} (λ_g)	P(TM_{01}) (%)	P(TM_{02}) (%)
0.487	84.01616	15.98384
0.823	90.13251	9.867487
1.159	92.64038	7.359615
1.495	92.75314	7.246861
2	98.05915	1.940844

Table 3.18: Percentage of modal power for the nine element microstrip-fed Yagi (ε_r=2.5, a=0.013λ_g, b=1.316λ_g, freq = 10GHz) with plate length equal to 3λ_g, λ_g=19mm, Figure 3.39.

L_{cut} (λ_g)	P(TM_{01}) (%)	P(TM_{02}) (%)
0.487	82.8254	17.1746
0.823	89.4647	10.53521
1.159	90.89098	9.109021
1.495	92.70438	7.295623
1.831	92.66305	7.336949
2.167	91.66599	8.334009
2.5	90.76714	9.23285
3	97.94414	2.055858

As we correlate the pattern performance with figure 3.39 on page 68, we notice that directors can control the rate of dissipation of a higher order mode. This extends and improves the pattern bandwidth but only up to a certain point. This point is reached when we observe an actual deceleration of the curve (as shown by the yellow curve in figure 3.39) at which point the dominant mode is allowed to take more action in the radiation and bring back the dominant condition closer to center frequency.

Comparing figures 3.22 with 3.39 we notice how essential the inclusion of directors is in improving pattern bandwidth and directivity but only up to a point.

Comparing figures 3.15 and 3.22 with figures 3.30 and 3.39 we definitely see the importance of parasitics on plates with low as well as high dielectric constant. However,

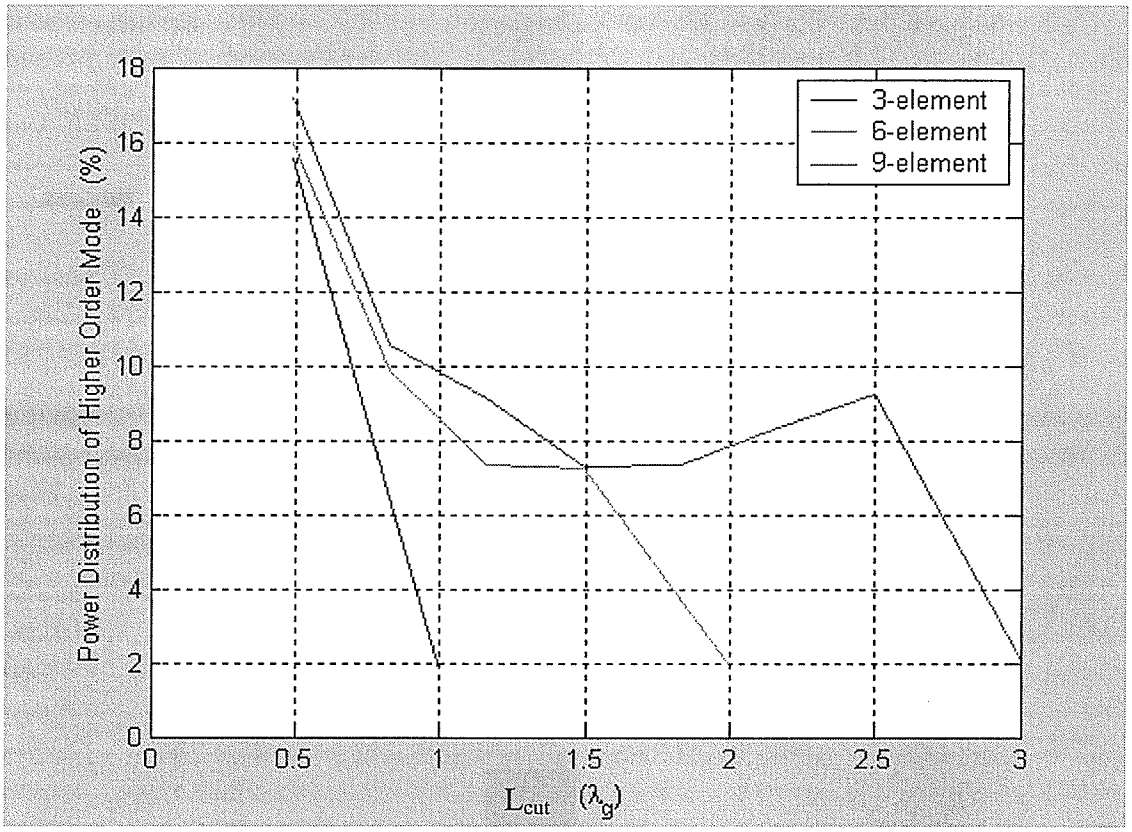

Figure 3.39. Percentage of Power Distribution of Higher Order (TM_{02}) Mode vs. Plate Length for the microstrip-fed Yagi with three different plate lengths and directors (ε_r=2.5, a=0.013λ_g, b=1.316λ_g, freq = 10GHz).

they are needed even more on plates with a low dielectric constant. Such plates experience higher degrees of dissipation of a higher order mode than the plates with higher dielectric constant. The directors also act better in reducing the dissipation of a higher order mode in plates with lower dielectric constant than in plates with higher dielectric constant. This shows that the lower the dielectric constant the greater the need for directors. One could technically maintain good directive behavior without the use of directors for dielectrics with high dielectric constant but would have to make the plate longer (which could be cumbersome for some applications depending on frequency of operation). Plate extensions would not however be viable alternatives in case of plates with low dielectric constant since they fail to improve the directivity.

3.6: Comparison Studies

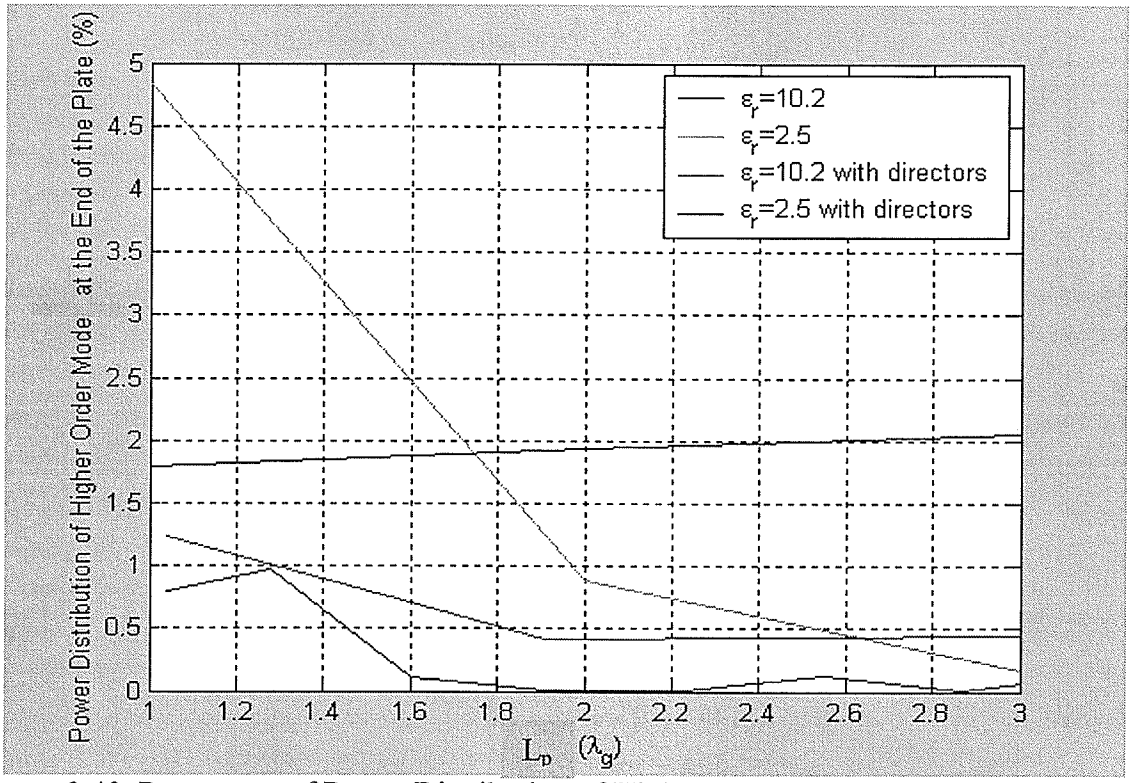

Figure 3.40. Percentage of Power Distribution of Higher Order (TM_{02}) Mode at the End of the Plate vs. Plate Length for the microstrip-fed Yagi ($a=0.06755\lambda_g$, $b=1.3163\lambda_g$, freq = 10GHz).

Figure 3.40 shows how directors act in controlling the decay of a higher order mode and making it radiate less. The gap between curves with and without directors is of course much wider in case of plates with low dielectric constant than in case of plates with high dielectric constant which again is to be expected as directors play a much more significant role in plates with low dielectric constant than high.

As we examine figures 3.41 to 3.43 below we deduce four relationships, the relationship between high and low dielectrics, the relationship between high and low dielectrics with directors, the relationship between high dielectrics without and with directors and the relationship between low dielectrics without and with directors.

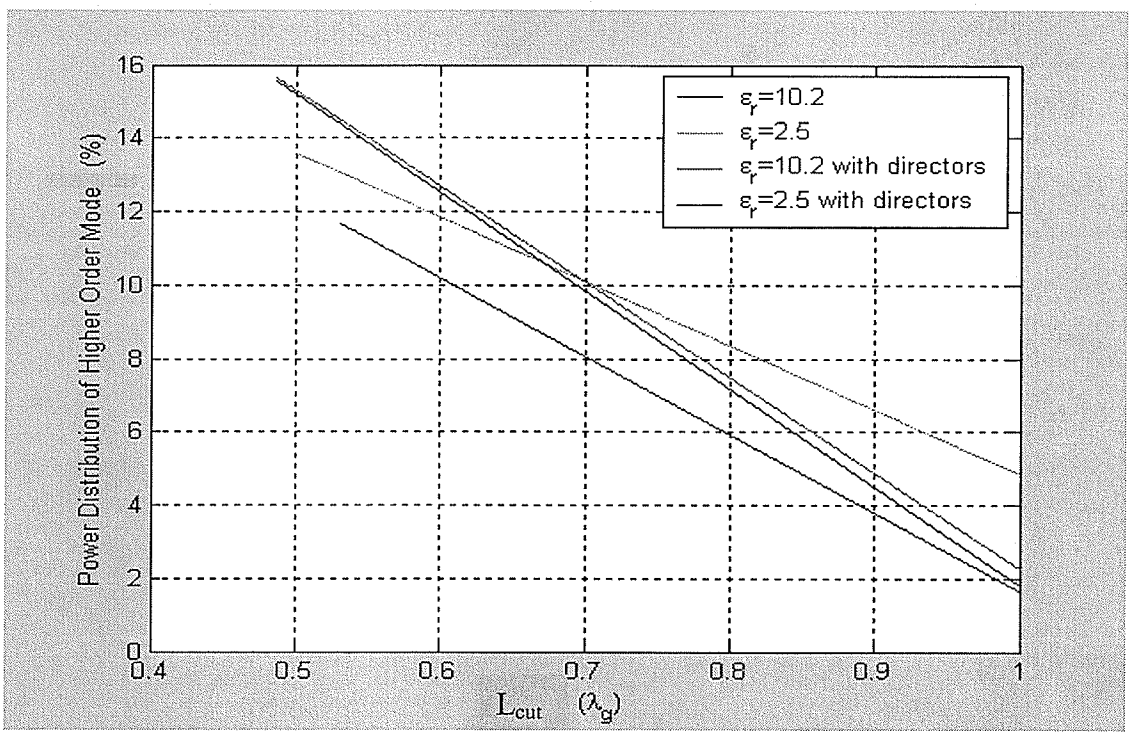

Figure 3.41. Percentage of Power Distribution of Higher Order (TM_{02}) Mode vs. Plate Length for the microstrip-fed Yagi with the plate length equal to λ_g (freq = 10GHz).

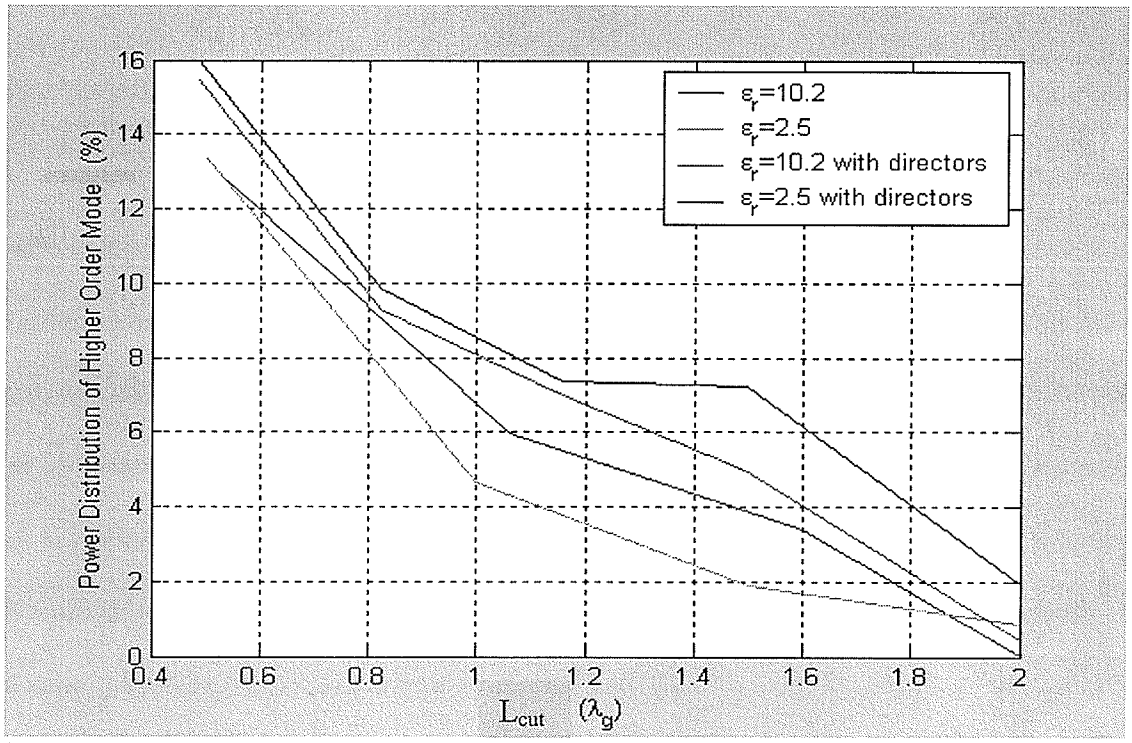

Figure 3.42. Percentage of Power Distribution of Higher Order (TM_{02}) Mode vs. Plate Length for the microstrip-fed Yagi with the plate length equal to $2\lambda_g$ (freq = 10GHz).

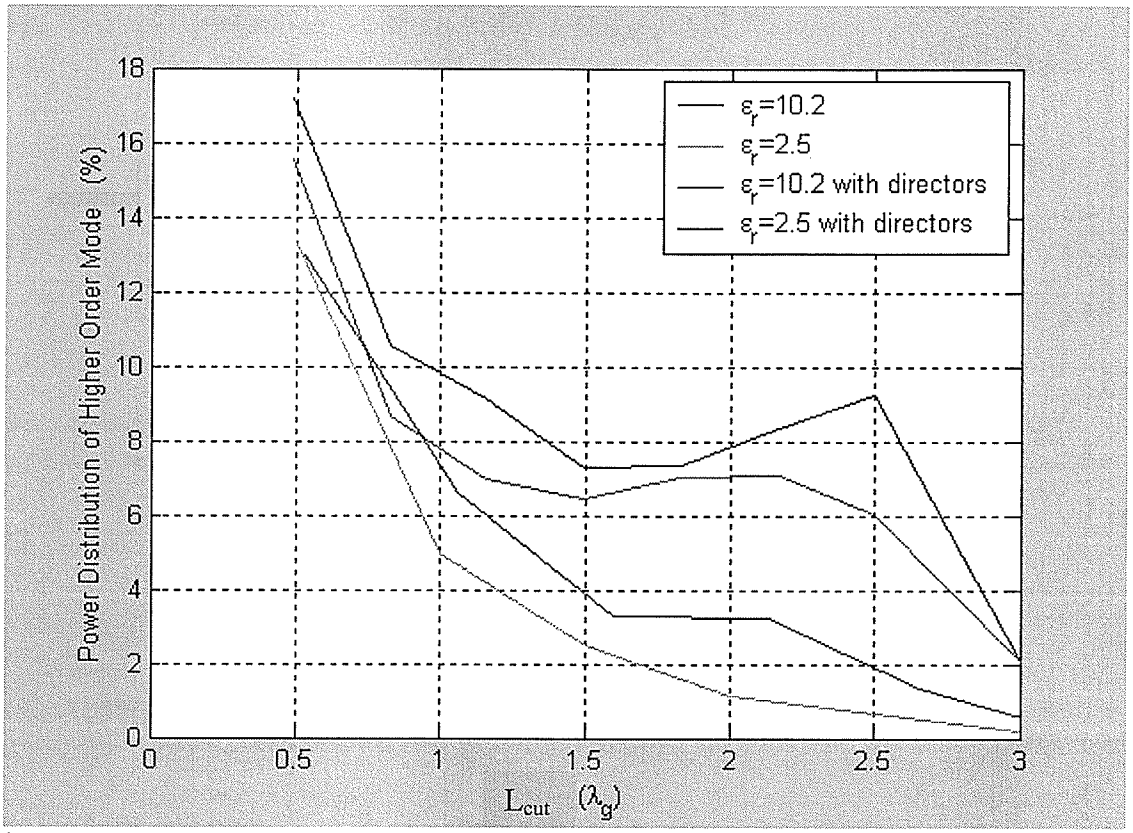

Figure 3.43. Percentage of Power Distribution of Higher Order (TM_{02}) Mode vs. Plate Length for the microstrip-fed Yagi with the plate length equal to $3\lambda_g$ (freq = 10GHz).

We will now go through each of these relationships as we extend plate length. The first relationship (or the relationship between high and low dielectrics) demonstrates that plates with higher dielectric constant have a much better ability to reduce the participation of the higher order mode in radiation than do plates with lower dielectric constant as we increase plate length. The second relationship (or the relationship between high and low dielectrics with directors) shows how the influence of directors is much more pronounced in low permittivity plates as compared with high permittivity plates. The next two relationships demonstrate that as we decrease the dielectric constant of the plate, the gap between the percentage of power of a higher order mode inside the plate with and without directors widens proving the necessity of their inclusion. There is no

such urgency in case of higher dielectric constants, as the gap is smaller. Ideally, with the use of very high permittivities, the gap should collapse and become very small. Therefore, in case of very high dielectrics, the directors would no longer be needed and directivity could be and should be improved with plate alone.

3.7: Discussion

Microstrip-fed Yagis placed on high permittivity plates showed pattern asymmetry within impedance bandwidth occurring at the upper side of the bandwidth. These asymmetric patterns proved to be less directive. It was found that this asymmetry could be corrected by increasing the plate length. Increases in plate length also improved directivity at the upper side of the frequency bandwidth.

Microstrip-fed Yagis placed on low permittivity plates likewise showed pattern asymmetry and distortion within impedance bandwidth occurring at the upper side of the bandwidth. These asymmetric patterns also suffered from lower values of directivity. However, this asymmetry and distortion could not be corrected by merely increasing the plate length.

Microstrip-fed Yagis placed on high permittivity plates with directors showed good radiation pattern performance within impedance bandwidth. It was found that increasing the number of directors does increase directivity levels but at the expense of side lobes. Directivity proved to be higher at the upper side of the impedance bandwidth as did the level of side lobes. Addition of parasitics likewise introduced a second resonance condition at which the basic shape of the pattern was changed although it did maintain good directivity.

Microstrip-fed Yagis placed on low permittivity plates with directors also showed good radiation pattern performance within impedance bandwidth. As in the case of high permittivity plates, inclusion of parasitics on low permittivity plates improved directivity but at the expense of higher side lobes. Addition of parasitics introduced multiple resonances at which the pattern maintained its symmetry and good directivity but also showed multiple side lobes at high level.

3.8: Concluding Remarks

This chapter studied radiation pattern bandwidth, directivity and return loss as functions of plate length and dielectric constant with or without directors.

It was concluded that as plate length and permittivity increased, directivity and pattern bandwidth also increased. Increases in plate length and permittivity did not have a significant effect on return loss and impedance bandwidth.

It was then determined that as plate length and permittivity increased with inclusion of directors, directivity and pattern bandwidth also increased but at the expense of higher side lobes. Side lobe level decreased as permittivity increased.

Increases in plate length and permittivity with directors also caused an increase in impedance bandwidth and a reduction in return loss.

Chapter 4: Effects of Plate Thickness With and Without Directors

4.1: Introduction

Changing thickness introduces higher order slab modes, which reduce the effect of directors as will be shown in this chapter. Modal coefficient theory is applied to understand pattern performance as we increase the plate thickness. It will be shown why director effects diminish as we increase the thickness of the plate.

4.2: Effects of Changing Thickness On High Permittivity Plates

Patterns in figures 4.1 through 4.6 (pages 75 to 80) show a stable pattern performance over specified frequency bandwidth (as indicated in table 4.2 on page 86). Figures 4.7 and 4.8 (pages 81 and 82) demonstrate how higher order slab modes introduce a double resonance condition, thus extending the impedance bandwidth. The pattern is however distorted at the upper side of the frequency range (2nd resonance) and suffers from increased levels of cross-polarization (as indicated by figures 4.8c and 4.8d); this condition occurs for the plate thickness of $0.266\lambda_g$. Increasing the thickness further to $0.3195\lambda_g$, reduces pattern distortion and lowers cross-polarization (by 2.5 dB) at the upper side of the frequency range (as indicated by figures 4.10c and 4.10d on page 84) but at the expense of pattern bandwidth (figures 4.9 and 4.10 on pages 83 and 84).

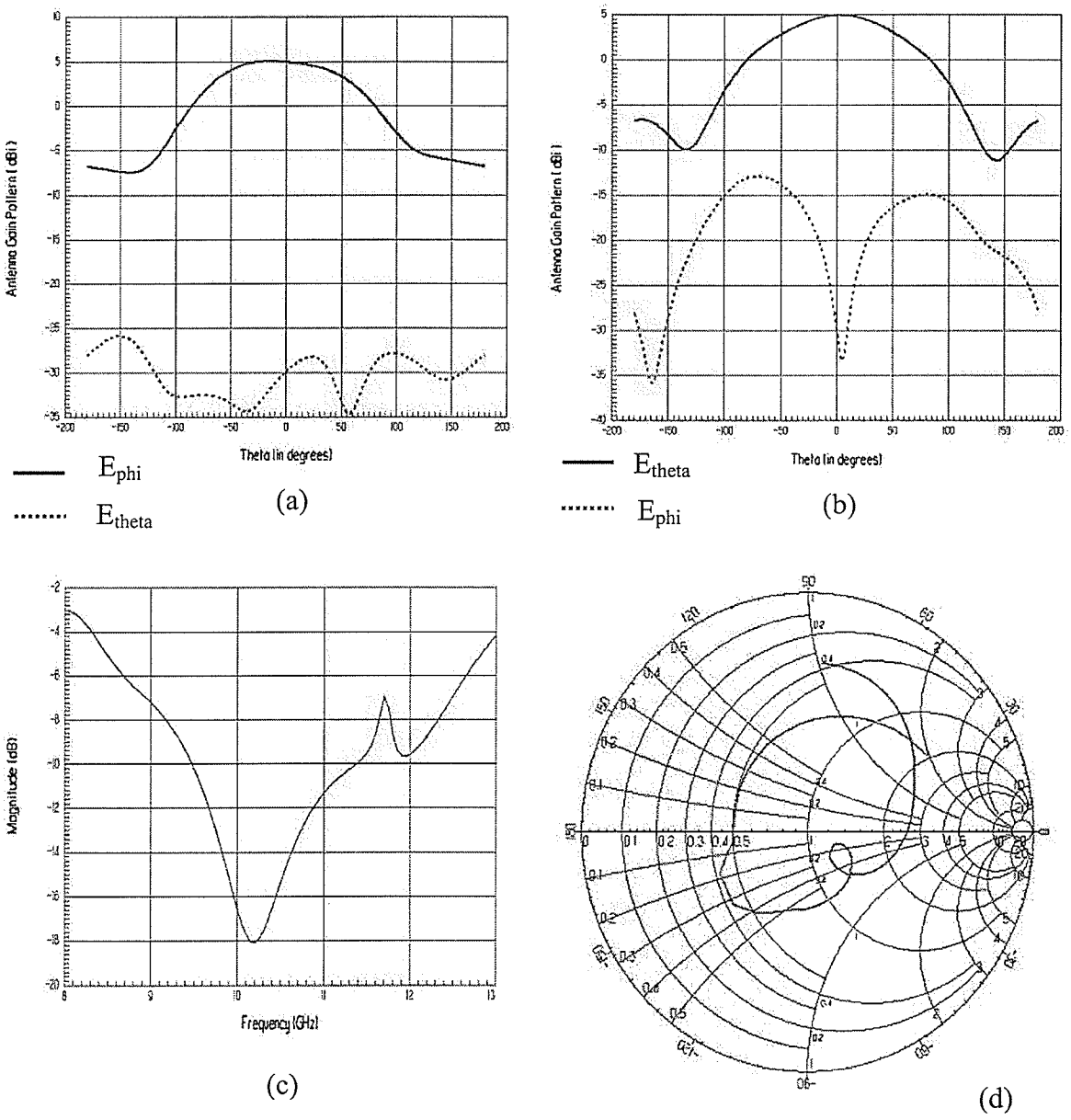

Figure 4.1. Antenna Gain Patterns and Return Loss at the center frequency of a Yagi on a plate with a dielectric constant of 10.2, an electrical length of $1.04\lambda_g$ and the thickness of $0.1065\lambda_g$, (a) radiation pattern at 10 GHz at phi=0, (b) radiation pattern at 10 GHz at phi=90, (c) linear plot of a return loss, (d) return loss on a smith chart.

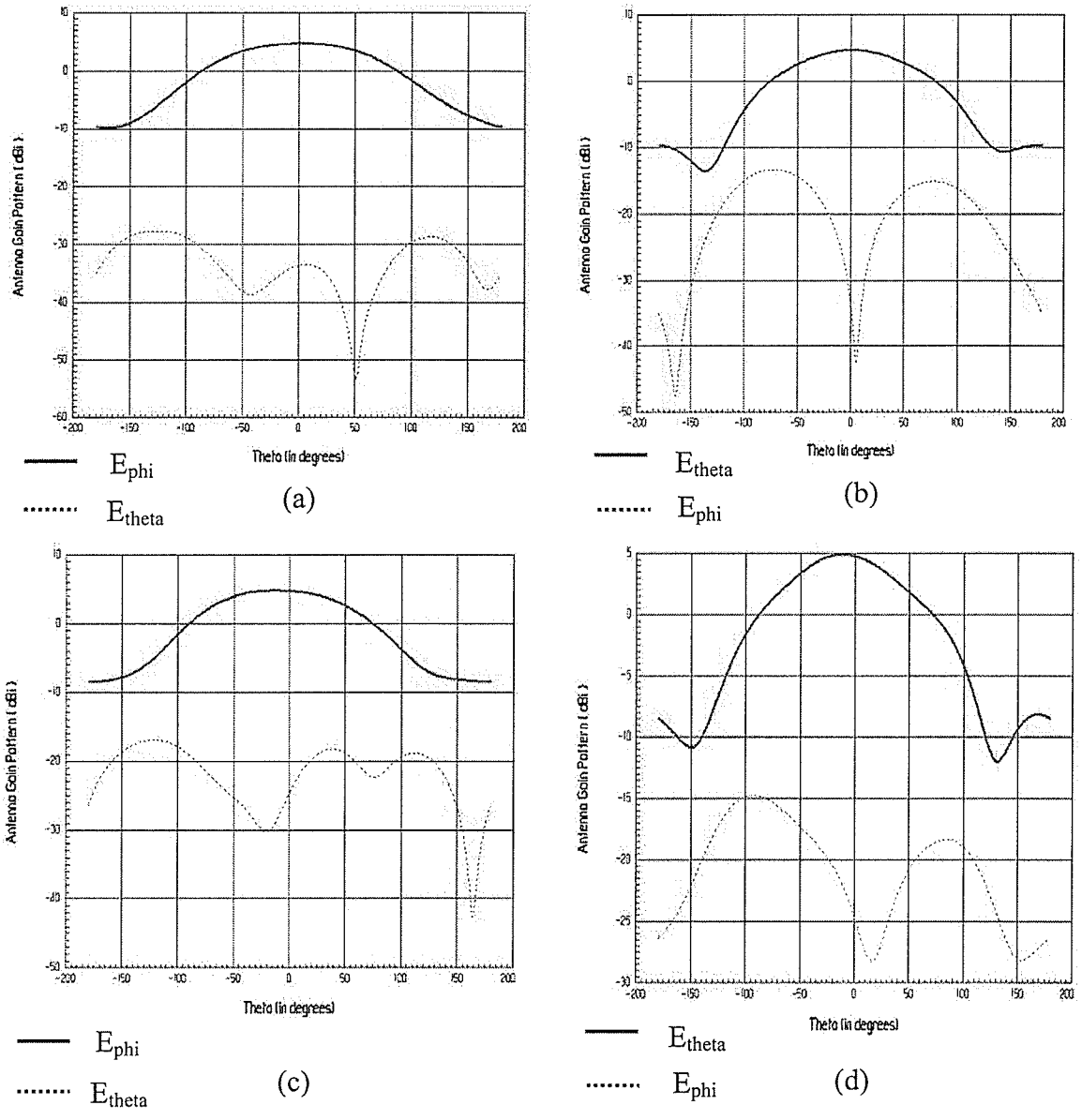

Figure 4.2. Antenna Gain Patterns within the impedance bandwidth of a Yagi on a plate with a dielectric constant of 10.2, an electrical length of $1.04\lambda_g$ and the thickness of $0.1065\lambda_g$, (a) radiation pattern at 9.5 GHz at phi=0, (b) radiation pattern at 9.5 GHz at phi=90, (c) radiation pattern at 11.4 GHz at phi=0, (d) radiation pattern at 11.4 GHz at phi=90.

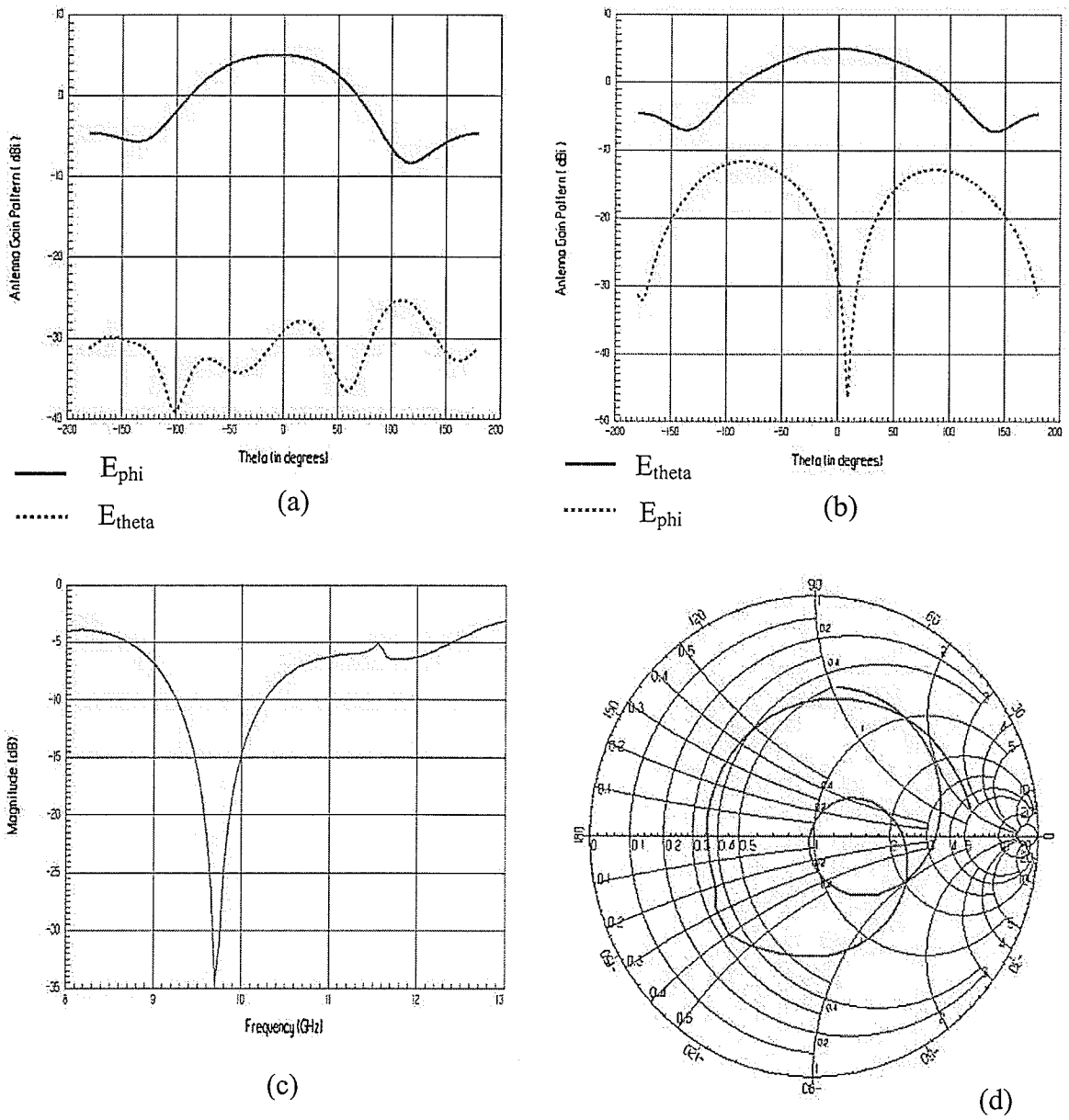

Figure 4.3. Antenna Gain Patterns and Return Loss at the center frequency of a Yagi on a plate with a dielectric constant of 10.2, an electrical length of $1.04\lambda_g$ and the thickness of $0.1597\lambda_g$, (a) radiation pattern at 10 GHz at phi=0, (b) radiation pattern at 10 GHz at phi=90, (c) linear plot of a return loss, (d) return loss on a smith chart.

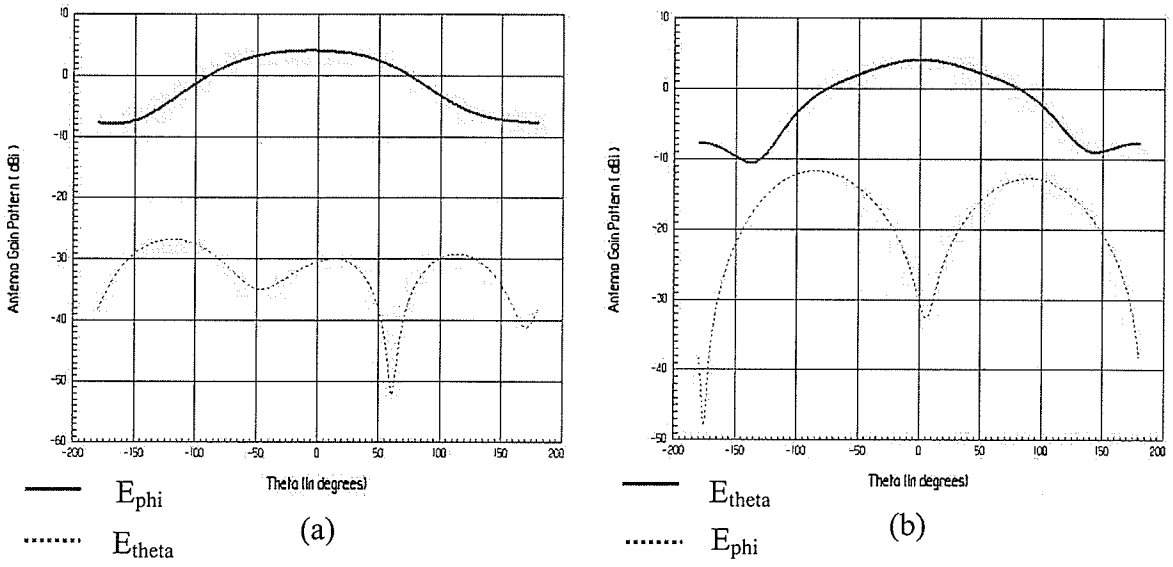

Figure 4.4. Antenna Gain Patterns at the lower part of the frequency range of a Yagi on a plate with a dielectric constant of 10.2, an electrical length of $1.04\lambda_g$ and the thickness of $0.1597\lambda_g$, (a) radiation pattern at 9.3 GHz at phi=0, (b) radiation pattern at 9.3 GHz at phi=90.

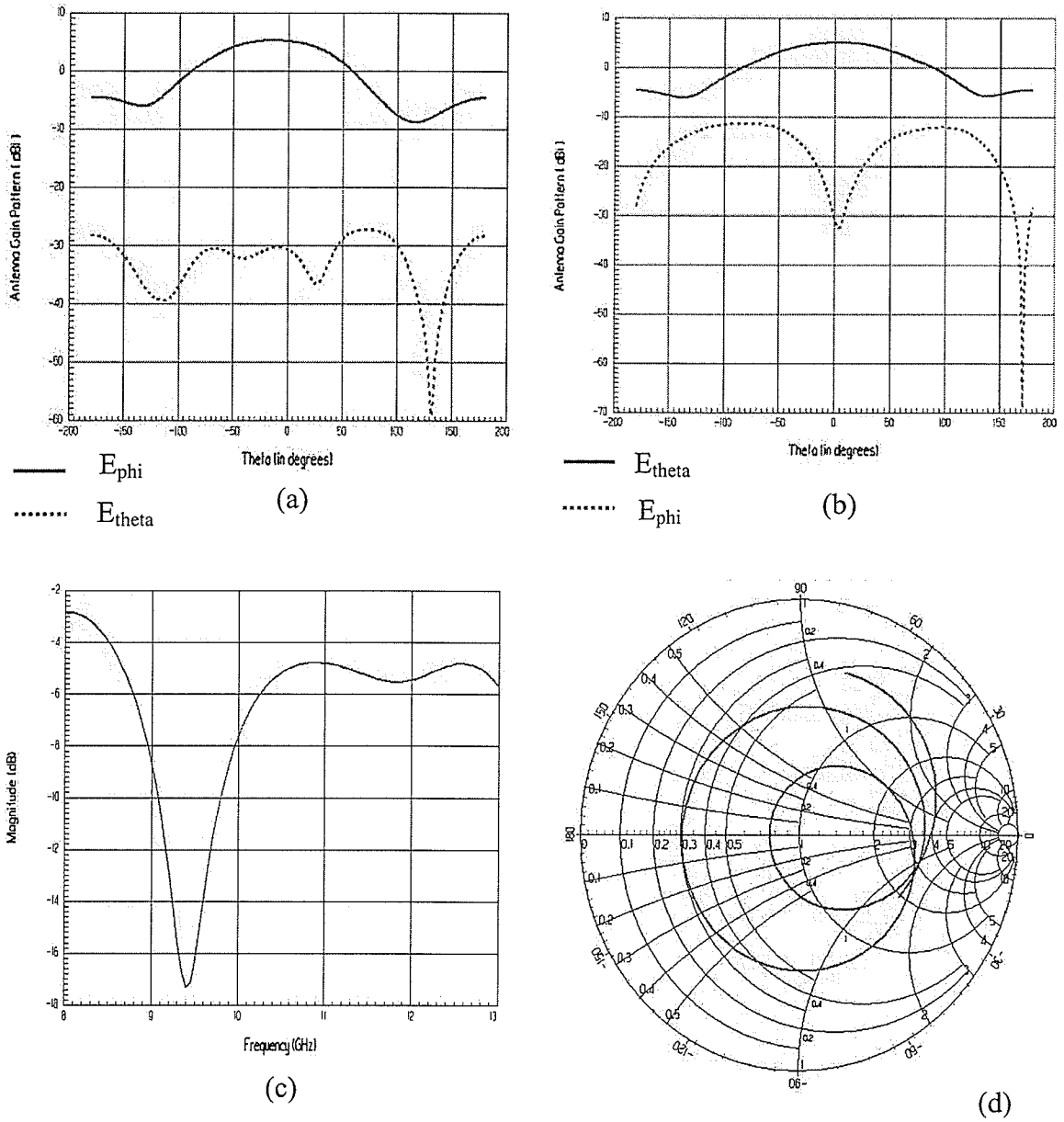

Figure 4.5. Antenna Gain Patterns and Return Loss at the center frequency of a Yagi on a plate with a dielectric constant of 10.2, an electrical length of $1.04\lambda_g$ and the thickness of $0.213\lambda_g$, (a) radiation pattern at 10 GHz at phi=0, (b) radiation pattern at 10 GHz at phi=90, (c) linear plot of a return loss, (d) return loss on a smith chart.

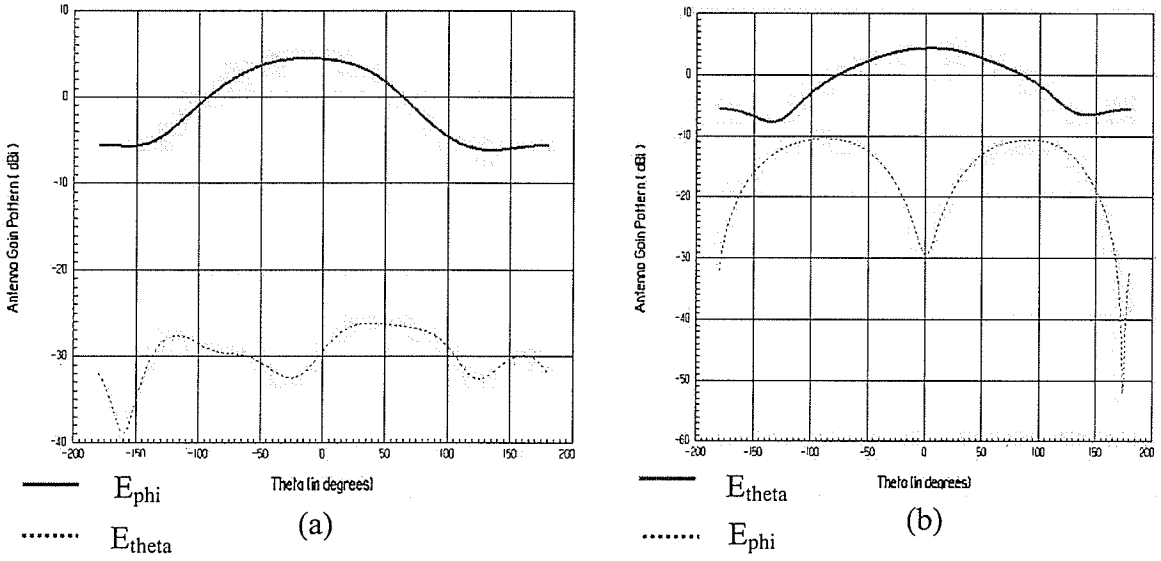

Figure 4.6. Antenna Gain Patterns at the lower part of the frequency range of a Yagi on a plate with a dielectric constant of 10.2, an electrical length of $1.04\lambda_g$ and the thickness of $0.213\lambda_g$, (a) radiation pattern at 9.1 GHz at phi=0, (b) radiation pattern at 9.1 GHz at phi=90.

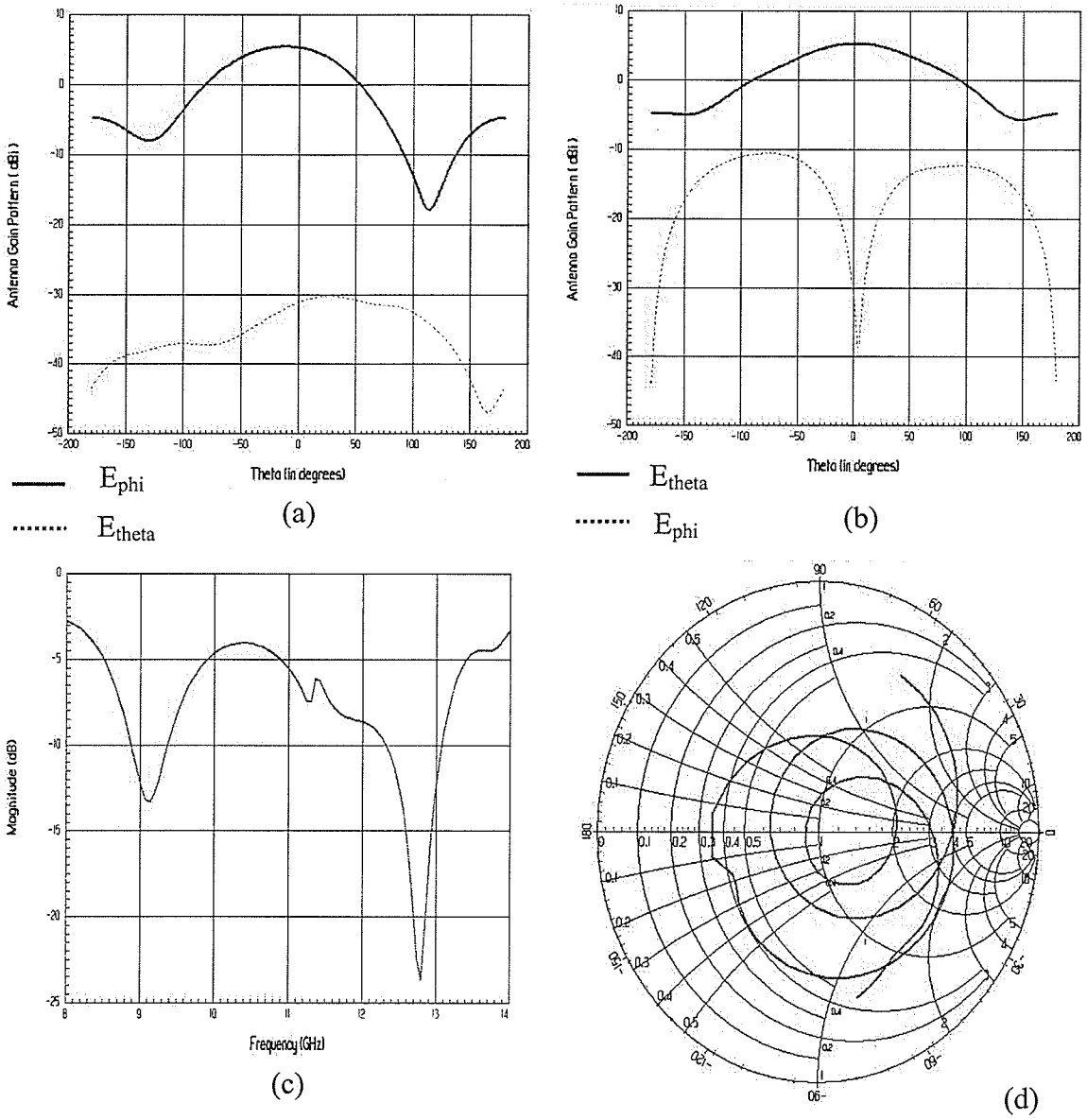

Figure 4.7. Antenna Gain Patterns and Return Loss at the center frequency of a Yagi on a plate with a dielectric constant of 10.2, electrical length of $1.04\lambda_g$ and thickness of $0.266\lambda_g$, (a) radiation pattern at 10 GHz at phi=0, (b) radiation pattern at 10 GHz at phi=90, (c) linear plot of a return loss, (d) return loss on a smith chart.

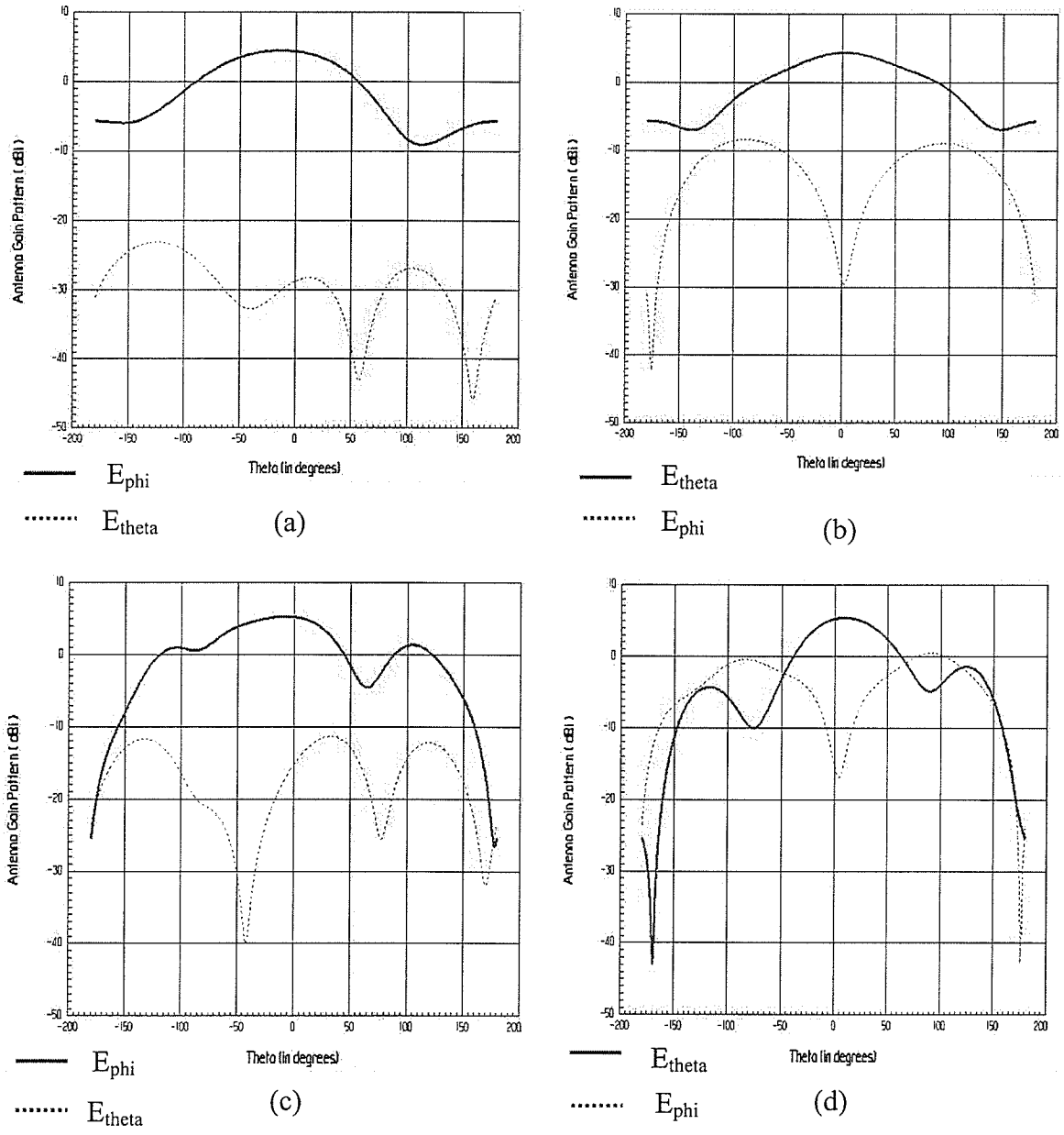

Figure 4.8. Antenna Gain Patterns at 2 resonances of a Yagi on a plate with a dielectric constant of 10.2, electrical length of $1.04\lambda_g$ and thickness of $0.266\lambda_g$, (a) radiation pattern at 9.1 GHz at phi=0, (b) radiation pattern at 9.1 GHz at phi=90, (c) radiation pattern at 12.8 GHz at phi=0, (d) radiation pattern at 12.8 GHz at phi=90.

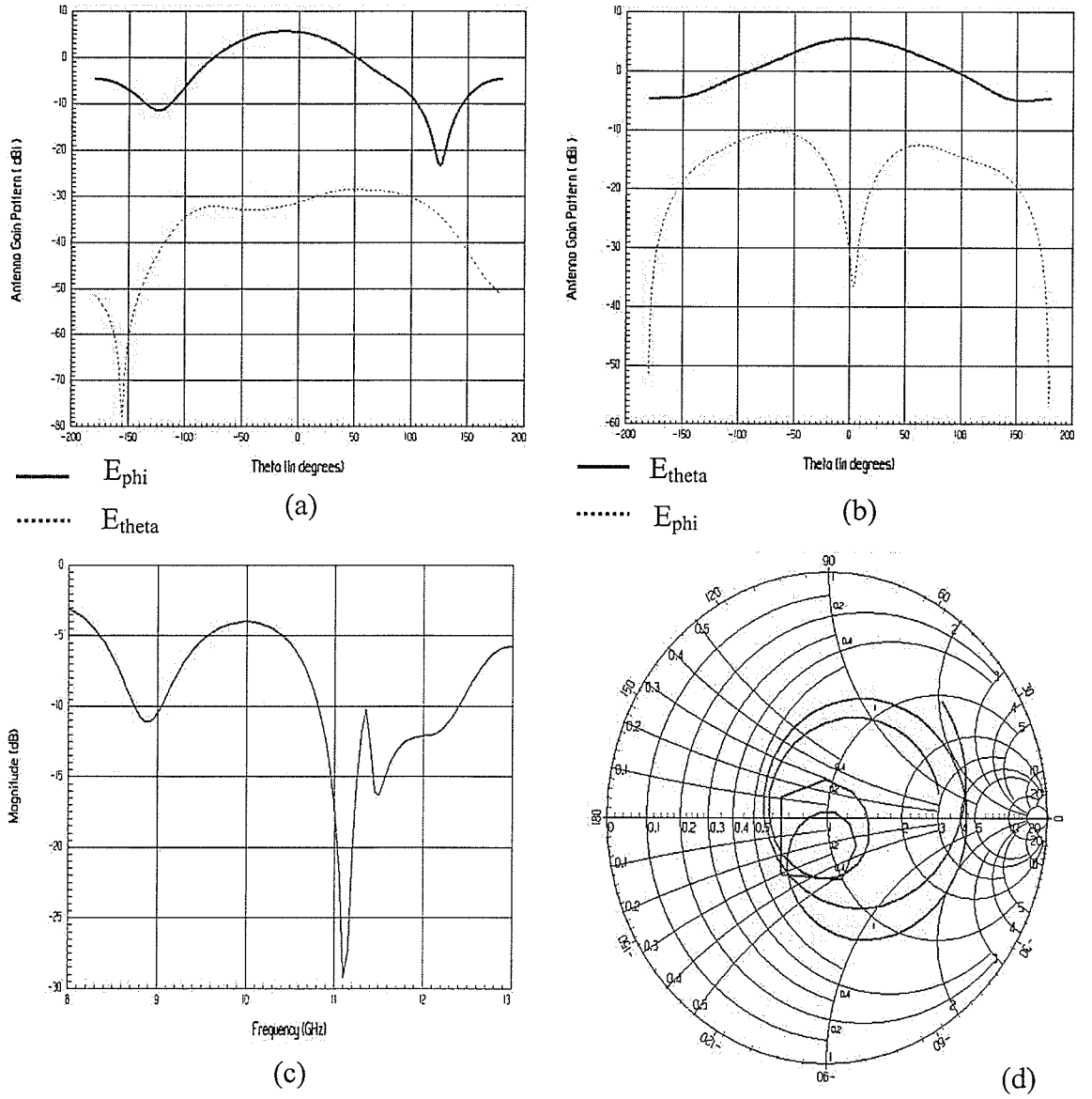

Figure 4.9. Antenna Gain Patterns and Return Loss at the center frequency of a Yagi on a plate with a dielectric constant of 10.2, electrical length of $1.04\lambda_g$ and thickness of $0.3195\lambda_g$, (a) radiation pattern at 10 GHz at phi=0, (b) radiation pattern at 10 GHz at phi=90, (c) linear plot of a return loss, (d) return loss on a smith chart.

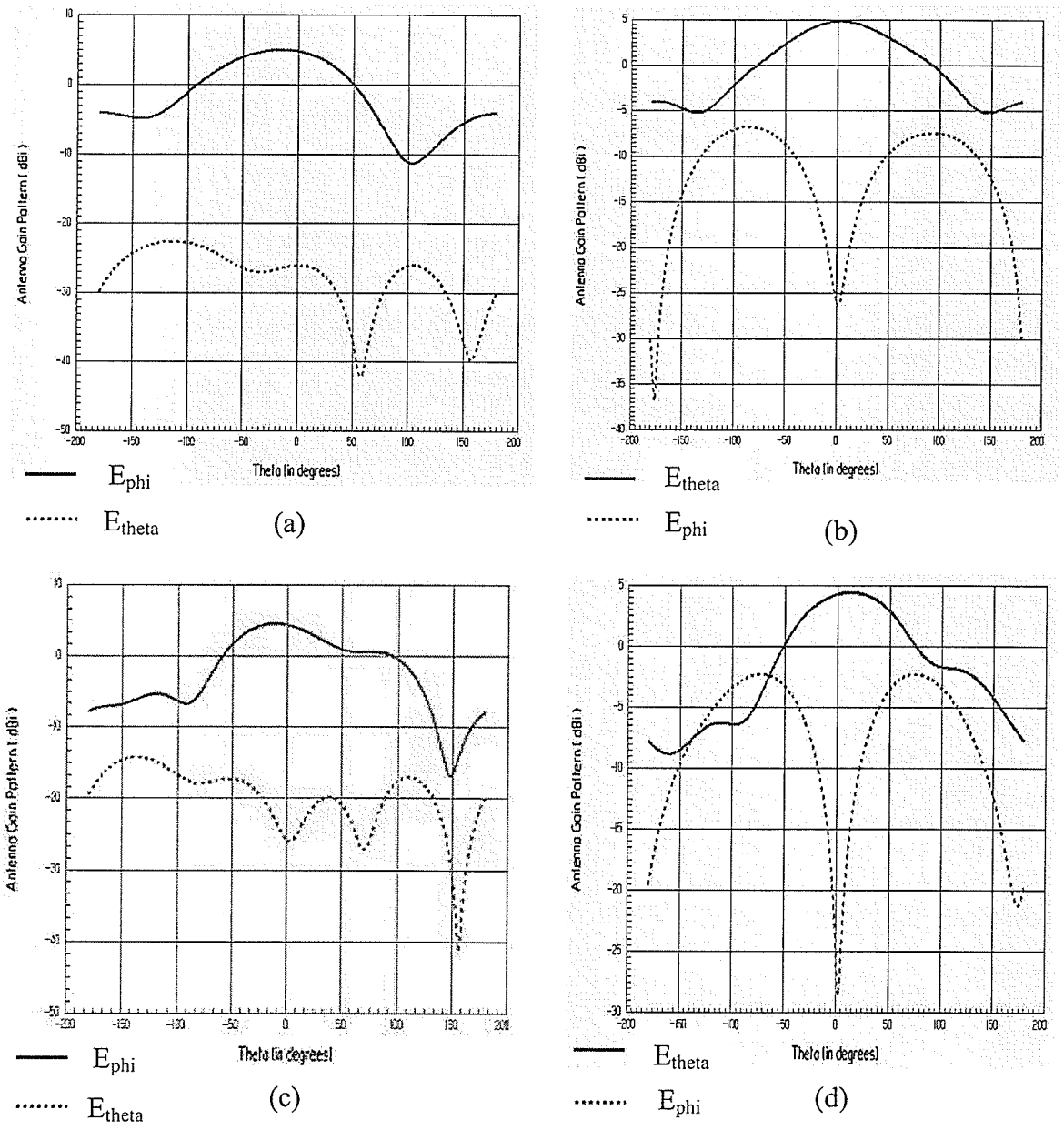

Figure 4.10. Antenna Gain Patterns at 2 resonances a Yagi on a plate with a dielectric constant of 10.2, electrical length of $1.04\lambda_g$ and thickness of $0.3195\lambda_g$, (a) radiation pattern at 8.9 GHz at phi=0, (b) radiation pattern at 8.9 GHz at phi=90, (c) radiation pattern at 11.1 GHz at phi=0, (d) radiation pattern at 11.1 GHz at phi=90.

Table 4.1 summarizes the above data and indicates that as plate thickness increases, we observe that the directivity also increases. Studies demonstrate that the beam tilt can also be controlled as it appears to oscillate in both phi=0° and phi=90° planes (more so in phi=0° plane than in phi=90° plane). It is worthwhile to observe row 2 in the table, which shows the least tilt. Next point (in row 3) is when higher order slab modes start coming into play. As we increase the thickness of the plate from this point on, we observe further changes in the tilt due to the influence of higher order slab modes which however appear to be less rapid than before the appearance of higher order slab modes. Hence, higher order slab modes slow down or bring balance to the beam tilt.

Table 4.1: Pattern data for the microstrip-fed yagi (ε_r=10.2, length=λ_g, b=1.3163λ_g, freq = 10GHz), λ_g=9.4mm.

Plate thickness (λ_g)	Maximum Gain (dB) E-plane (phi=90)	Maximum Gain (dB) H-plane (phi=0)	Beam Tilt (θ) E-plane (phi=90)	Beam Tilt (θ) H-plane (phi=0)
0.1065	4.956592	5.047873	2	-15
0.1597	4.993862	5.008629	0	-6
0.213	5.163792	5.292143	4	-14
0.266	5.372999	5.599435	2	-15
0.3195	5.847584	5.944378	-1	-10

Table 4.2 illustrates that as plate thickness increases, we observe rapid changes in return loss, center frequency as well as the impedance bandwidth before reaching the plate thickness of 0.213λ_g when higher order slab modes start coming into play. In this range we observe that the values of center frequency and impedance bandwidth both decrease more so for thinner plates than for thicker. We also observe a rapid decrease in the return loss until the point when higher order modes start coming into play beyond which values of return loss rise again. Further increases in the thickness cause a split in

the return loss, center frequency and impedance bandwidth causing two resonances. The center frequency and impedance bandwidth for the first resonance continue to decrease although not as rapidly as before. On the other hand, values of the return loss continue to increase for first resonance condition and decrease for second resonance condition. The center frequency for second resonance condition first shifts up in frequency and then starts decreasing with the gap between the two resonances closing. The impedance bandwidth at second resonance starts rapidly increasing and the gap between the values at two resonances grows or diverges.

Table 4.2: Return Loss data for the microstrip-fed yagi (ε_r=10.2, length=λ_g, b=1.3163λ_g, freq = 10GHz), λ_g=9.4mm.

Plate thickness (λ_g)	Return Loss (dB)	Frequency (GHz)	Impedance Bandwidth (%)
0.1065	-18	10.2	18.63
0.1597	-34.5	9.7	10.31
0.213	-17.2	9.4	7.45
0.266	-13.5/-23.5	9.1/12.8	4.95/6.25
0.3195	-11/-29	8.9/11.1	3.93/14.41

4.3: Effects of Changing Thickness On High Permittivity Plates With a Parasitic

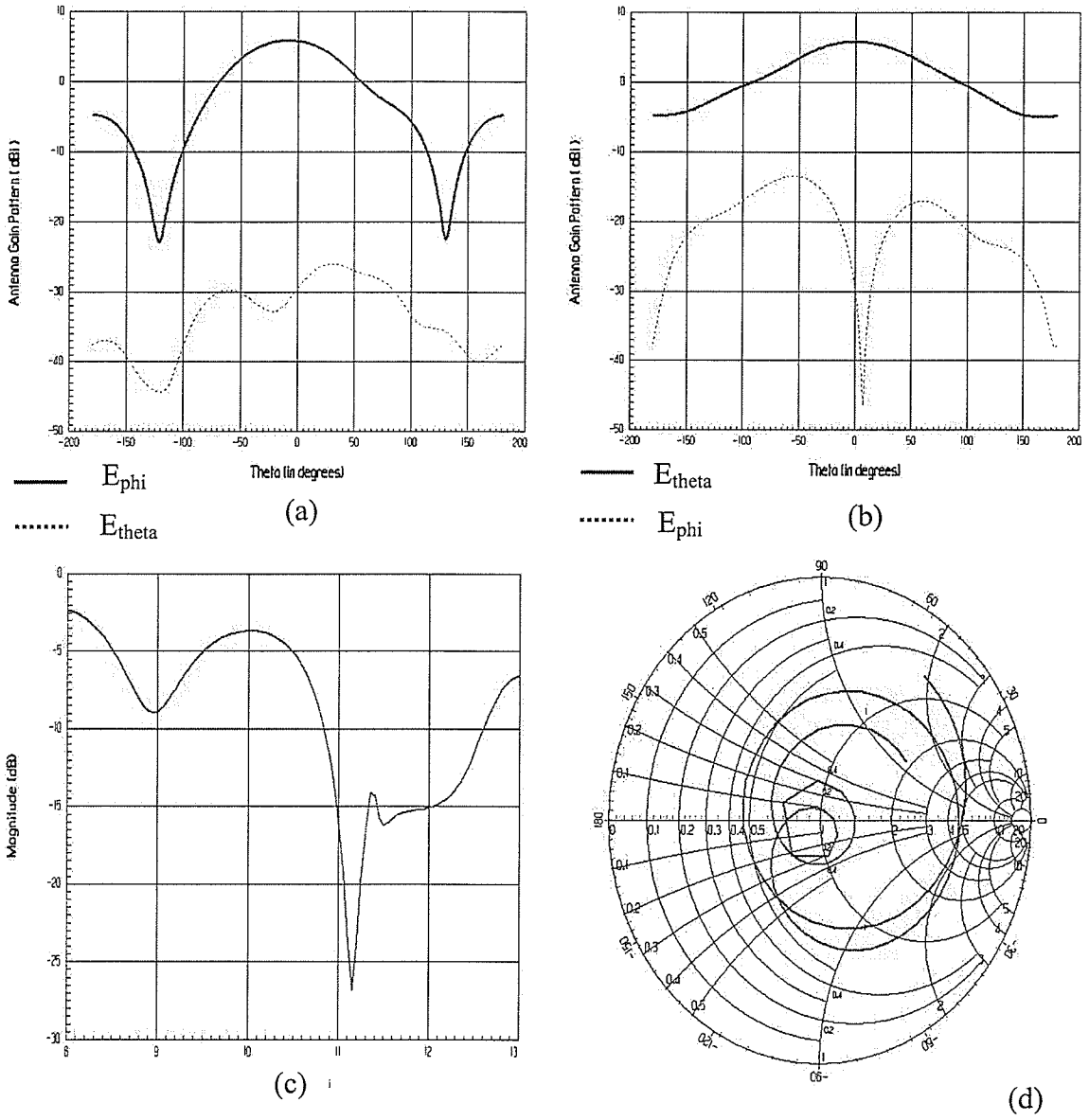

Figure 4.11. Antenna Gain Patterns and Return Loss at the center frequency of a Yagi on a plate with a director, dielectric constant of 10.2, electrical length of $1.04\lambda_g$ and thickness of $0.3195\lambda_g$, (a) radiation pattern at 10 GHz at phi=0, (b) radiation pattern at 10 GHz at phi=90, (c) linear plot of a return loss, (d) return loss on a smith chart.

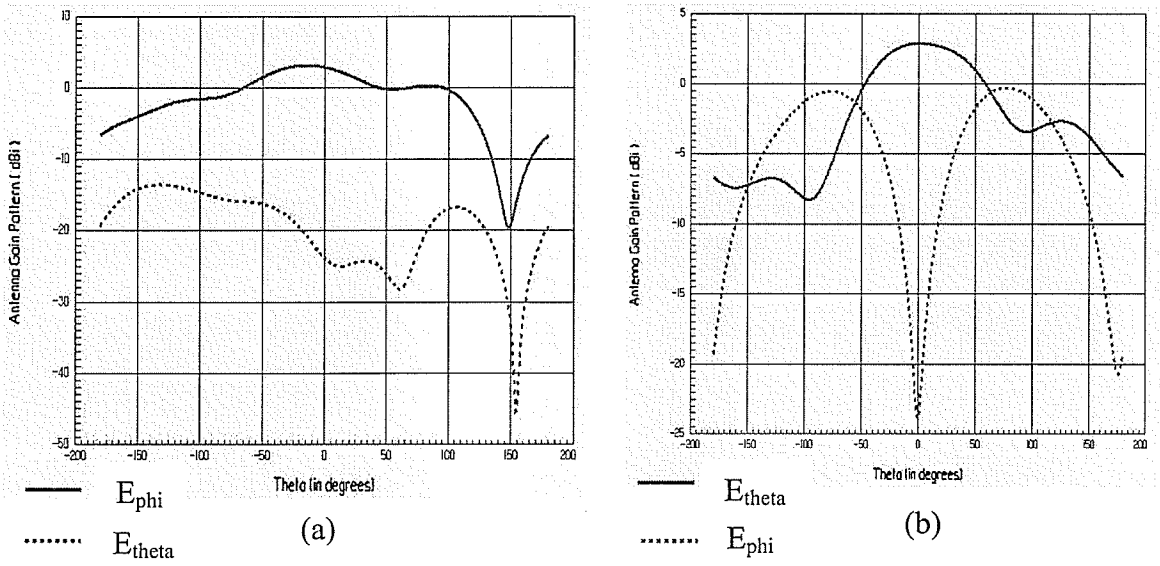

Figure 4.12. Antenna Gain Patterns at resonance of a Yagi on a plate with a director, dielectric constant of 10.2, electrical length of $1.04\lambda_g$ and thickness of $0.3195\lambda_g$, (a) radiation pattern at 11.15 GHz at phi=0, (b) radiation pattern at 11.15 GHz at phi=90.

Figures 4.11 (page 87) and 4.12 demonstrate that although the director effect on pattern directivity is negligible for deeper plates, we observe that it is detrimental in terms of pattern bandwidth (as shown in figure 4.12 and compared with figure 4.10).

At first glance table 4.3 indicates that the slab modes prevent any increases in directivity despite the director placement; directors though are able to stabilize the beam tilt, which oscillates without them (as shown in table 4.1).

Table 4.3: Pattern data for the microstrip-fed yagi (ε_r=10.2, length=λ_g, b=1.3163λ_g, freq = 10GHz) with director, λ_g=9.4mm.

Plate thickness (λ_g)	Maximum Gain (dB) E-plane (phi=90)	Maximum Gain (dB) H-plane (phi=0)	Beam Tilt (θ) E-plane (phi=90)	Beam Tilt (θ) H-plane (phi=0)
0.213	5.654739	5.704916	0	-7
0.266	5.814426	5.916715	-1	-9
0.3195	5.820048	5.919864	-1	-9

Table 4.4 shows that directors increase the return loss for the first resonance (which is kept constant) and reduce its value for the 2nd resonance. The center frequency and impedance bandwidth remain virtually unchanged, except that the impedance bandwidth at the first resonance is discounted because the value of its return loss is above –10dB.

Table 4.4: Return Loss data for the microstrip-fed yagi (ε_r=10.2, length=λ_g, b=1.3163λ_g, freq = 10GHz) with director, λ_g=9.4mm.

Plate thickness (λ_g)	Return Loss (dB)	Frequency (GHz)	Impedance Bandwidth (%)
0.213	-9.5	9.3	0
0.266	-9/-32.5	9.1/12.8	6.25
0.3195	-9/-26.75	8.95/11.15	16.14

4.4: Effects of Changing Thickness On Low Permittivity Plates

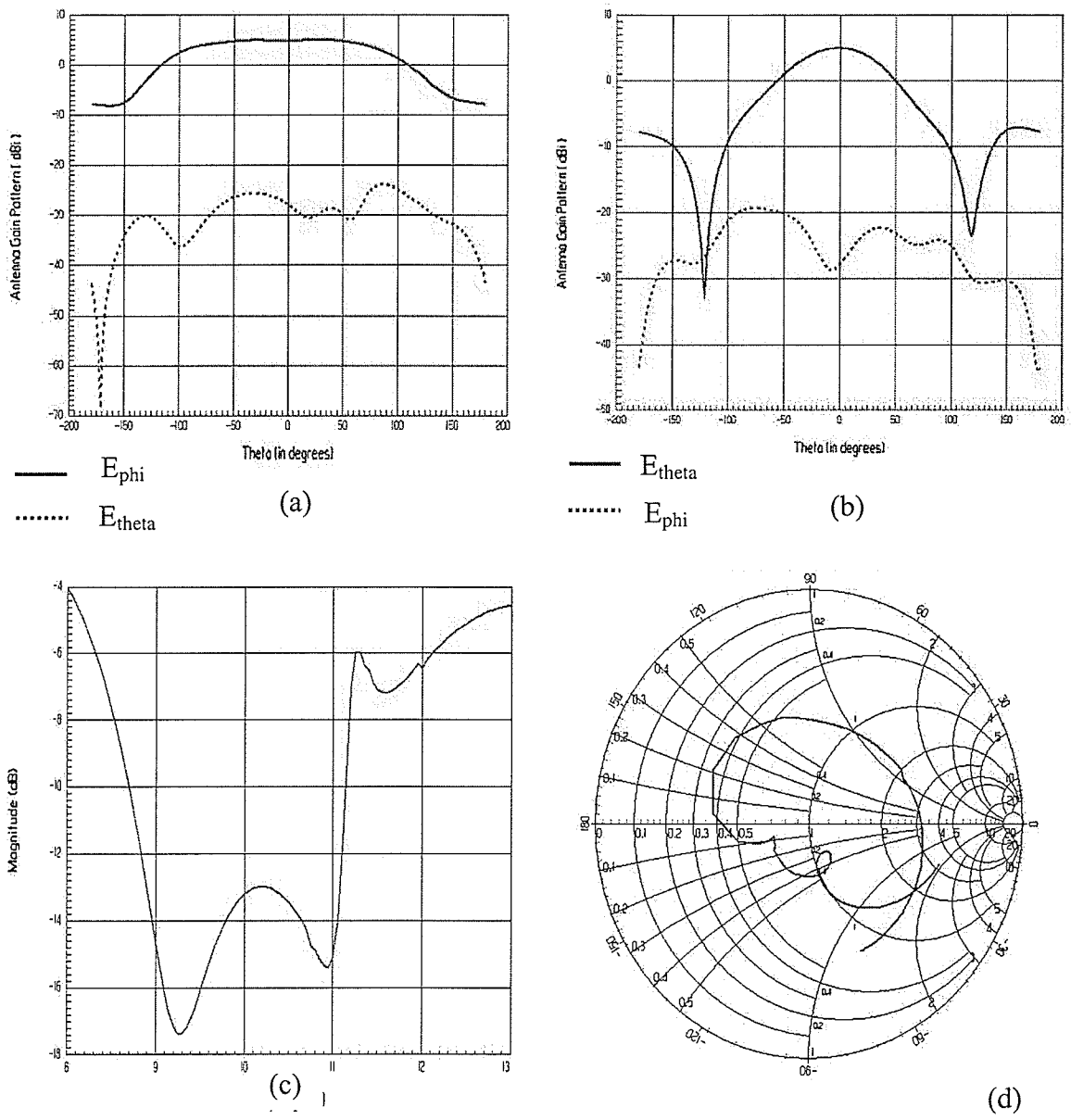

Figure 4.13. Antenna Gain Patterns and Return Loss at the center frequency of a Yagi on a plate with a dielectric constant of 2.5, electrical length of λ_g and thickness of $0.0526\lambda_g$, (a) radiation pattern at 10 GHz at phi=0, (b) radiation pattern at 10 GHz at phi=90, (c) linear plot of a return loss, (d) return loss on a smith chart.

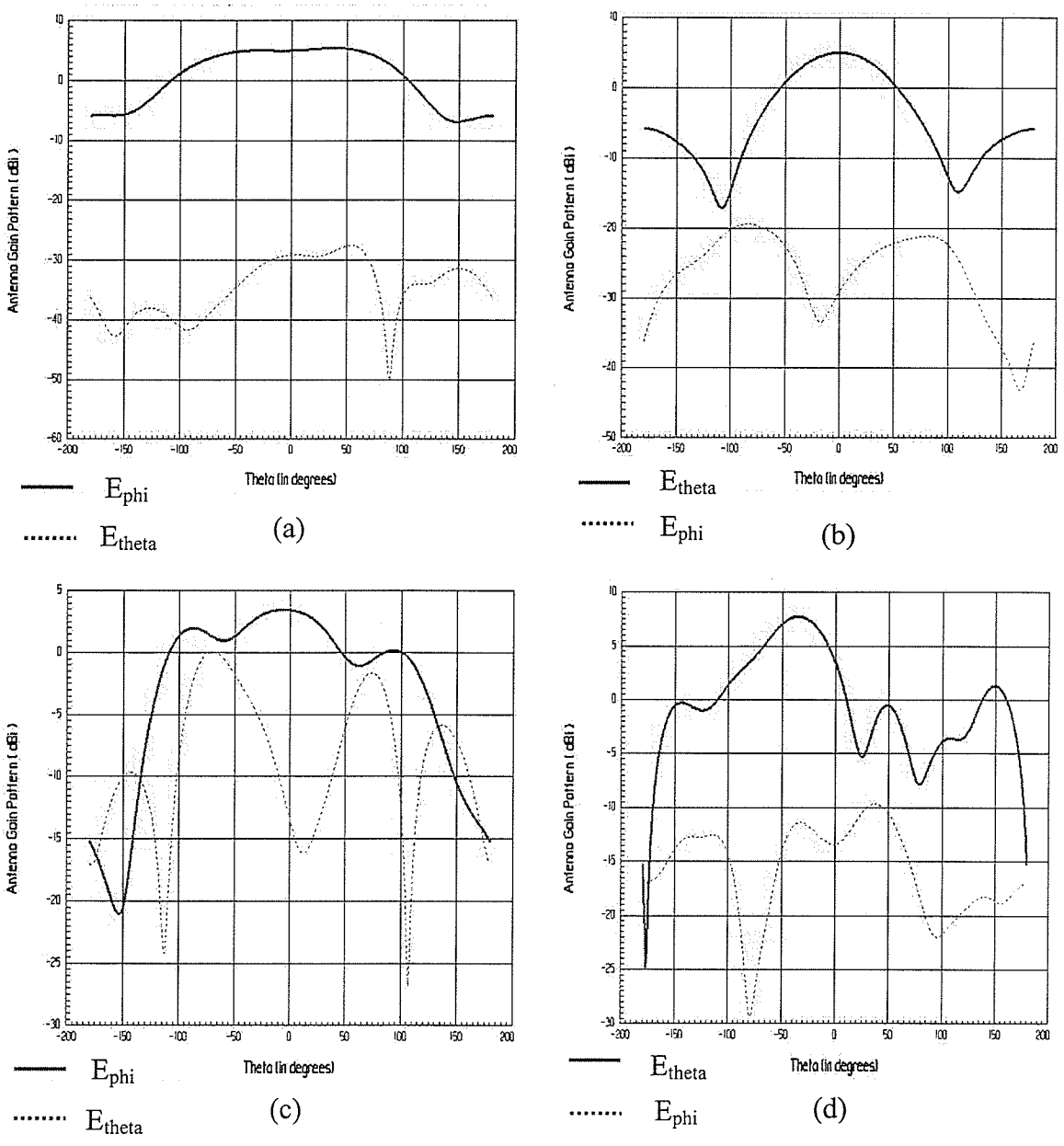

Figure 4.14. Antenna Gain Patterns within the impedance bandwidth of a Yagi on a plate with a dielectric constant of 2.5, electrical length of λ_g and thickness of $0.0526\lambda_g$, (a) radiation pattern at 8.7 GHz at phi=0, (b) radiation pattern at 8.7 GHz at phi=90, (c) radiation pattern at 11.2 GHz at phi=0, (d) radiation pattern at 11.2 GHz at phi=90.

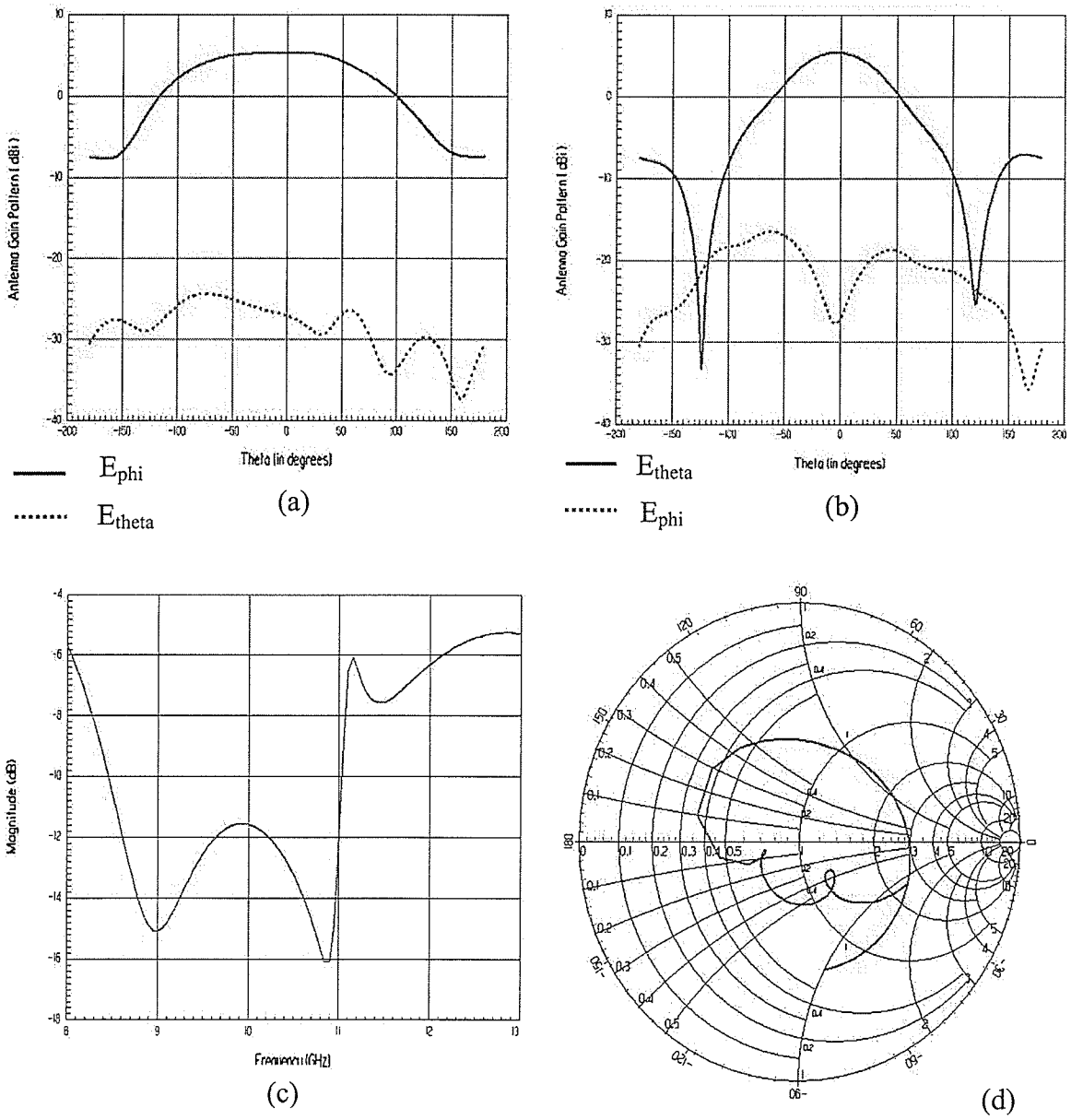

Figure 4.15. Antenna Gain Patterns and Return Loss at the center frequency of a Yagi on a plate with a dielectric constant of 2.5, electrical length of λ_g and thickness of $0.10526\lambda_g$, (a) radiation pattern at 10 GHz at phi=0, (b) radiation pattern at 10 GHz at phi=90, (c) linear plot of a return loss, (d) return loss on a smith chart.

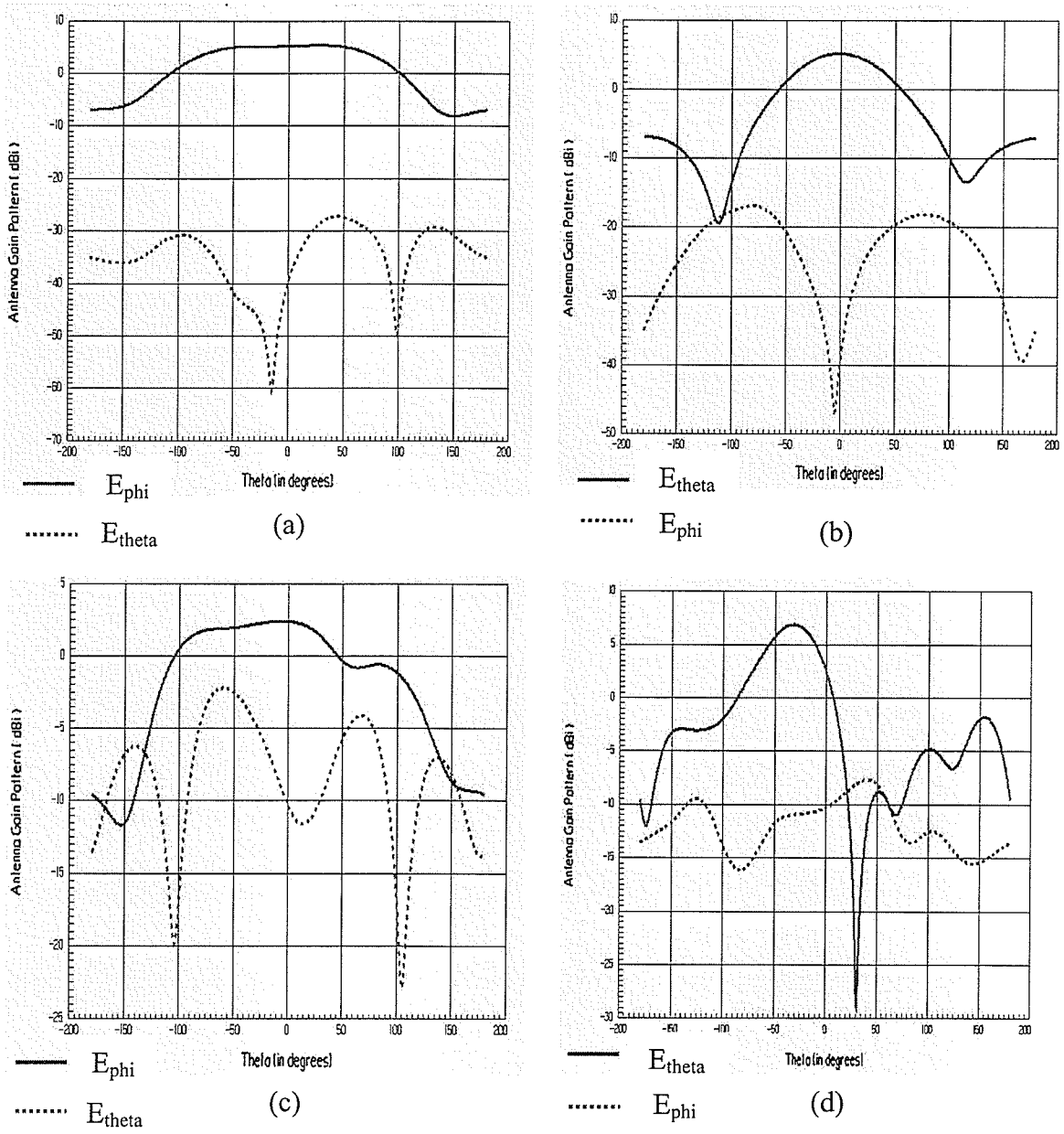

Figure 4.16. Antenna Gain Patterns within the impedance bandwidth of a Yagi on a plate with a dielectric constant of 2.5, electrical length of λ_g and thickness of $0.10526\lambda_g$, (a) radiation pattern at 8.45 GHz at phi=0, (b) radiation pattern at 8.45 GHz at phi=90, (c) radiation pattern at 11.05 GHz at phi=0, (d) radiation pattern at 11.05 GHz at phi=90.

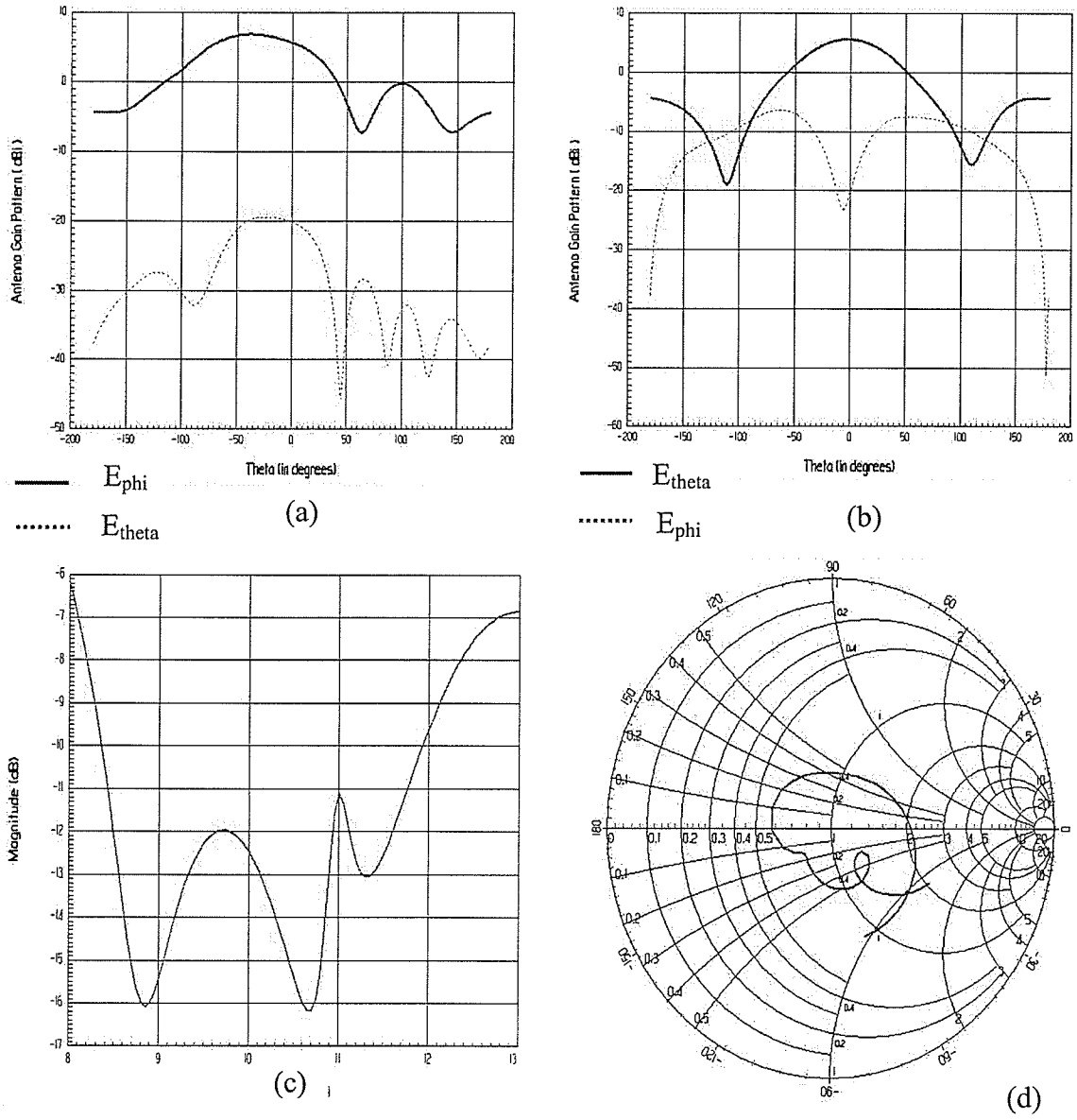

Figure 4.17. Antenna Gain Patterns and Return Loss at the center frequency of a Yagi on a plate with a dielectric constant of 2.5, electrical length of λg and thickness of $0.3158\lambda_g$, (a) radiation pattern at 10 GHz at phi=0, (b) radiation pattern at 10 GHz at phi=90, (c) linear plot of a return loss, (d) return loss on a smith chart.

As illustrated in figures 4.13 through 4.18 (pages 90 to 95), extending the plate thickness and addition of slab modes has no effect on pattern bandwidth.

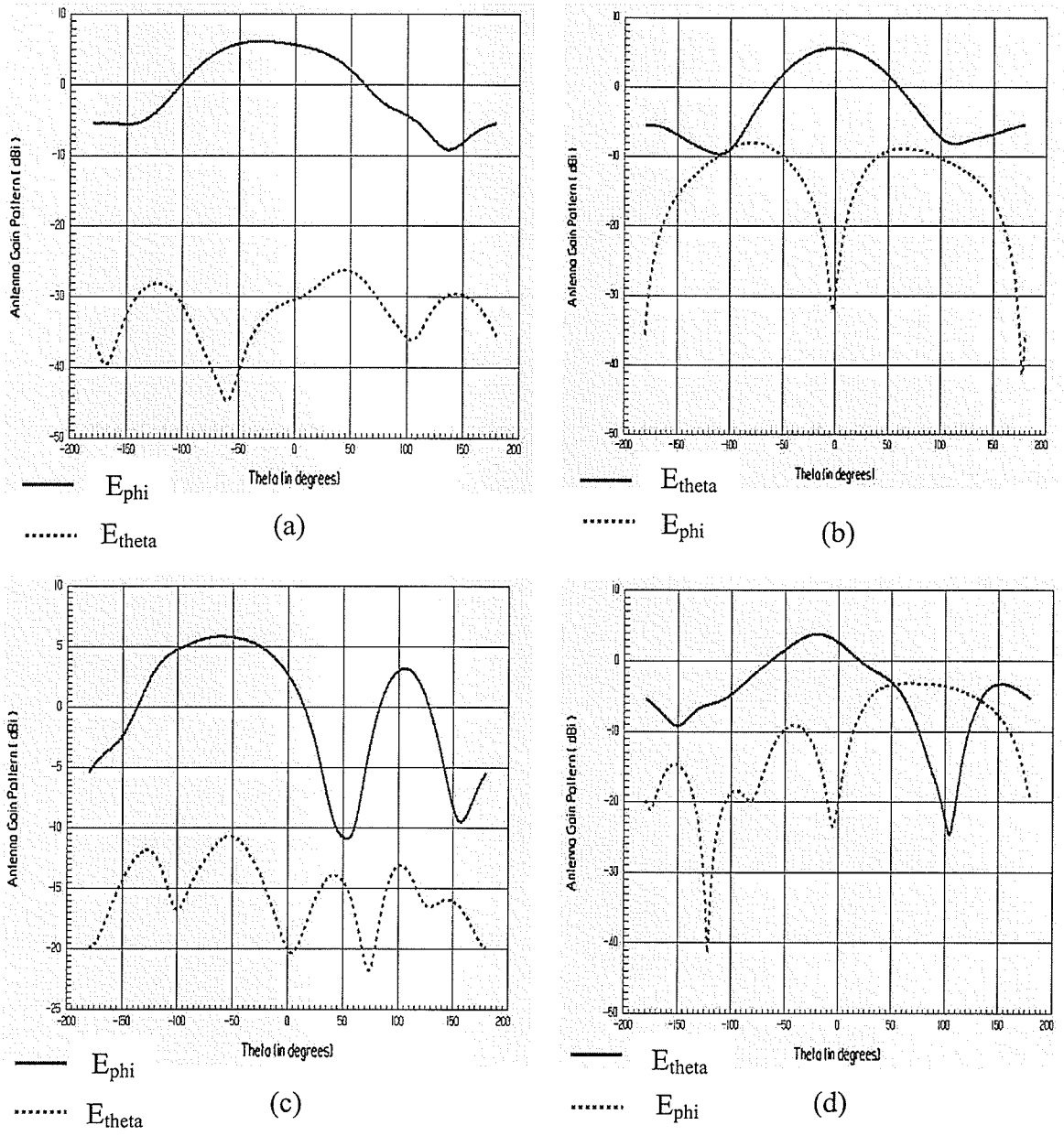

Figure 4.18. Antenna Gain Patterns for a Yagi on a plate with a dielectric constant of 2.5, electrical length of λ_g and thickness of $0.3158\lambda_g$, (a) radiation pattern at 8.35 GHz at phi=0, (b) radiation pattern at 8.35 GHz at phi=90, (c) radiation pattern at 11.95 GHz at phi=0, (d) radiation pattern at 11.95 GHz at phi=90.

Table 4.5 (page 96) illustrates that as plate thickness increases, directivity also increases. We also observe that beam tilt can be controlled as it moves from positive to negative values with respect to $\theta = 0°$ axis (visible mainly in phi=0° plane). Again, let us

Table 4.5: Pattern data for the microstrip-fed yagi (ε_r=2.5, length=λ_g, b=1.3158λ_g, freq = 10GHz), λ_g=19mm.

Plate thickness (λ_g)	Maximum Gain (dB) E-plane (phi=90)	Maximum Gain (dB) H-plane (phi=0)	Beam Tilt (θ) E-plane (phi=90)	Beam Tilt (θ) H-plane (phi=0)
0.0526	4.933858	5.077752	-1	29
0.10526	5.406892	5.391827	-5	10
0.1579	5.710546	5.959967	-2	-30
0.2105	5.759572	6.392823	-2	-35
0.263	6.088521	6.783485	-2	-31
0.3158	5.692418	7.127588	-4	-40

observe row 2 in the table. That is where we see the least tilt. Next point (in row 3) is when higher order slab modes start coming into play. There, we observe a dramatic shift in the tilt.

Table 4.6: Return Loss data for the microstrip-fed yagi (ε_r=2.5, length=λ_g, b=1.3158λ_g, freq = 10GHz), λ_g=19mm.

Plate thickness (λ_g)	Return Loss (dB)	Frequency (GHz)	Impedance Bandwidth (%)
0.0526	-17.4	9.25	25.95
0.10526	-16	10.85	23
0.1579	-16.1	10.85	23.96
0.2105	-16.4	10.8	30.1
0.263	-16.2	10.7	35
0.3158	-16.4	10.7	33.18

As we analyze the first two rows of table 4.6, we observe a change in the value or return loss and center frequency as the slab mode comes into play (in the 2nd row of the table, i.e. for plate thickness of 0.10526λ_g). Further increases in plate thickness and addition of higher order slab modes have little or no effect on values of the return loss or center frequency. They do however increase the impedance bandwidth.

4.5: Effects of Changing Thickness On Low Permittivity Plates With a Parasitic

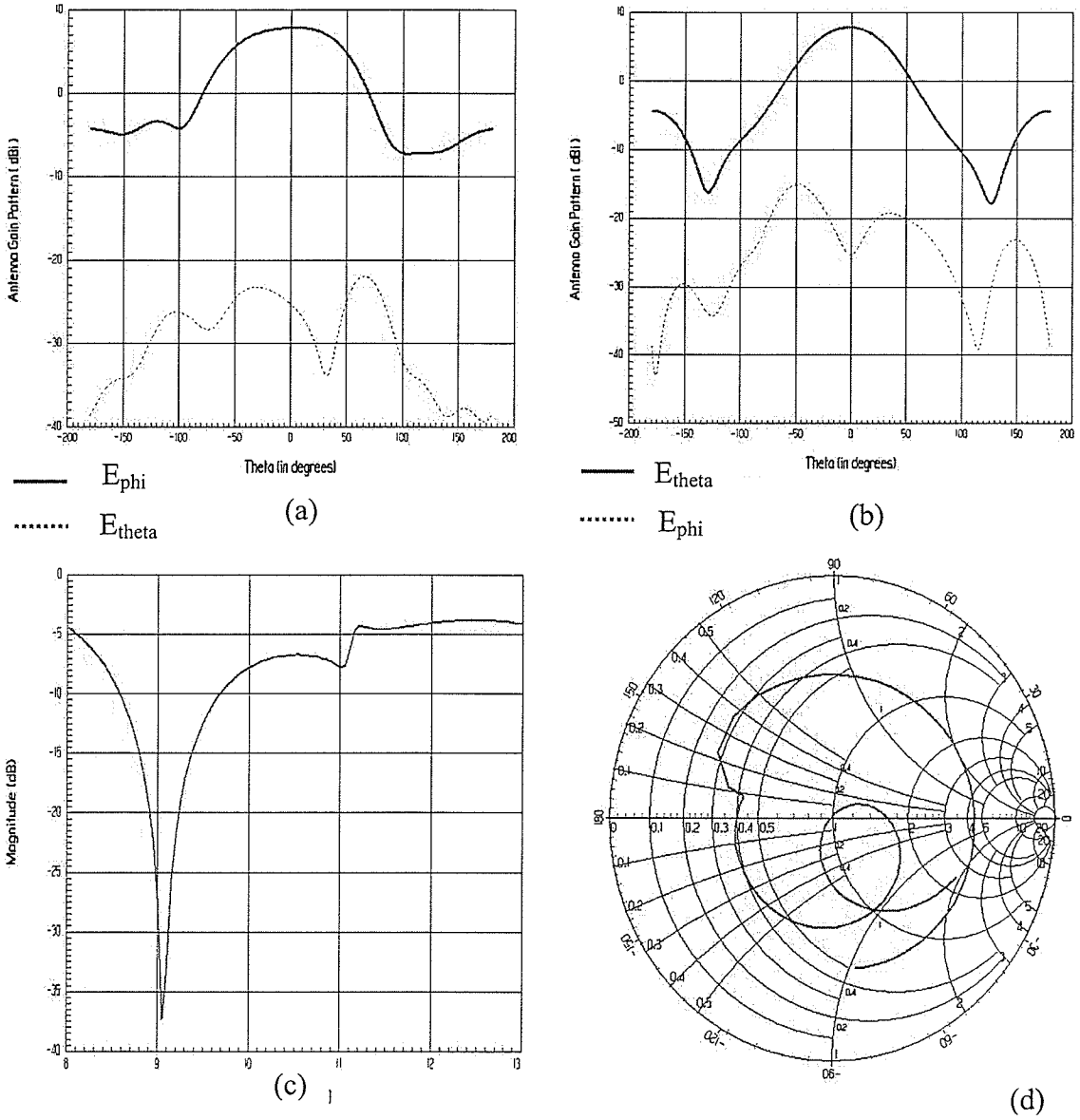

Figure 4.19. Antenna Gain Patterns and Return Loss at the center frequency of a Yagi on a plate with a director, dielectric constant of 2.5, electrical length of λ_g and thickness of $0.10526\lambda_g$, (a) radiation pattern at 10 GHz at phi=0, (b) radiation pattern at 10 GHz at phi=90, (c) linear plot of a return loss, (d) return loss on a smith chart.

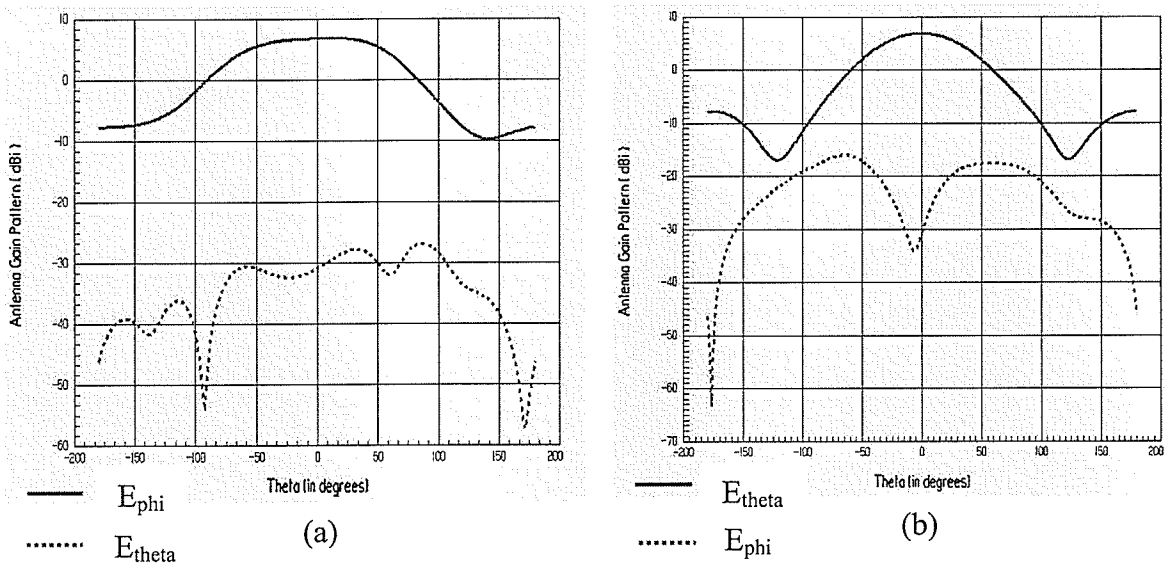

Figure 4.20. Antenna Gain Patterns at resonance of a Yagi on a plate with a director, dielectric constant of 2.5, electrical length of λ_g and thickness of $0.10526\lambda_g$, (a) radiation pattern at 9 GHz at phi=0, (b) radiation pattern at 9 GHz at phi=90.

Figures 4.19 (page 97) and 4.20 show good pattern performance over the specified bandwidth. The pattern bandwidth does not improve with the formation of 2nd resonance as shown in figures 4.21 and 4.22 (pages 99 and 100).

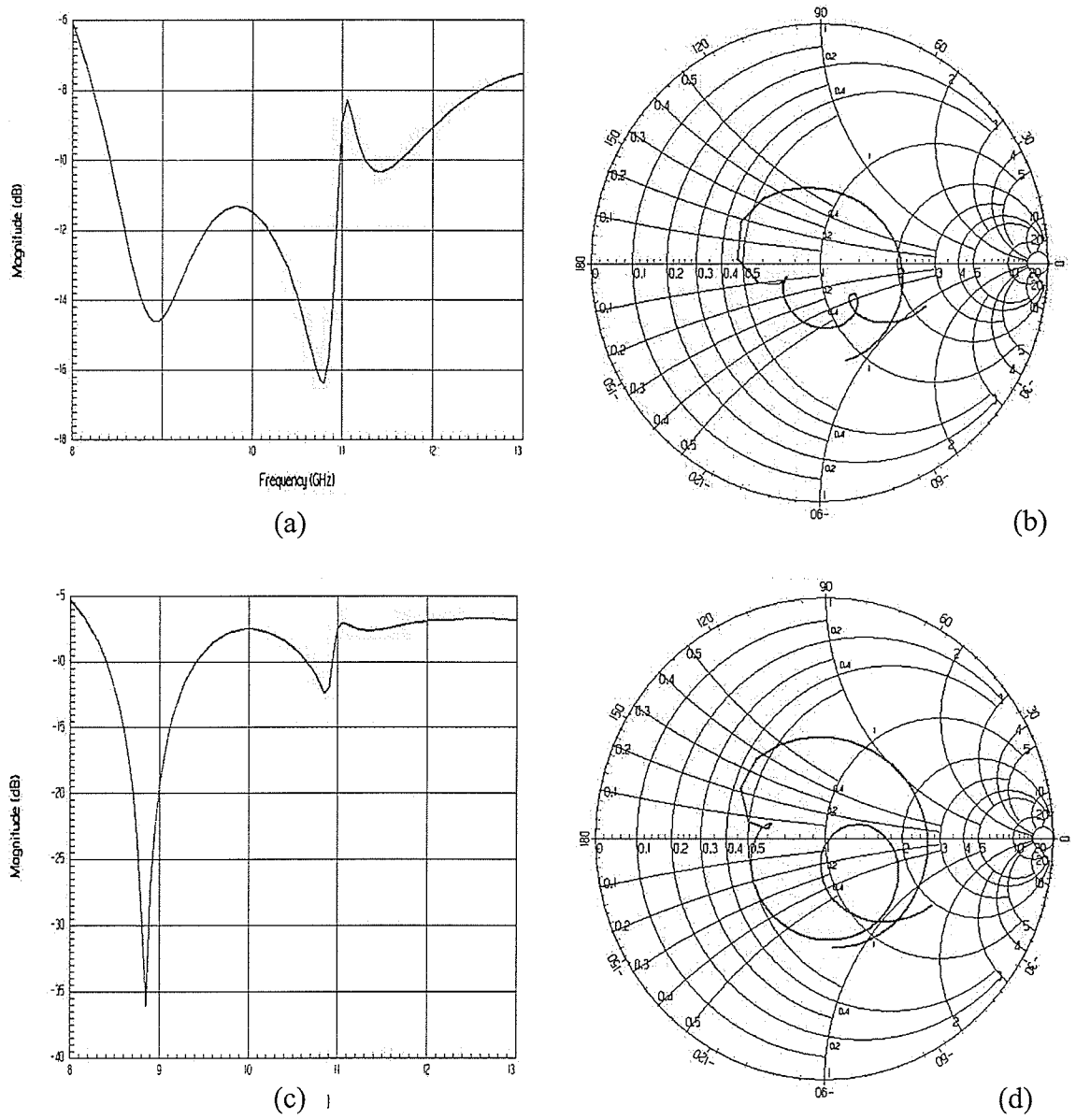

Figure 4.21. Antenna Return Loss for a Yagi on a plate with a dielectric constant of 2.5, electrical length of λg and thickness of $0.21\lambda_g$, (a) linear plot of a return loss without a director, (b) return loss on a smith chart without a director, (c) linear plot of a return loss with a director, (d) return loss on a smith chart with a director.

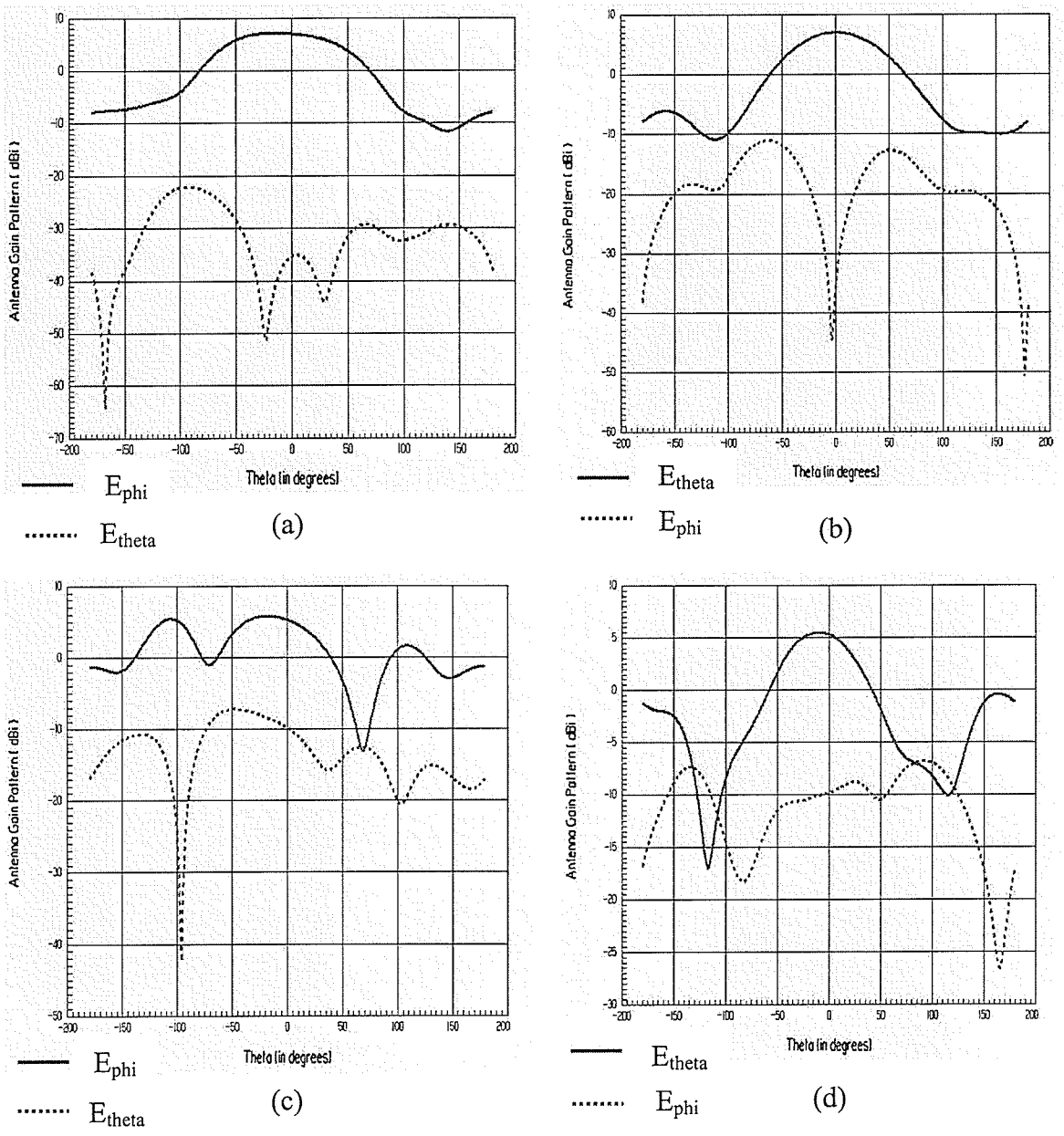

Figure 4.22. Antenna Gain Patterns at 2 resonances of a Yagi on a plate with a director, dielectric constant of 2.5, electrical length of λ_g and thickness of $0.21\lambda_g$, (a) radiation pattern at 8.85 GHz at phi=0, (b) radiation pattern at 8.85 GHz at phi=90, (c) radiation pattern at 10.85 GHz at phi=0, (d) radiation pattern at 10.85 GHz at phi=90.

According to table 4.7 as plate thickness increases, directivity decreases. This shows that the effect of parasitics diminishes with extended thickness and additional slab modes. Beam tilt can also be controlled.

Table 4.7: Pattern data for the microstrip-fed yagi (ε_r=2.5, length=λ_g, b=1.3158λ_g, freq = 10GHz) with director, λ_g=19mm.

Plate thickness (λ_g)	Maximum Gain (dB) E-plane (phi=90)	Maximum Gain (dB) H-plane (phi=0)	Beam Tilt (θ) E-plane (phi=90)	Beam Tilt (θ) H-plane (phi=0)
0.10526	7.844536	7.83955	-2	3
0.1579	8.010752	8.009761	-2	-2
0.2105	7.743955	7.88455	-1	-13
0.263	7.630514	7.779899	-2	-12
0.3158	6.947628	7.533318	-2	-24

Table 4.8 shows that for thinner plates, the dominant slab mode decreases the return loss and impedance bandwidth. Center frequency remains practically unaffected. Higher order slab mode causes two resonances, increasing the return loss and impedance bandwidth at the first resonance. The value of return loss at second resonance decreases; the impedance bandwidth is smaller than at the first resonance but increases more rapidly. The third slab mode cancels the dual frequency behavior. The values of return loss and impedance bandwidth continue to increase.

Table 4.8: Return Loss data for the microstrip-fed yagi (ε_r=2.5, length=λ_g, b=1.3158λ_g, freq = 10GHz) with director, λ_g=19mm.

Plate thickness (λ_g)	Return Loss (dB)	Frequency (GHz)	Impedance Bandwidth (%)
0.10526	-37.5	9.05	12.15
0.1579	-53	8.95	11.17
0.2105	-36/-12	8.85/10.85	11.3/2.76
0.263	-29.5/-13.5	8.75/10.7	11.43/4.67
0.3158	-28	8.75	37.71

4.6: Comparison Studies

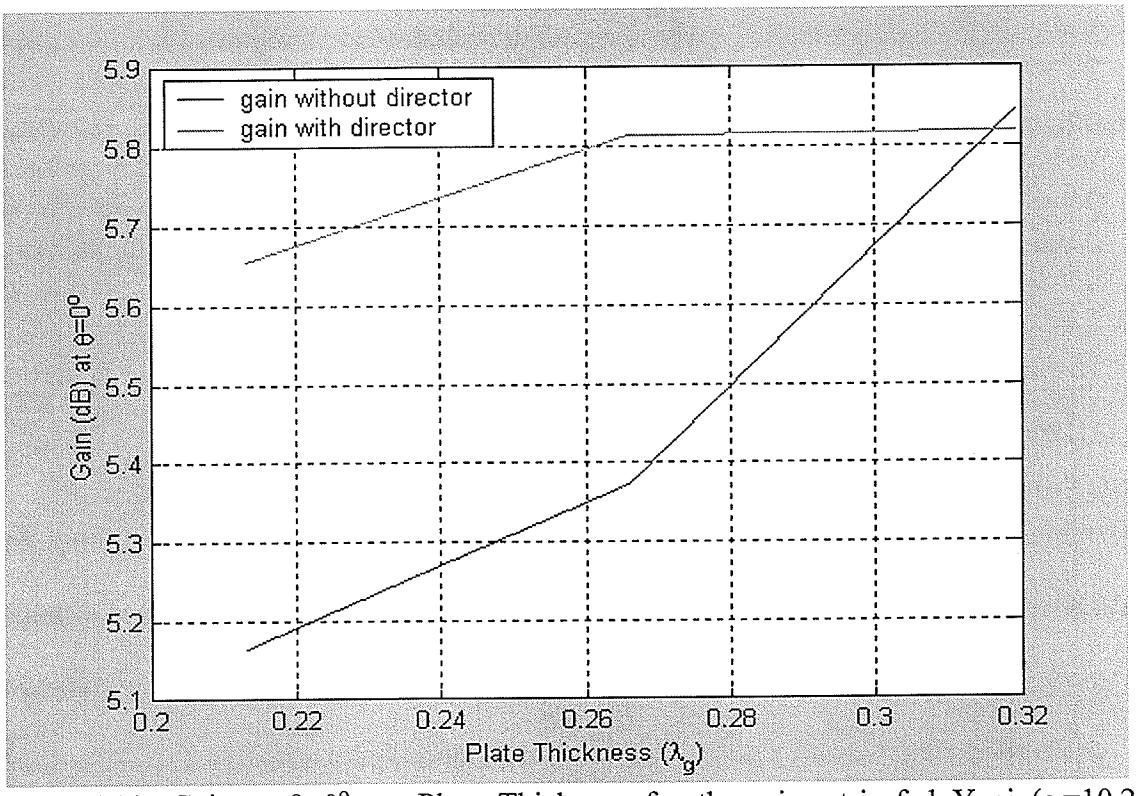

Figure 4.23. Gain at $\theta=0^{\circ}$ vs. Plate Thickness for the microstrip-fed Yagi (ε_r=10.2, length=λ_g, b=1.3163λ_g, freq = 10GHz).

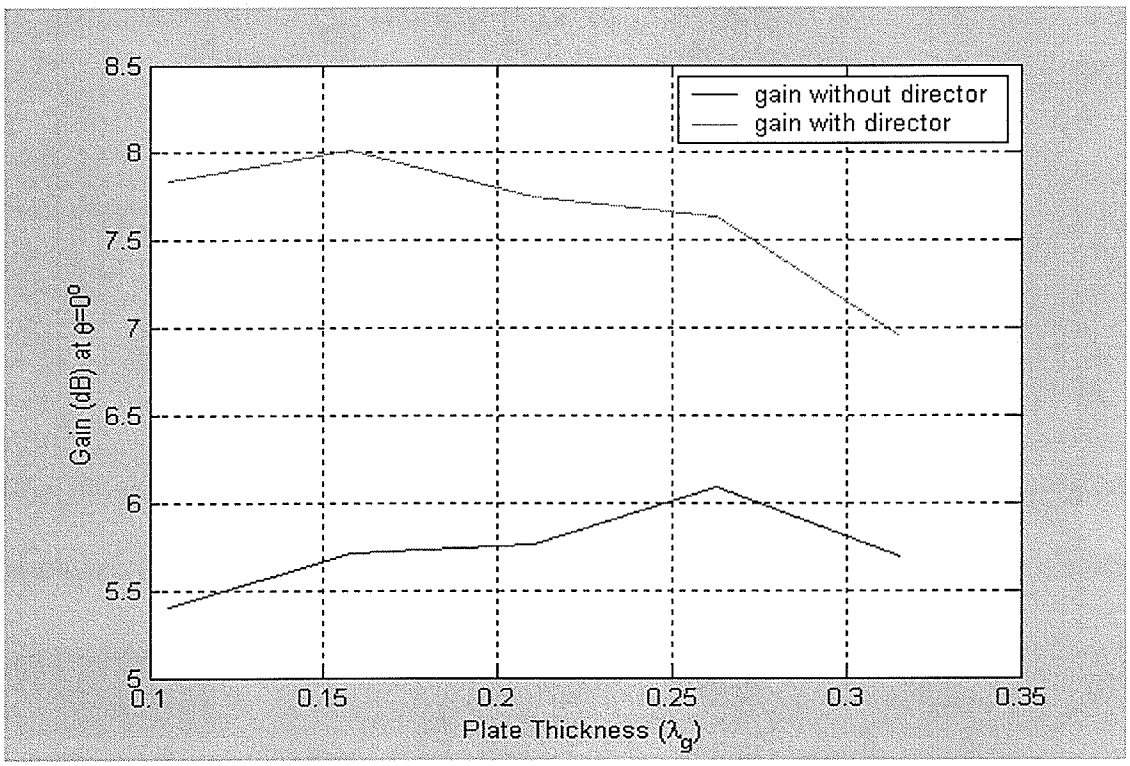

Figure 4.24. Gain at $\theta=0^{o}$ vs. Plate Thickness for the microstrip-fed Yagi (ε_r=2.5, length=λ_g, b=1.3158λ_g, freq = 10GHz).

The gain curves in figures 4.23 (page 102) and 4.24 demonstrate that as plate thickness increases, the effect of parasitics decreases. It appears that the effect is slower in case of plates with lower dielectric constant (as shown in figure 4.24) and greater thicknesses are needed to obtain the crossover between curves as was obtained for plates with higher dielectric constant (shown in figure 4.23).

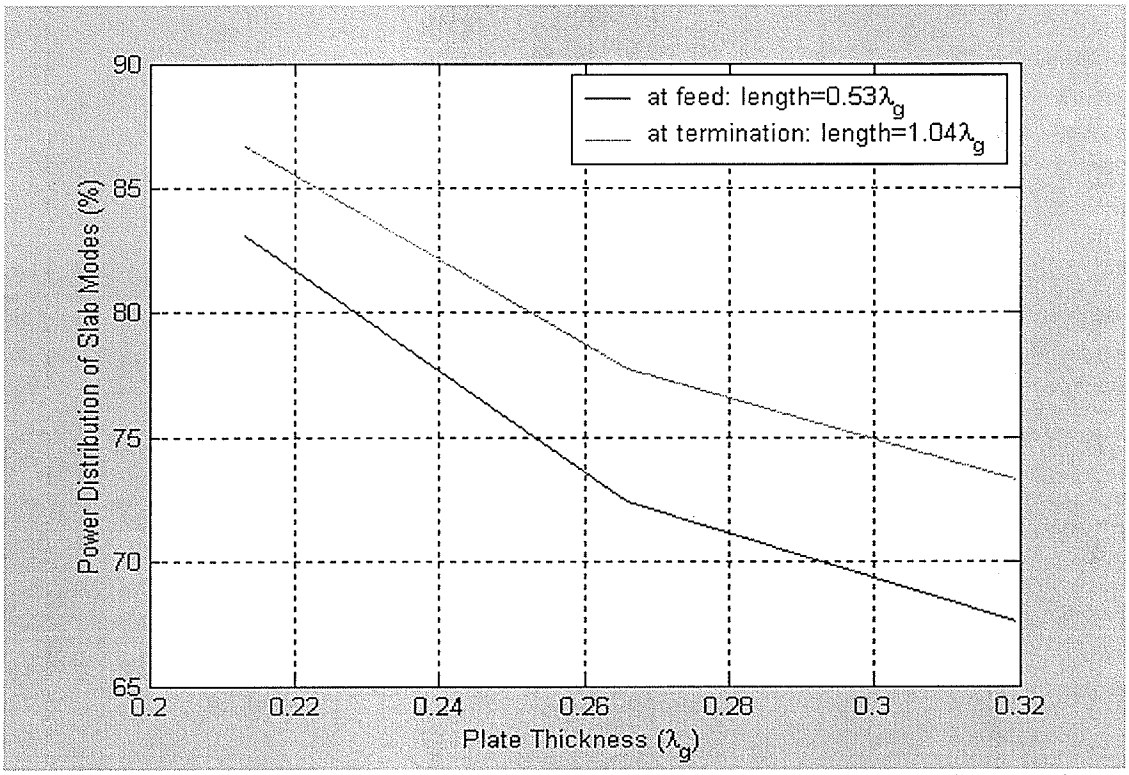

Figure 4.25. Percentage of Power Distribution of Slab Modes vs. Plate Thickness for the two element microstrip-fed Yagi (ε_r=10.2, b=1.3163λ_g, freq = 10GHz) with plate length equal to λ_g.

Figure 4.25 shows rate of decay of slab modes (sum of TM_{10} and TM_{11}) with increasing thickness in higher permittivity plates. It illustrates how slab modes continue to affect the pattern as thickness increases. The two curves diverge from each other indicating that this trend could not be continued indefinitely.

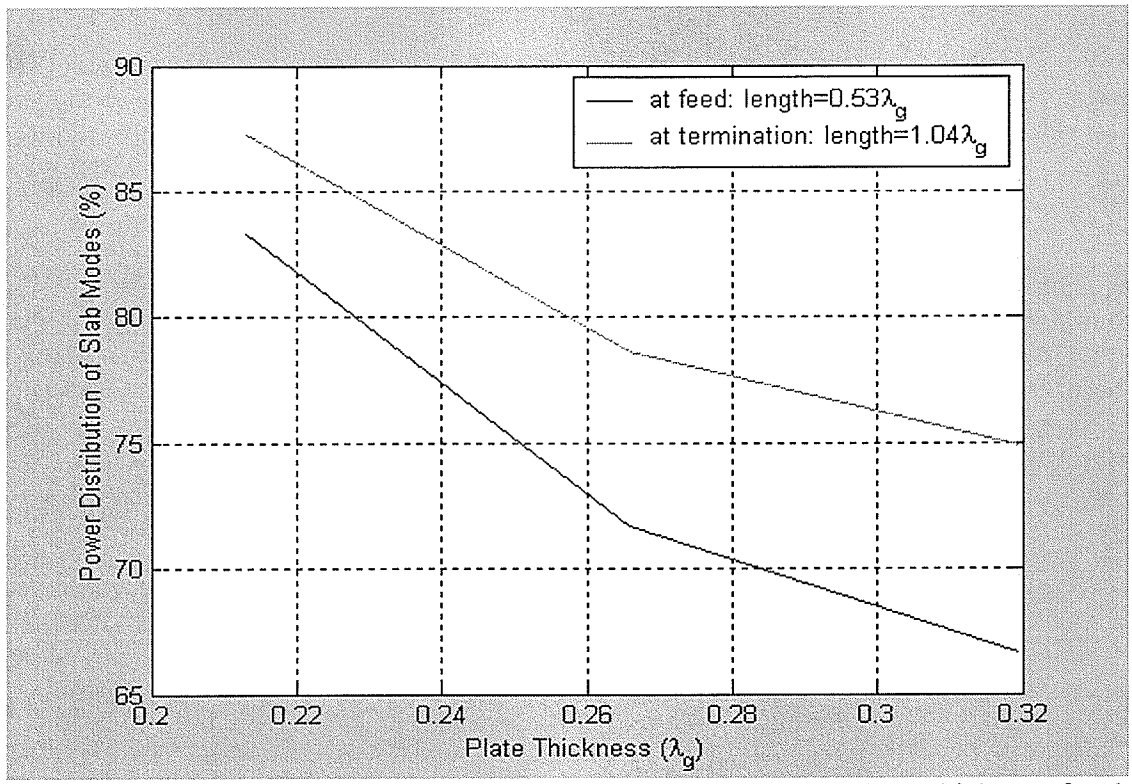

Figure 4.26. Percentage of Power Distribution of Slab Modes vs. Plate Thickness for the three element microstrip-fed Yagi (ε_r=10.2, b=1.3163λ_g, freq = 10GHz) with plate length equal to λ_g.

Figure 4.26 shows the effect of a parasitic on the rate of decay of slab modes (sum of TM_{10} and TM_{11}) with increasing thickness in higher permittivity plates. The figure illustrates how slab modes continue to affect the pattern as thickness increases. The two curves diverge from each other indicating that this trend could not be continued indefinitely. The divergence is however greater in this case than in the case without a parasitic indicating that the director is able to slow down the decay of slab modes.

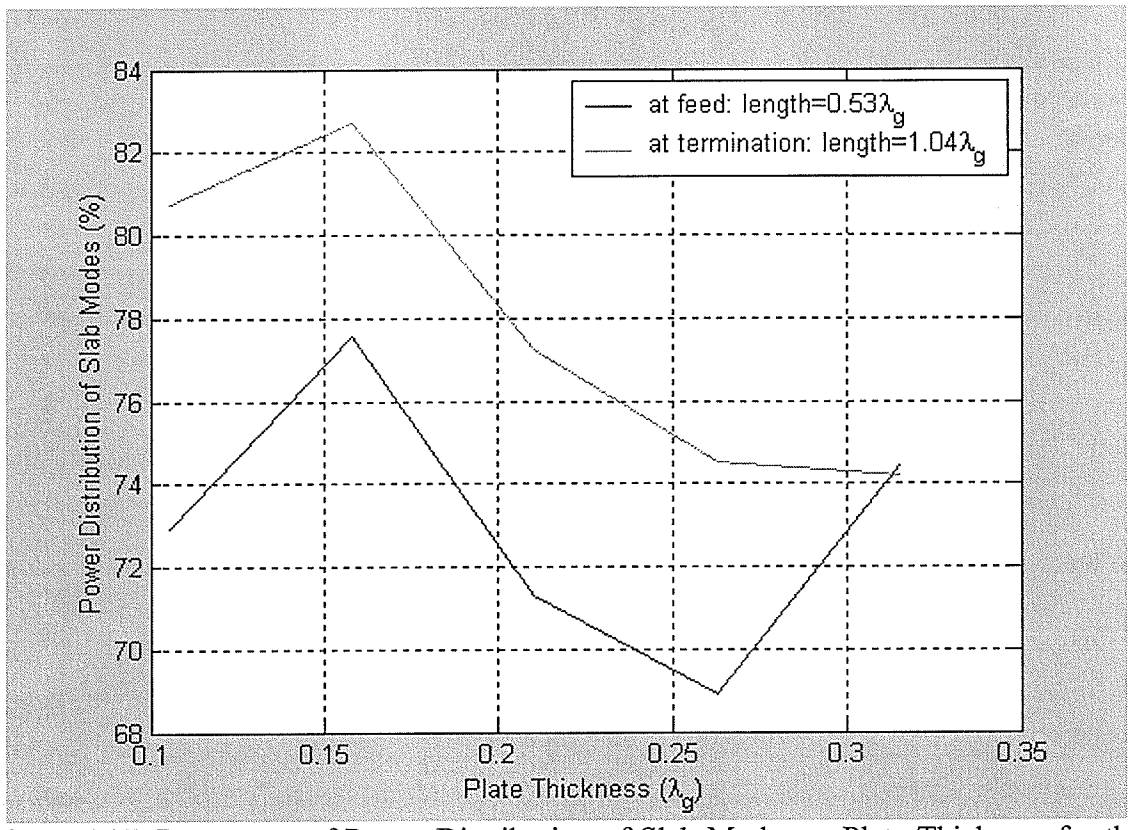

Figure 4.27. Percentage of Power Distribution of Slab Modes vs Plate Thickness for the two element microstrip-fed Yagi (ε_r=2.5, b=1.3158λ_g, freq = 10GHz) with plate length equal to λ_g.

Figures 4.27 and 4.28 (page 107) show the total rate of decay of slab modes (TM_{10}, TM_{11} and TM_{12}) with increasing plate thickness. The behavior appears more complicated in case of plates with lower dielectric constant than in case of plates with higher dielectric constant. It appears that in the region of plate thickness of 0.10526λ_g to plate thickness of 0.1579λ_g, the dominant slab mode (TM_{10}) does not appear to participate in radiation that much. As the higher order mode (TM_{11}) gets introduced, the two slab modes act to radiate. Finally, introduction of a third slab mode (TM_{12}) reduces the effects of slab modes on radiation pattern evident from the rise of the blue curve and its eventual crossover with the green curve. The two curves are almost alike showing that modes decay almost the same way for low-permittivity plates regardless of parasitics.

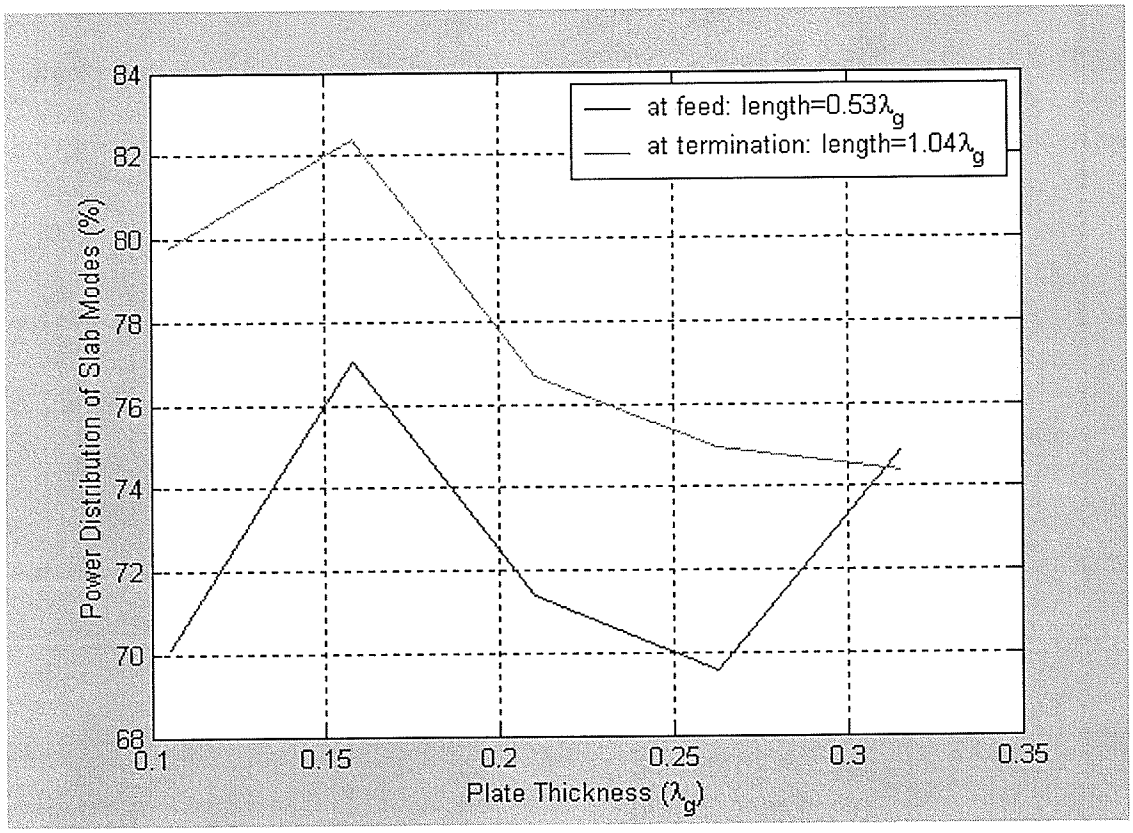

Figure 4.28. Percentage of Power Distribution of Slab Modes vs. Plate Thickness for the three element microstrip-fed Yagi (ε_r=2.5, b=1.3158λ_g, freq = 10GHz) with plate length equal to λ_g.

4.7: Discussion

As we increased the thickness of high permittivity plates we observed a stable radiation pattern performance over the impedance bandwidth. We also observed a formation of a 2^{nd} resonance condition at which radiation pattern became distorted and experienced high levels of cross-polarization. Further increases in thickness reduced radiation pattern distortion and lowered cross-polarization at the 2^{nd} resonance at the expense of impedance bandwidth. The above effects could be attributed to both the destructive as well as constructive interference of higher order slab modes. It was found that adding a parasitic on deeper plates had negligible effect on pattern directivity but it was detrimental in terms of pattern bandwidth.

As we increased the thickness of low permittivity plates, radiation pattern bandwidth remained unaffected with or without directors. The 2^{nd} resonance condition following the placement of a director did not extend the pattern bandwidth. The impedance bandwidth became narrower following the placement of a parasitic as long as the plate remained electrically thin.

4.8: Concluding Remarks

This chapter studied radiation pattern bandwidth, directivity and return loss as functions of plate thickness and dielectric constant with or without directors.

It was concluded that as plate thickness and permittivity increased, directivity and pattern bandwidth remained virtually unchanged. Increases in plate thickness and permittivity did however have a significant effect on return loss and impedance

bandwidth. Two pass bands formed causing an enhancement in impedance bandwidth. At 2^{nd} resonance, radiation pattern experienced distortion and high levels of cross-polarization.

It was then determined that as plate thickness and permittivity increased with inclusion of directors, directivity remained unaffected but there was a reduction in pattern bandwidth.

Increases in plate length and permittivity with directors also caused a reduction in impedance bandwidth and return loss.

Chapter 5: Conclusion and Summary of Future Work

5.1: Conclusion

Chapter 1 gave an overview of an evolution of microstrip-fed Yagi Uda antennas, which are basically a combination of wire Yagis and dielectric rod antennas both of which have been studied in the past.

Modal analysis of chapter 2 has shed light on the radiation characteristics of microstrip-fed Yagi-Uda antennas placed on plates of different dimensions and varying dielectric constants. The percentage of power carried by each mode demonstrated the effects of higher order modes on the far field radiation pattern as a function of plate length, thickness and permittivity with and without parasitics.

To this effect, chapter 3 demonstrated that the lower the dielectric constant, the higher the pattern distortion and the influence of the higher order modes. For the materials with higher dielectric constant the amount of power carried by a higher order mode was higher at the feed point than at the termination, which explains a tilt in the beam pattern (less destructive interference in the end fire region). On the other hand, for the materials with lower dielectric constant the amount of power carried by a higher order mode was lower at the feed point than at the termination, which explains a split beam pattern (more destructive interference in the end fire region) [10]. This approach allowed for a thorough examination of the radiation characteristics of antennas of this type.

Research presented in chapter 3 has also shown that as plate length and permittivity increases, directivity and pattern bandwidth also increase. Addition of parasitics causes an increase in directivity and pattern bandwidth but at the expense of higher side lobes; side lobe level decreases as permittivity increases. Increases in plate length and permittivity with directors also cause an increase in impedance bandwidth and a reduction in return loss. It was found that parasitics are far more needed on low permittivity plates than on high permittivity plates. In fact, it was determined that in case of very high dielectrics, the directors would no longer be needed and a plate alone could be used in order to improve the directivity. It could then be deduced that the higher the permittivity the shorter the plate extensions required.

Thickness studies of chapter 4 demonstrated that as plate thickness and permittivity increase, directivity and pattern bandwidth remain virtually unchanged. Increases in plate thickness and permittivity do however cause an enhancement in impedance bandwidth. Inclusion of parasitics as plate thickness and permittivity increase does not affect pattern directivity but it does cause a reduction in pattern and impedance bandwidths and return loss.

5.2: Summary of Future Work

Figure 5.1 on page 112 shows electromagnetic wave propagation through three different plate configurations. The first (figure 5.1a) represents the plate without directors. In this case the wave reflects and refracts on both sides of the plate as it travels through it. More constructive (due to dominant mode) as well as destructive (due to higher order mode(s)) radiation takes place along the surface of the plate affecting the pattern and directivity as was shown in this work. In order to remedy the problem,

parasitics can be included as shown in figure 5.1b; in that case the wave is kept more inside the plate and cannot refract that much as is illustrated in the figure. Improvement

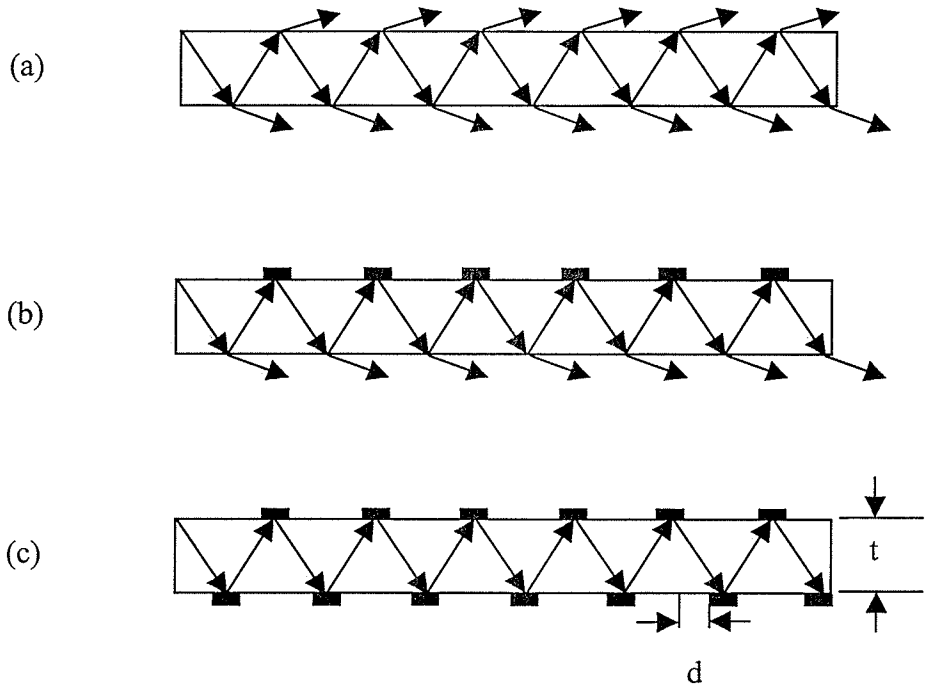

Figure 5.1: Problem Geometry (a) plate without directors (b) plate with directors on one side (c) plate with directors on both sides [1]

in pattern and directivity can be seen as was demonstrated. Refraction is further limited as directors slow down the wave by increasing the effective permittivity of the medium as seen by the traveling wave. A slower wave is a wave that possesses less energy as it hits the boundary between the dielectric and air from the physical optics point of view; thus, the magnitude of refraction decreases.

In a proposed model shown in figure 5.1c parasitics are added to the bottom of the plate. The two design parameters in this case would of course be the distance of

separation d between the two parasitics (one at the bottom and the other at the top of the plate) and the thickness t of the plate. It is hoped that effective permittivity of the plate would further increase thus improving pattern and directivity and reducing refraction even more as is shown in the figure. The modal coefficient theory could again be used to extract the necessary coefficients and study pattern behavior.

It should be noted that figure 5.1 shows reflection and refraction mechanism only and not radiation. Obviously, wave hitting the directors in figures 5.1b and 5.1c will induce currents that will radiate.

Back in 1979, Kahn analyzed an infinite linear array consisting of dipoles oriented at an arbitrary angle with respect to the array axis [11]. It is suggested in this case that the designer study the directivity and pattern characteristics of microstrip-fed Yagis as a function of an inclined angle of tilted parasitics.

In their work on Yagi Arrays of Two Concentric Loops Shoamanesh and Shafai loaded the array elements with reactive impedance elements in order to observe their effect on impedance bandwidth [21]. Similar study could be performed when we wrap the plate with an array of copper loops filling it in with an array of concentric loops as shown in figure 5.2 on page 114. The study could be made with and without the concentric loops and the reactive loading provided by various permittivities.

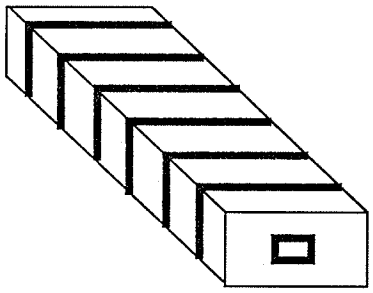

Figure 5.2: Microstrip-fed Yagi Uda antenna of loops.

APPENDIX A.1

```
                              PROGRAM PEAK

      INTEGER i, degree, max_deg, mark, kount(10), j
      REAL gain, curr, top

      OPEN (UNIT=10,FILE='h_plane.txt',status='old')
      OPEN (UNIT=20,FILE='beam.dat')

      read (10,*) degree, gain
      top = gain
      do i = 1,360
         read (10,*) degree, gain
         curr = gain
         if (curr.gt.top) then
            top = curr
            max_deg = degree
         endif
      enddo
      print*,' THE MAXIMUM GAIN IS: ',top
      print*
      print*,' THE ANGLE AT WHICH THE MAXIMUM GAIN OCCURS IS:
',max_deg
      print*
*
      rewind (unit=10)
      read (10,*) degree, gain
      prev = degree
      j=1
      kount(j) = -1
      do i = 1,360
         read (10,*) degree, gain
         curr = degree
         if (gain.ge.(top-3)) then
            kount(j) = kount(j)+1
            mark = 1
            if ((curr-prev).gt.1) then
               write (20,*)
               j = j+1
               kount(j) = 0
               mark = mark+1
            endif
            write (20,*) degree, mark
          endif
         prev = curr
      enddo
      if (j.eq.1) then
         print*,' THE BEAMWIDTH IS: ',kount(1)
      else
         do i = 1,j
            print*,' Beamwidth no.',i,' is: ',kount(j)
         enddo
      endif
*
      end
```

APPENDIX A.2

PROGRAM MODE_CHECK

```
*       This program computes axial propagation constants and guide
*       wavelengths of dielectric rods of rectangular cross section.

        DOUBLE PRECISION K(5), lambda_not, eps_r(5), eps_rr, AA(5), a, b
        DOUBLE PRECISION lambda_z
        DOUBLE PRECISION FREQ, OMEGA, pi, MU_not
        DOUBLE PRECISION factor
        DOUBLE PRECISION kx, ky, kz
        INTEGER p, q, i, dir
*
*       opening a ready input file...
        open (unit=10,file='prep.dat',status='old')
*       defining constants...
        pi = 3.141592654
        MU_not = (4*pi)/(10**7)
*       reading dielectric constants of all 5 regions...
        do i = 1,5
           read(10,*) eps_r(i)
        enddo
        eps_rr = eps_r(1)
*       entering guide width...
        read(10,*) a
*       entering guide thickness...
        read(10,*) b
*       entering the value of the mode number p...
        read(10,*) p
*       entering the value of the mode number q...
        read(10,*) q
*       choosing the direction of guide polarization (x=1 and y=2)...
        read(10,*) dir
*       entering the frequency in GHz...
        do FREQ = 100,0.01,-0.01
        OMEGA = 2*pi*FREQ*(10**9)
        lambda_not = 0.3/FREQ
*       defining wave numbers in all 5 regions...
        do i = 1,5
           K(i) = (2*pi*sqrt(eps_r(i)))/lambda_not
        enddo
        do i = 2,5
           AA(i) = pi/sqrt((K(1)**2)-(K(i)**2))
        enddo
*       calculating the transverse propagation constants...
        if (dir.eq.1) then
           kx = ((p*pi)/a)*((1+(((eps_r(3)*AA(3))+(eps_r(5)*AA(5)))/
     &          (pi*eps_rr*a)))**(-1))
           ky = ((q*pi)/b)*((1+((AA(2)+AA(4))/(pi*b)))**(-1))
        elseif (dir.eq.2) then
           kx = ((p*pi)/a)*((1+((AA(3)+AA(5))/(pi*a)))**(-1))
           ky = ((q*pi)/b)*((1+(((eps_r(2)*AA(2))+(eps_r(4)*AA(4)))/
     &          (pi*eps_rr*b)))**(-1))
        endif
*       finding mode cutoff frequency...
```

```
      factor = (K(1)**2)-(kx**2)-(ky**2)
      if (factor.le.0) then
         print*
         print*,'Cutoff frequency for this mode is',freq,'GHz'
         print*
         goto 101
      endif
      enddo
      print*
      print*,'There is no cutoff frequency for this mode.'
      print*
*
 101  continue
      end
```

APPENDIX A.3

PROGRAM FIELDS

```
*       This program computes axial propagation constants and guide
*       wavelengths of dielectric rods of rectangular cross-section.
*       It then computes mode contributions of y-polarized rods. To
*       that effect it must be used in unison with software for
*       cross-sectional field computation such as Ansoft's HFSS.

        REAL K(5), lambda_not, eps_r(5), eps_rr, AA(5), a, b
        REAL lambda_z, initial_y, final_y, delta3, power(5)
        REAL FREQ, OMEGA, pi, MU_not, x, y, delta4, z, eps_not
        REAL factor, magEx, magEy, magEz, magHx, magHy, magHz
        REAL phEx, phEy, phEz, phHx, phHy, phHz, term, term2
        REAL kx, ky, kz, initial_x, final_x, delta, delta2
        REAL initial_x2, initial_x3, final_x2, final_x3
        REAL initial_y2, initial_y3, final_y2, final_y3
        REAL rEx, rEy, rEz, rHx, rHz, k_not, const(5), fac(5)
        REAL sum_rEx, sum_rEy, sum_rEz, sum_rHx, sum_rHz
        COMPLEX lEx, lEy, lEz, lHx, lHz
        COMPLEX sum_lEx, sum_lEy, sum_lEz, sum_lHx, sum_lHz
        COMPLEX co_rEx(5), co_rEy(5), co_rEz(5), co_rHx(5)
        COMPLEX co_rHz(5), co_lEx(5), co_lEy(5), xx, yy, zz
        COMPLEX co_lEz(5), co_lHx(5), co_lHz(5)
        COMPLEX tot_coEx, tot_coEy, tot_coEz, tot_coHx, tot_coHz
        COMPLEX Ex_pq(5), Ey_pq(5), Ez_pq(5), Hx_pq(5), Hz_pq(5), j
        INTEGER  p, q, i, dir, choice, count_x, count_y
*
*       opening magnitude of cross sectional electric field in region 1
file...
!       open (unit=11,file='Emag.txt',status='old')
*       opening phase of cross sectional electric field in region 1
file...
!       open (unit=12,file='Ephase.txt',status='old')
*       opening magnitude of cross sectional electric field in region 2
file...
!       open (unit=13,file='Emag2.txt',status='old')
*       opening phase of cross sectional electric field in region 2
file...
!       open (unit=14,file='Ephase2.txt',status='old')
*       opening magnitude of cross sectional electric field in region 3
file...
!       open (unit=15,file='Emag3.txt',status='old')
*       opening phase of cross sectional electric field in region 3
file...
!       open (unit=16,file='Ephase3.txt',status='old')
*       opening magnitude of cross sectional electric field in region 4
file...
!       open (unit=17,file='Emag4.txt',status='old')
*       opening phase of cross sectional electric field in region 4
file...
!       open (unit=18,file='Ephase4.txt',status='old')
*       opening magnitude of cross sectional electric field in region 5
file...
!       open (unit=19,file='Emag5.txt',status='old')
```

```
*       opening phase of cross sectional electric field in region 5
file...
!       open (unit=20,file='Ephase5.txt',status='old')
*       opening magnitude of cross sectional magnetic field in region 1
file...
        open (unit=21,file='Hmag2.txt',status='old')
*       opening phase of cross sectional magnetic field in region 1
file...
        open (unit=22,file='Hphase2.txt',status='old')
*       opening magnitude of cross sectional magnetic field in region 2
file...
!       open (unit=23,file='H3mag2.txt',status='old')
*       opening phase of cross sectional magnetic field in region 2
file...
!       open (unit=24,file='H3phase2.txt',status='old')
*       opening magnitude of cross sectional magnetic field in region 3
file...
!       open (unit=25,file='H3mag3.txt',status='old')
*       opening phase of cross sectional magnetic field in region 3
file...
!       open (unit=26,file='H3phase3.txt',status='old')
*       opening magnitude of cross sectional magnetic field in region 4
file...
!       open (unit=27,file='H3mag4.txt',status='old')
*       opening phase of cross sectional magnetic field in region 4
file...
!       open (unit=28,file='H3phase4.txt',status='old')
*       opening magnitude of cross sectional magnetic field in region 5
file...
!       open (unit=29,file='H3mag5.txt',status='old')
*       opening phase of cross sectional magnetic field in region 5
file...
!       open (unit=30,file='H3phase5.txt',status='old')

*
        j = (0.0,1.0)
*       opening a ready input file...
        open (unit=10,file='prep.dat',status='old')
*       defining constants...
        pi = 3.141592654
        eps_not = 8.841941283E-12
        MU_not = (4*pi)/(10**7)
        d = 0.01
*       reading dielectric constants of all 5 regions...
        do i = 1,5
           read(10,*) eps_r(i)
        enddo
        eps_rr = eps_r(1)
*       entering guide thickness...
        read(10,*) a
*       entering guide width...
        read(10,*) b
*       entering the value of the mode number p...
        read(10,*) p
*       entering the value of the mode number q...
        read(10,*) q
*       entering the frequency in GHz...
```

```
      read(10,*) FREQ
      OMEGA = 2*pi*FREQ*1E9
      lambda_not = 0.3/FREQ
      k_not = (2*pi)/lambda_not
*     defining wave numbers in all 5 regions...
      do i = 1,5
         K(i) = (2*pi*sqrt(eps_r(i)))/lambda_not
      enddo
      do i = 2,5
         AA(i) = pi/sqrt((K(1)**2)-(K(i)**2))
      enddo
*     choosing the direction of guide polarization (x=1 and y=2)...
      read(10,*) dir
*     calculating the transverse propagation constants...
      if (dir.eq.1) then
         kx = ((p*pi)/a)*((1+(((eps_r(3)*AA(3))+(eps_r(5)*AA(5)))/
     &        (pi*eps_rr*a)))**(-1))
         ky = ((q*pi)/b)*((1+((AA(2)+AA(4))/(pi*b)))**(-1))
      elseif (dir.eq.2) then
         kx = ((p*pi)/a)*((1+((AA(3)+AA(5))/(pi*a)))**(-1))
         ky = ((q*pi)/b)*((1+(((eps_r(2)*AA(2))+(eps_r(4)*AA(4)))/
     &        (pi*eps_rr*b)))**(-1))
      endif
*     calculating axial propagation constant and guide wavelength...
      factor = (K(1)**2)-(kx**2)-(ky**2)
      term = (a/2) + ((sin(2*kx*a))/(4*kx))
      term2 = (b/2) + ((sin(2*ky*b))/(4*ky))
      if (kx.eq.0) then
         term = a
      elseif (ky.eq.0) then
         term2 = b
      endif
      if (factor.lt.0) then
         print*
         print*,'This mode cannot propagate.'
         print*
         goto 101
      elseif (factor.ge.0) then
         kz = sqrt(factor)
         print*
         print*,'kx = ',kx
         print*,'ky = ',ky
         print*,'kz = ',kz
         print*,'K(1) = ',K(1)
         lambda_z = (2*pi)/kz
      endif
      do i = 1,5
         const(i) = (omega*eps_not*eps_r(i)*kz)
         fac(i) = abs((ky**2) - ((k_not**2)*(eps_r(i))))/const(i)
      enddo
      print*
      print*,' THE GUIDED WAVELENGTH IS:    ',lambda_z
      print*
      print*,' p = ',p,' q = ',q
      print*
*
*     This part of the program calculates mode contributions of
```

```
*       y-polarized rods. Since qualitatively mode contributions of
*       y-polarized rods are the same as those of x-polarized rods it
*       is sufficient to analyze one polarization only.
*
        if (dir.eq.1) then
           print*,'Choose y-polarization for mode contribution'
           print*,'                calculation'
           print*
           goto 101
        elseif (dir.eq.2) then
           print*,'To exit press (1)...'
           print*,'To calculate mode contributions press (2)...'
           read*,choice
           if (choice.eq.1) then
              goto 101
           elseif (choice.eq.2) then
              goto 102
           endif
        endif
*
 102    continue
*       choosing first lower and upper limits of x integration...
        read(10,*) initial_x, final_x
*       choosing second lower and upper limits of x integration...
*       read(10,*) initial_x2, final_x2
*       choosing third lower and upper limits of x integration...
*       read(10,*) initial_x3, final_x3
*       choosing first lower and upper limits of y integration...
        read(10,*)
        read(10,*)
        read(10,*) initial_y, final_y
*       choosing second lower and upper limits of y integration...
*       read(10,*) initial_y2, final_y2
*       choosing third lower and upper limits of y integration...
*       read(10,*) initial_y3, final_y3
*       choosing the first delta...
        read(10,*)
        read(10,*)
        read(10,*) delta
*       choosing the second delta...
*       read(10,*) delta2
*       choosing the third delta...
*       read(10,*) delta3
*       choosing the fourth delta...
        read(10,*)
        read(10,*)
        read(10,*) delta4
*
*       calculating coefficient contributions in region 1...
*
!       sum_rEx = 0.0
!       sum_rEy = 0.0
!       sum_rEz = 0.0
        sum_rHx = 0.0
!       sum_rHz = 0.0
!       sum_lEx = 0.0
!       sum_lEy = 0.0
```

```
!       sum_lEz = 0.0
        sum_lHx = 0.0
!       sum_lHz = 0.0
        count_x = 0
        do x = initial_x, final_x, delta
           count_x = count_x+1
           print*,x,count_x
           count_y = 0
           do y = initial_y, final_y, delta4
!             read (11,*) xx, yy, zz, magEx, magEy, magEz
!             read (12,*) xx, yy, zz, phEx, phEy, phEz
              read (21,*) xx, yy, zz, magHx, magHy, magHz
              read (22,*) xx, yy, zz, phHx, phHy, phHz
              z = zz/1000
!             Ex_pq(1) = -sin(kx*x)*sin(ky*y)*(sin(kz*z)+j*cos(kz*z))
!             Ey_pq(1) = cos(kx*x)*cos(ky*y)*(cos(kz*z)-j*sin(kz*z))
!             Ez_pq(1) = -cos(kx*x)*sin(ky*y)*(sin(kz*z)+j*cos(kz*z))
              Hx_pq(1) = cos(kx*(x-(final_x/2)))*cos(ky*(y
     &                   -(final_y/2)))*(cos(kz*z)-j*sin(kz*z))
!             Hz_pq(1) = -sin(kx*x)*sin(ky*(y-(final_y/2)))*(sin(kz*z)+
!    &                   j*cos(kz*z))
!             rEx = (cabs(Ex_pq(1)))**2
!             rEy = (cabs(Ey_pq(1)))**2
!             rEz = (cabs(Ez_pq(1)))**2
              rHx = (cabs(Hx_pq(1)))**2
!             rHz = (cabs(Hz_pq(1)))**2
!             lEx = magEx*(cos(phEx)+j*sin(phEx))*conjg(Ex_pq(1))
!             lEy = magEy*(cos(phEy)+j*sin(phEy))*conjg(Ey_pq(1))
!             lEz = magEz*(cos(phEz)+j*sin(phEz))*conjg(Ez_pq(1))
              lHx = magHx*(cos(phHx*(pi/180))+j*sin(phHx*(pi/180)))*
     &              conjg(Hx_pq(1))
!             lHz = magHz*(cos(phHz*(pi/180))+j*sin(phHz*(pi/180)))*
!    &              conjg(Hz_pq(1))
!             sum_rEx = sum_rEx + rEx
!             sum_rEy = sum_rEy + rEy
!             sum_rEz = sum_rEz + rEz
              sum_rHx = sum_rHx + rHx
!             sum_rHz = sum_rHz + rHz
!             sum_lEx = sum_lEx + lEx
!             sum_lEy = sum_lEy + lEy
!             sum_lEz = sum_lEz + lEz
              sum_lHx = sum_lHx + lHx
!             sum_lHz = sum_lHz + lHz
              count_y = count_y+1
              print*,y,count_y
           enddo
        enddo
!       co_rEx(1) = sum_rEx
!       co_rEy(1) = sum_rEy
!       co_rEz(1) = sum_rEz
        co_rHx(1) = sum_rHx
!       co_rHz(1) = sum_rHz
!       co_lEx(1) = sum_lEx
!       co_lEy(1) = sum_lEy
!       co_lEz(1) = sum_lEz
        co_lHx(1) = sum_lHx
!       co_lHz(1) = sum_lHz
```

```
*
*       calculating coefficient contributions in region 2...
*
!       sum_rEx = 0.0
!       sum_rEy = 0.0
!       sum_rEz = 0.0
!       sum_rHx = 0.0
!       sum_rHz = 0.0
!       sum_lEx = 0.0
!       sum_lEy = 0.0
!       sum_lEz = 0.0
!       sum_lHx = 0.0
!       sum_lHz = 0.0
!       do x = initial_x, final_x, delta
!          do y = initial_y2, final_y2, delta2
!             read (13,*) xx, yy, zz, magEx, magEy, magEz
!             read (14,*) xx, yy, zz, phEx, phEy, phEz
!             read (23,*) xx, yy, zz, magHx, magHy, magHz
!             read (24,*) xx, yy, zz, phHx, phHy, phHz
!             z = zz/1000
!             Ex_pq(2) = sin(kx*x)*(cos(ky*y)-j*sin(ky*y))*(cos(kz*z)-
!     &                  j*sin(kz*z))
!             Ey_pq(2) = cos(kx*x)*(cos(ky*y)-j*sin(ky*y))*(cos(kz*z)-
!     &                  j*sin(kz*z))
!             Ez_pq(2) = cos(kx*x)*(cos(ky*y)-j*sin(ky*y))*(cos(kz*z)-
!     &                  j*sin(kz*z))
!             Hx_pq(2) = cos(kx*x)*(cos(ky*(y-(final_y/2)))-
!     &                  j*sin(ky*(y-(final_y/2))))*(cos(kz*z)-
!     &                  j*sin(kz*z))
!             Hz_pq(2) = sin(kx*x)*(cos(ky*y)-j*sin(ky*y))*(cos(kz*z)-
!     &                  j*sin(kz*z))
!             rEx = (cabs(Ex_pq(2)))**2
!             rEy = (cabs(Ey_pq(2)))**2
!             rEz = (cabs(Ez_pq(2)))**2
!             rHx = (cabs(Hx_pq(2)))**2
!             rHz = (cabs(Hz_pq(2)))**2
!             lEx = magEx*(cos(phEx)+j*sin(phEx))*conjg(Ex_pq(2))
!             lEy = magEy*(cos(phEy)+j*sin(phEy))*conjg(Ey_pq(2))
!             lEz = magEz*(cos(phEz)+j*sin(phEz))*conjg(Ez_pq(2))
!             lHx = magHx*(cos(phHx*(pi/180))+j*sin(phHx*(pi/180)))*
!     &             conjg(Hx_pq(2))
!             lHz = magHz*(cos(phHz)+j*sin(phHz))*conjg(Hz_pq(2))
!             sum_rEx = sum_rEx + rEx
!             sum_rEy = sum_rEy + rEy
!             sum_rEz = sum_rEz + rEz
!             sum_rHx = sum_rHx + rHx
!             sum_rHz = sum_rHz + rHz
!             sum_lEx = sum_lEx + lEx
!             sum_lEy = sum_lEy + lEy
!             sum_lEz = sum_lEz + lEz
!             sum_lHx = sum_lHx + lHx
!             sum_lHz = sum_lHz + lHz
!          enddo
!       enddo
!       co_rEx(2) = sum_rEx
!       co_rEy(2) = sum_rEy
!       co_rEz(2) = sum_rEz
```

```
!       co_rHx(2) = sum_rHx
!       co_rHz(2) = sum_rHz
!       co_lEx(2) = sum_lEx
!       co_lEy(2) = sum_lEy
!       co_lEz(2) = sum_lEz
!       co_lHx(2) = sum_lHx
!       co_lHz(2) = sum_lHz
*
*       calculating coefficient contributions in region 3...
*
!       sum_rEx = 0.0
!       sum_rEy = 0.0
!       sum_rEz = 0.0
!       sum_rHx = 0.0
!       sum_rHz = 0.0
!       sum_lEx = 0.0
!       sum_lEy = 0.0
!       sum_lEz = 0.0
!       sum_lHx = 0.0
!       sum_lHz = 0.0
!       do x = initial_x2, final_x2, delta2
!          do y = initial_y, final_y, delta4
!             read (15,*) xx, yy, zz, magEx, magEy, magEz
!             read (16,*) xx, yy, zz, phEx, phEy, phEz
!             read (25,*) xx, yy, zz, magHx, magHy, magHz
!             read (26,*) xx, yy, zz, phHx, phHy, phHz
!             z = zz/1000
!             Ex_pq(3) = sin(ky*y)*(cos(kx*x)-j*sin(kx*x))*(cos(kz*z)-
!     &                  j*sin(kz*z))
!             Ey_pq(3) = cos(ky*y)*(cos(kx*x)-j*sin(kx*x))*(cos(kz*z)-
!     &                  j*sin(kz*z))
!             Ez_pq(3) = -sin(ky*y)*(cos(kx*x)-j*sin(kx*x))*(sin(kz*z)+
!     &                  j*cos(kz*z))
!             Hx_pq(3) = cos(ky*(y-(final_y/2)))*(cos(kx*x)-
!     &                  j*sin(kx*x))*(cos(kz*z)-j*sin(kz*z))
!             Hz_pq(3) = sin(ky*y)*(cos(kx*x)-j*sin(kx*x))*(cos(kz*z)-
!     &                  j*sin(kz*z))
!             rEx = (cabs(Ex_pq(3)))**2
!             rEy = (cabs(Ey_pq(3)))**2
!             rEz = (cabs(Ez_pq(3)))**2
!             rHx = (cabs(Hx_pq(3)))**2
!             rHz = (cabs(Hz_pq(3)))**2
!             lEx = magEx*(cos(phEx)+j*sin(phEx))*conjg(Ex_pq(3))
!             lEy = magEy*(cos(phEy)+j*sin(phEy))*conjg(Ey_pq(3))
!             lEz = magEz*(cos(phEz)+j*sin(phEz))*conjg(Ez_pq(3))
!             lHx = magHx*(cos(phHx*(pi/180))+j*sin(phHx*(pi/180)))*
!     &             conjg(Hx_pq(3))
!             lHz = magHz*(cos(phHz)+j*sin(phHz))*conjg(Hz_pq(3))
!             sum_rEx = sum_rEx + rEx
!             sum_rEy = sum_rEy + rEy
!             sum_rEz = sum_rEz + rEz
!             sum_rHx = sum_rHx + rHx
!             sum_rHz = sum_rHz + rHz
!             sum_lEx = sum_lEx + lEx
!             sum_lEy = sum_lEy + lEy
!             sum_lEz = sum_lEz + lEz
!             sum_lHx = sum_lHx + lHx
```

```
!              sum_lHz = sum_lHz + lHz
!           enddo
!        enddo
!        co_rEx(3) = sum_rEx
!        co_rEy(3) = sum_rEy
!        co_rEz(3) = sum_rEz
!        co_rHx(3) = sum_rHx
!        co_rHz(3) = sum_rHz
!        co_lEx(3) = sum_lEx
!        co_lEy(3) = sum_lEy
!        co_lEz(3) = sum_lEz
!        co_lHx(3) = sum_lHx
!        co_lHz(3) = sum_lHz
*
*        calculating coefficient contributions in region 4...
*
!        sum_rEx = 0.0
!        sum_rEy = 0.0
!        sum_rEz = 0.0
!        sum_rHx = 0.0
!        sum_rHz = 0.0
!        sum_lEx = 0.0
!        sum_lEy = 0.0
!        sum_lEz = 0.0
!        sum_lHx = 0.0
!        sum_lHz = 0.0
!        do x = initial_x, final_x, delta
!           do y = initial_y3, final_y3, delta2
!              read (17,*) xx, yy, zz, magEx, magEy, magEz
!              read (18,*) xx, yy, zz, phEx, phEy, phEz
!              read (27,*) xx, yy, zz, magHx, magHy, magHz
!              read (28,*) xx, yy, zz, phHx, phHy, phHz
!              z = zz/1000
!              Ex_pq(4) = sin(kx*x)*(cos(ky*y)+j*sin(ky*y))*(-cos(kz*z)+
!     &                   j*sin(kz*z))
!              Ey_pq(4) = cos(kx*x)*(cos(ky*y)+j*sin(ky*y))*(cos(kz*z)-
!     &                   j*sin(kz*z))
!              Ez_pq(4) = cos(kx*x)*(cos(ky*y)+j*sin(ky*y))*(cos(kz*z)+
!     &                   j*sin(kz*z))
!              Hx_pq(4) = cos(kx*x)*(cos(ky*(y-(final_y/2)))+
!     &                   j*sin(ky*(y-(final_y/2))))*(cos(kz*z)-
!     &                   j*sin(kz*z))
!              Hz_pq(4) = sin(kx*x)*(cos(ky*y)+j*sin(ky*y))*(cos(kz*z)+
!     &                     j*sin(kz*z))
!              rEx = (cabs(Ex_pq(4)))**2
!              rEy = (cabs(Ey_pq(4)))**2
!              rEz = (cabs(Ez_pq(4)))**2
!              rHx = (cabs(Hx_pq(4)))**2
!              rHz = (cabs(Hz_pq(4)))**2
!              lEx = magEx*(cos(phEx)+j*sin(phEx))*conjg(Ex_pq(4))
!              lEy = magEy*(cos(phEy)+j*sin(phEy))*conjg(Ey_pq(4))
!              lEz = magEz*(cos(phEz)+j*sin(phEz))*conjg(Ez_pq(4))
!              lHx = magHx*(cos(phHx*(pi/180))+j*sin(phHx*(pi/180)))*
!     &              conjg(Hx_pq(4))
!              lHz = magHz*(cos(phHz)+j*sin(phHz))*conjg(Hz_pq(4))
!                sum_rEx = sum_rEx + rEx
!                sum_rEy = sum_rEy + rEy
```

```
!              sum_rEz = sum_rEz + rEz
!              sum_rHx = sum_rHx + rHx
!              sum_rHz = sum_rHz + rHz
!              sum_lEx = sum_lEx + lEx
!              sum_lEy = sum_lEy + lEy
!              sum_lEz = sum_lEz + lEz
!              sum_lHx = sum_lHx + lHx
!              sum_lHz = sum_lHz + lHz
!         enddo
!      enddo
!      co_rEx(4) = sum_rEx
!      co_rEy(4) = sum_rEy
!      co_rEz(4) = sum_rEz
!      co_rHx(4) = sum_rHx
!      co_rHz(4) = sum_rHz
!      co_lEx(4) = sum_lEx
!      co_lEy(4) = sum_lEy
!      co_lEz(4) = sum_lEz
!      co_lHx(4) = sum_lHx
!      co_lHz(4) = sum_lHz
*
*      calculating coefficient contributions in region 5...
*
!      sum_rEx = 0.0
!      sum_rEy = 0.0
!      sum_rEz = 0.0
!      sum_rHx = 0.0
!      sum_rHz = 0.0
!      sum_lEx = 0.0
!      sum_lEy = 0.0
!      sum_lEz = 0.0
!      sum_lHx = 0.0
!      sum_lHz = 0.0
!      do x = initial_x3, final_x3, delta3
!         do y = initial_y, final_y, delta4
!            read (19,*) xx, yy, zz, magEx, magEy, magEz
!            read (20,*) xx, yy, zz, phEx, phEy, phEz
!            read (29,*) xx, yy, zz, magHx, magHy, magHz
!            read (30,*) xx, yy, zz, phHx, phHy, phHz
!            z = zz/1000
!            Ex_pq(5) = sin(ky*y)*(cos(kx*x)+j*sin(kx*x))*(-cos(kz*z)+
!     &                  j*sin(kz*z))
!            Ey_pq(5) = cos(ky*y)*(cos(kx*x)+j*sin(kx*x))*(cos(kz*z)-
!     &                  j*sin(kz*z))
!            Ez_pq(5) = sin(ky*y)*(cos(kx*x)+j*sin(kx*x))*(sin(kz*z)+
!     &                  j*cos(kz*z))
!            Hx_pq(5) = cos(ky*(y(final_y/2)))*(cos(kx*x)+j*sin(kx*x))*
!     &                  (cos(kz*z)-j*sin(kz*z))
!            Hz_pq(5) = sin(ky*y)*(cos(kx*x)+j*sin(kx*x))*(-cos(kz*z)+
!     &                  j*sin(kz*z))
!            rEx = (cabs(Ex_pq(5)))**2
!            rEy = (cabs(Ey_pq(5)))**2
!            rEz = (cabs(Ez_pq(5)))**2
!            rHx = (cabs(Hx_pq(5)))**2
!            rHz = (cabs(Hz_pq(5)))**2
!            lEx = magEx*(cos(phEx)+j*sin(phEx))*conjg(Ex_pq(5))
!            lEy = magEy*(cos(phEy)+j*sin(phEy))*conjg(Ey_pq(5))
```

```
!             lEz = magEz*(cos(phEz)+j*sin(phEz))*conjg(Ez_pq(5))
!             lHx = magHx*(cos(phHx*(pi/180))+j*sin(phHx*(pi/180)))*
!     &               conjg(Hx_pq(5))
!             lHz = magHz*(cos(phHz)+j*sin(phHz))*conjg(Hz_pq(5))
!             sum_rEx = sum_rEx + rEx
!             sum_rEy = sum_rEy + rEy
!             sum_rEz = sum_rEz + rEz
!             sum_rHx = sum_rHx + rHx
!             sum_rHz = sum_rHz + rHz
!             sum_lEx = sum_lEx + lEx
!             sum_lEy = sum_lEy + lEy
!             sum_lEz = sum_lEz + lEz
!             sum_lHx = sum_lHx + lHx
!             sum_lHz = sum_lHz + lHz
!          enddo
!       enddo
!       co_rEx(5) = sum_rEx
!       co_rEy(5) = sum_rEy
!       co_rEz(5) = sum_rEz
!       co_rHx(5) = sum_rHx
!       co_rHz(5) = sum_rHz
!       co_lEx(5) = sum_lEx
!       co_lEy(5) = sum_lEy
!       co_lEz(5) = sum_lEz
!       co_lHx(5) = sum_lHx
!       co_lHz(5) = sum_lHz
*
*       calculating coefficients...
*
!       print*,'Ex...'
!       print*
!       print*,co_lEx(1)/co_rEx(1)
!       print*,co_lEx(2)/co_rEx(2)
!       print*,co_lEx(3)/co_rEx(3)
!       print*,co_lEx(4)/co_rEx(4)
!       print*,co_lEx(5)/co_rEx(5)
!       print*
!       print*,'Ey...'
!       print*
!       print*,co_lEy(1)/co_rEy(1)
!       print*,co_lEy(2)/co_rEy(2)
!       print*,co_lEy(3)/co_rEy(3)
!       print*,co_lEy(4)/co_rEy(4)
!       print*,co_lEy(5)/co_rEy(5)
!       print*
!       print*,'Ez...'
!       print*
!       print*,co_lEz(1)/co_rEz(1)
!       print*,co_lEz(2)/co_rEz(2)
!       print*,co_lEz(3)/co_rEz(3)
!       print*,co_lEz(4)/co_rEz(4)
!       print*,co_lEz(5)/co_rEz(5)
!       print*
        print*,'Hx...'
        print*
        print*,cabs(co_lHx(1)/co_rHx(1))
!       print*,cabs(co_lHx(2)/co_rHx(2))
```

```
!       print*,cabs(co_lHx(3)/co_rHx(3))
!       print*,cabs(co_lHx(4)/co_rHx(4))
!       print*,cabs(co_lHx(5)/co_rHx(5))
        do i = 1,1
           power(i) = (((cabs(co_lHx(i)/co_rHx(i)))**2)*fac(i))/2
        enddo
        power(1) = power(1)*term*term2
!       power(2) = power(2)*term
!       power(3) = power(3)*term2
!       power(4) = power(4)*term
!       power(5) = power(5)*term2
        print*
        do i = 1,1
           print*,' power flowing through region',i,'=',power(i)
        enddo
!       print*
!       print*,'Hz...'
!       print*
!       print*,co_lHz(1)/co_rHz(1)
!       print*,co_lHz(2)/co_rHz(2)
!       print*,co_lHz(3)/co_rHz(3)
!       print*,co_lHz(4)/co_rHz(4)
!       print*,co_lHz(5)/co_rHz(5)
*
 101    continue
        end
```

APPENDIX A.4

```
                              PROGRAM PERCENT

      INTEGER num, i, j, modes
      REAL power(50,20), summ(50), per(50,20)

      OPEN (UNIT=10,FILE='data.txt',status='old')
      OPEN (UNIT=20,FILE='data2.txt')
*
      READ (10,*) num, modes
      do i = 1,num
         read (10,*) power(i,1), power(i,2), power(i,3), power(i,4),
     &               power(i,5)
      enddo
*
      rewind (unit=10)
      read (10,*) num, modes
      do i = 1,num
         summ(i) = 0
         do j = 1,modes
            summ(i) = summ(i)+power(i,j)
         enddo
      enddo
*
      rewind (unit=10)
      read (10,*) num, modes
      do i = 1,num
         read (10,*) power(i,1), power(i,2), power(i,3), power(i,4),
     &               power(i,5)
         do j = 1,modes
            per(i,j) = power(i,j)/summ(i)
         enddo
      enddo
*
      do i = 1,num
         write (20,*) 100*per(i,1), 100*per(i,2), 100*per(i,3),
     &                100*per(i,4), 100*per(i,5)
      enddo
*
      end
```

APPENDIX B

According to Trim [24], a sequence of functions $\{f_n(x)\}$ is said to be orthonormal on $a \le x \le b$ with respect to the weight function w(x) if

$$\int_a^b w(x) f_n(x) f_m(x) dx = 1 \text{ if } n = m \qquad \text{(i)}$$

$$\int_a^b w(x) f_n(x) f_m(x) dx = 0 \text{ if } n \neq m$$

Now, in our case we have

$$\int_0^L \cos(\frac{n\pi x}{L}) \cos(\frac{m\pi x}{L}) dx = \frac{1}{2}\int_0^L \cos((n-m)x) dx + \frac{1}{2}\int_0^L \cos((n+m)x) dx = \frac{L}{2},\ n = m \quad \text{(ii)}$$

$$\int_0^L \cos(\frac{n\pi x}{L}) \cos(\frac{m\pi x}{L}) dx = \frac{1}{2}\int_0^L \cos((n-m)x) dx + \frac{1}{2}\int_0^L \cos((n+m)x) dx = 0,\ n \neq m$$

or,

$$\int_0^L \sin(\frac{n\pi x}{L}) \sin(\frac{m\pi x}{L}) dx = \frac{1}{2}\int_0^L \cos((n-m)x) dx - \frac{1}{2}\int_0^L \cos((n+m)x) dx = \frac{L}{2},\ n = m \quad \text{(iii)}$$

$$\int_0^L \sin(\frac{n\pi x}{L}) \sin(\frac{m\pi x}{L}) dx = \frac{1}{2}\int_0^L \cos((n-m)x) dx - \frac{1}{2}\int_0^L \cos((n+m)x) dx = 0,\ n \neq m$$

REFERENCES

1. Alexopoulos, N.G., Katehi, P.B. and Rutledge, D.B., "Substrate Optimization for Integrated Circuit Antennas", *IEEE Transactions On Microwave Theory And Techniques*, Vol. MTT-31, pp. 550-553, 1983.
2. Ansoft Corporation, *AnsoftHFSS Technical Notes*, 1996-1999.
3. Balanis, C.A., *Advanced Engineering Electromagnetics*, New York, 1989.
4. Balanis, C.A., *Antenna Theory*, John Wiley & Sons, Inc., New York, 1997.
5. Barlow, H.M. and Brown, J., *Radio Surface Waves*, Clarendon Press, Oxford, 1962.
6. Bridges, E., *Microwave Engineering*, University of Manitoba, Winnipeg, 1998.
7. Brown, J. and Spector, J.O., "The Radiating Properties of End-Fire Aerials", *Proceedings of The Institution of Electrical Engineers*, Vol. 104B, pp. 27-34, 1957.
8. Cendes, Z.J. and Lee, Jin-Fa, "The Transfinite Element Method for Modeling MMIC Devices", *IEEE Transactions On Microwave Theory And Techniques*, vol. 36, pp. 1639-1649, 1988.
9. Deal, W.R., Kaneda, N., Sor, J., Qian, Y. and Itoh, T., "A New Quasi-Yagi Antenna for Planar Active Antenna Arrays", *IEEE Transactions On Microwave Theory And Techniques*, Vol. 48, pp. 910-916, 2000.
10. Jasik, H. and Johnson, R.C., *Antenna Engineering Handbook*, McGraw-Hill, New York, 1993.
11. Kahn, W.K., "Currents on Generalized Yagi Structures", *IEEE Transactions On Antennas And Propagation*, Vol. AP-27, pp. 788-797, 1979.
12. Kiely, D.G., *Dielectric Aerials*, London, 1953.
13. Love, A.W., *Electromagnetic Horn Antennas*, IEEE Press, New York, 1976.
14. Marcatili, E. A. J., "Dielectric Rectangular Waveguide and Dielectric Coupler for Integrated Optics", *The Bell System Technical Journal*, Vol. (September), pp. 2071-2102, 1969.
15. Marcuse, D., *Theory of Dielectric Optical Waveguides*, Academic Press, Boston, 1991.

16. Mueller, G.E. and Tyrell, W.A., "Polyrod Antennas", *The Bell System Technical Journal*, Vol. 26, pp. 837-851, 1947.
17. Nielsen, E.D. and Pontoppidan, K., "Backfire Antennas with Dipole Elements", *IEEE Transactions On Antennas And Propagation*, Vol. AP-18, pp. 367-374, 1970.
18. Petosa, Aldo, "Ferrite and Dielectric Antennas for Personal Communications", PhD THESIS, Carleton University, Ottawa, 1995.
19. Qassim, K.A.S. and McEwan, N.J., "Printed Yagi Antennas as a Focal Plane Array In an Imaging System", *Seventh International Conference on Antennas and Propagation ICAP 91*, pp. 193-196, 1991.
20. Qian, Y., Deal, W.R., Kaneda, N. and Itoh, T., "Microstrip-fed quasi-Yagi antenna with broadband characteristics", *Electronics Letters*, Vol. 34, pp. 2194-2196, 1998.
21. Shoamanesh, A. and Shafai, L., "Characteristics of Yagi Arrays of Two Concentric Loops with Loaded Elements", *IEEE Transactions On Antennas And Propagation*, Vol. AP-28, pp. 871-874, 1980.
22. Syms, R. and Cozens, J., *Optical Guided Waves and Devices*, McGraw-Hill, New York, 1992.
23. Thiele, G.A., "Analysis of Yagi-Uda-Type Antennas", *IEEE Transactions On Antennas And Propagation*, Vol. AP-17, pp. 24-31, 1969.
24. Trim, D., *Ordinary Differential Equations With Variable Coefficients*, University of Manitoba, Winnipeg, 1995.
25. Watson, R.B. and Horton, C.W., "The Radiation Patterns of Dielectric Rods: Experiment and Theory", *Journal of Applied Physics*, p. 661, 1948.
26. Kaneda Noriaki, Deal W.R., Qian Yongxi, Waterhouse Rod, and Itoh Tatsuo, "A Broad-Band Planar Quasi-Yagi Antenna", *IEEE Transactions On Antennas And Propagation*, Vol. 50, pp. 1158-1160, 2002.
27. Song J. Hyok and Bialkowski Marek E., "Investigations Into The Operation of a Microstrip-Fed Uniplanar Quasi-Yagi Antenna", University of Queensland, Brisbane, Australia.